THERMAL DISSOCIATION AND DESORPTION: A NOSÉ EQUATION APPROACH

Li Liu

Thesis submitted to the

School of Graduate Studies and Research

University of Ottawa

in partial fulfilment of the requirements for the

M.Sc. degree in the

Ottawa-Carleton Chemistry Institute

Thèse soumise à

l'Ecole des études supérieures et de la recherche

Université d'Ottawa

en vue de l'obtention de la maîtrise ès sciences à

L'Institut de chimie d'Ottawa-Carleton

© Li LIU, Ottawa, Ontario, Canada, 1996

National Library of Canada
Acquisitions and Bibliographic Services Branch
395 Wellington Street
Ottawa, Ontario
K1A 0N4

Bibliothèque nationale du Canada
Direction des acquisitions et des services bibliographiques
395, rue Wellington
Ottawa (Ontario)
K1A 0N4

Your file Votre référence

Our file Notre référence

The author has granted an irrevocable non-exclusive licence allowing the National Library of Canada to reproduce, loan, distribute or sell copies of his/her thesis by any means and in any form or format, making this thesis available to interested persons.

L'auteur a accordé une licence irrévocable et non exclusive permettant à la Bibliothèque nationale du Canada de reproduire, prêter, distribuer ou vendre des copies de sa thèse de quelque manière et sous quelque forme que ce soit pour mettre des exemplaires de cette thèse à la disposition des personnes intéressées.

The author retains ownership of the copyright in his/her thesis. Neither the thesis nor substantial extracts from it may be printed or otherwise reproduced without his/her permission.

L'auteur conserve la propriété du droit d'auteur qui protège sa thèse. Ni la thèse ni des extraits substantiels de celle-ci ne doivent être imprimés ou autrement reproduits sans son autorisation.

ISBN 0-612-15736-9

Canada

UNIVERSITÉ D'OTTAWA
UNIVERSITY OF OTTAWA

Abstract

In this theoretical study, I have applied the Nosé-Hoover equations of motion with and without rotational considerations to the thermal dissociation of a diatomic molecule, H_2, in an inert gas. I calculated the pseudo-unimolecular rate constants and activation energy of thermal dissociation. My calculated values of the activation energy agree with the results of other research quite well. In addition, I have shown that the inclusion of rotation in the Nosé-Hoover equations of motion does not cause the Nosé-Hoover dynamics to be more ergodic, but such inclusion does promote the dissociation of diatomics.

Moreover, I have demonstrated an example in which the Nosé-Hoover equations of motion can be applied to the thermal desorption of H atoms from a LiF (001) surface. In this case, the surface acts as a thermal bath.

dedicated to my husband and daughter

Wei and Susan Sheng .....

Acknowledgements

I would like to express my deepest gratitude to my supervisor Prof. Ian P. Hamilton for his guidance, encouragement and patience throughout the course of this work.

I would like to express my special thanks to my co-supervisor Prof. Margaret Back for her great assistance and kindness.

My thanks go to Prof. James S. Wright, Prof. Heshel Teitelbaum, Prof. Paul C. Wilde and Prof. H. J. Kreuzer for helpful discussions regarding this work.

I acknowledge and thank the University of Ottawa and Wilfrid Laurier University for a grant of computer time. I also acknowledge and thank PHH Engineering Ltd. in Calgary for the printer access.

Abstract

In this theoretical study, I have applied the Nosé-Hoover equations of motion with and without rotational considerations to the thermal dissociation of a diatomic molecule, H_2, in an inert gas. I calculated the pseudo-unimolecular rate constants and activation energy of thermal dissociation. My calculated values of the activation energy agree with the results of other research quite well. In addition, I have shown that the inclusion of rotation in the Nosé-Hoover equations of motion does not cause the Nosé-Hoover dynamics to be more ergodic, but such inclusion does promote the dissociation of diatomics.

I have also discussed and applied the *modified* Nosé-Hoover equations of motion to the thermal dissociation of the homonuclear diatomic molecule, H_2, and the heteronuclear diatomic molecule, HCl. My results show that the modified Nosé-Hoover equations of motion can cause the phase space dynamics to be more chaotic than the original Nosé-Hoover equations of motion.

Moreover, I have demonstrated an example in which the Nosé-Hoover equations of motion can be applied to the thermal desorption of H atoms from a LiF (001) surface. In this case, the surface acts as a thermal bath.

My results suggest that the Nosé-Hoover equations of motion or their modification should be applicable to pseudo-unimolecular reactions of polyatomics in inert gases or molecular reactions on a surface where other approaches may not be feasible. I show that the generalized Nosé-Hoover equations of motion,

combined with statistical models to predict product distributions, should be applicable to bimolecular reactions.

CONTENTS

List of Figures

Chapter 1

Introduction

Theoretical studies try to simulate conditions that are close to the experimental ones, and then develop these to provide valuable information or predictions. A chemical reaction normally takes place at constant temperature and at constant pressure or constant volume, depending on whether the container is open or closed, but the energy of the system is not constant. The standard molecular dynamics method is based on simulating a reaction system with constant total energy, which is different from most real experiments.

Simulation using constant temperature conditions was pursued by various groups for many years[1.1]. However, none of the attempts really succeeded until Nosé introduced an auxiliary equation with a free parameter Q into the original Hamiltonian equations of motion[1.2]. The resulting Nosé equations of motion are both deterministic and time-reversible and have received a great deal of attention in applications to set up simulation models, to study thermodynamic or thermophysical quantities, *etc.*[1.3]. However, the Nosé equation approach has not, until the present work, been applied to any chemical reaction. In this theoretical study, I have applied modifications of the Nosé equation approach to the thermal dissociation of diatomic molecules in inert gases and the thermal desorption of an atom from a surface.

Modifications to the Nosé equation approach simplify or improve the original Nosé equations of motion, and make it more practical. The first modification was made by

Hoover[1.4], and it simplified the Nosé dynamics. I call this the Nosé-Hoover equations of motion. Later, Hamilton[1.5] modified the Nosé-Hoover equation approach to be more suitable for a one-dimensional oscillator. I call this the modified Nosé-Hoover equations of motion.

In Chapter 2, I have provided background theories regarding the methods used in this work, *i.e.*, the Nosé equation approach and modifications.

In Chapter 3, I have applied the Nosé-Hoover equation approach to the thermal dissociation of a diatomic, H_2, in an inert gas which acts as a heat bath. The H_2 dissociation is assumed to be a bimolecular reaction in the case of infinite dilution, which means that only H_2 and inert ga[illegible]s are involved. If the concentration of inert gas is considered to be constant, t[illegible] be assumed to be a pseudo-unimolecular reaction. I have shown that the No[illegible]quation approach can thermalize the H_2 dynamics when the phase space dynamics is chaotic.

Theoretical studies have indicated that rotation is effective in promoting the dissociation of diatomics[1.6]. In order to examine this, I first calculated the rate constants and the activation energy of the H_2 dissociation without considering rotation[1.7]. I then added a rotation term to the Nosé-Hoover equations of motion and calculated the rate constants[1.8] and the activation energy. My results confirm that rotation is indeed effective in promoting the dissociation of diatomics.

For a one-dimensional oscillator, the Nosé-Hoover approach is not sufficiently chaotic for a fully statistical description. In Chapter 4, I have applied the modified Nosé-Hoover equations of motion to the thermal dissociation of diatomics, H_2 and HCl. The results show

that the modified Nosé-Hoover equations of motion thermalize the diatomic dynamics more efficiently than the original Nosé-Hoover equations of motion. I have also calculated the activation energies of H_2 dissociation and HCl dissociation in an infinitely diluted inert gas. My calculated values are very close to those measured by incident shock wave experiments[1.9, 1.10].

In Chapter 5, I have extended the Nosé-Hoover equation approach to the thermal desorption of hydrogen atoms from the LiF (001) surface. In this case, the surface acts as a heat bath. My results show that the Nosé-Hoover equations of motion can also thermalize the H/LiF dynamics. They indicate that the Nosé-Hoover equation approach is applicable to the thermal desorption of an atom or a molecule from a surface where other approaches may not be feasible.

Conclusions and predictions based on this work have been given in Chapter 6.

Chapter 2

The Nosé Equation Approach and Modifications

§2.1 A Few Concepts

§2.1.1 Hamiltonian Equations of Motion

The Hamiltonian, which was named after Irish mathematician Sir William Rowan Hamilton, is an expression which permits us to calculate the energy of a system. The Hamiltonian of an N-particle system is composed of kinetic energy and potential energy terms. It can be written as follows:

$$H(r,p_r) = \sum_{i}^{N} \frac{p_{ri}^2}{2m_i} + V_N(r) \quad , \qquad (2.1)$$

where the parameter m_i is the mass of the particle i, the function $V_N(r)$ represents the total potential energy of the system, the variable p_n is the momentum of the particle i, and the variables r and p_r in parentheses are general symbols of the configuration for the three dimensional motions of all the N particles (Note: Appendix A summarizes variables used).

The coordinate, r_i, and the momentum, p_n, are functions of time, t. Usually, velocity and acceleration are denoted as $\dot{r}_i$ and $\ddot{r}_i$, respectively, *i.e.*,

$$\dot{r}_i = \frac{dr_i}{dt} \quad , \quad \ddot{r}_i = \frac{d^2r_i}{dt^2} \quad . \qquad (2.2)$$

By definition,

$$\dot{r}_i = \frac{p_i}{m_i} \quad . \tag{2.3}$$

The time derivative of the momentum is denoted as $\dot{p}_i$, *i.e.*,

$$\dot{p}_i = \frac{dp_i}{dt} = m_i \ddot{r}_i \quad . \tag{2.4}$$

According to Newton's second law, the force acting on the particle i, $F_i(r)$, is

$$F_i(r) = m_i \ddot{r}_i = - \frac{\partial V_N(r)}{\partial r_i} \quad . \tag{2.5}$$

Comparing Eq. (2.4) with Eq. (2.5),

$$\dot{p}_i = - \frac{\partial V_N(r)}{\partial r_i} \quad . \tag{2.6}$$

Equations (2.3) and (2.6) are called the *Hamiltonian equations of motion*. They describe the time evolution for the N-particle system.

As well, from Eq. (2.1), the following relationships exist:

$$\frac{\partial H(r,p_r)}{\partial p_i} = \frac{p_i}{m_i} \quad , \tag{2.7}$$

and

$$\frac{\partial H(r,p_r)}{\partial r_i} = \frac{\partial V(r)}{\partial r_i} \quad . \tag{2.8}$$

Comparing Eq. (2.3) with Eq. (2.7) and Eq. (2.6) with Eq. (2.8), we obtain

$$\dot{r}_i = \frac{\partial H(r, p_r)}{\partial p_{ri}} \quad , \tag{2.9}$$

and

$$\dot{p}_{ri} = - \frac{\partial H(r, p_r)}{\partial r_i} \quad . \tag{2.10}$$

Equations (2.9) and (2.10) are called the *Hamiltonian formalism*, which indicates the important relations between the time derivatives of the variables r_i and p_{ri} for the particle i and the Hamiltonian of the N-particle system. For any simple N-particle system where the potential energy is a function of the coordinates only, the Hamiltonian equations of motion can be derived from the expression of the Hamiltonian for that system using Eqs. (2.9) and (2.10).

The Hamiltonian equations of motion are deterministic and time reversible, and the energy is constant. The Nosé equations of motion, which will be introduced in Section §2.2, are actually extended Hamiltonian equations of motion and have all the characteristics possessed by them.

§2.1.2 The Canonical Ensemble

A crucial concept in the treatment of systems of interacting particles is the *ensemble*. An ensemble is a collection of imaginary replications of the actual system. If the number of particles, N, the volume, V, and the temperature, T, are held constant in each imaginary replication, the ensemble is called the *canonical ensemble*. Figure 2.A[2.11] shows a

representation of a canonical ensemble with 20 imaginary replications.

As seen in Fig. 2.A, all the individual replications (a replication is also called a "cell") of the actual system have the same composition and volume. Since all identical replications are regarded to be in thermal contact with each other, they have the same temperature. However, the energy, E, of an individual replication may fluctuate and be transferred as heat; the total energy, E_N, of all 20 replications is a constant because the whole ensemble is isolated completely.

The important point about an ensemble is that it is a collection of the *imaginary* replications in the actual system. Therefore, the number of imaginary replications, denoted as N_N, can be as small as we need (*e.g.*, $N_N = 1$) or as large as we need (*e.g.*, $N_N = \infty$). Note that N_N is not related to N. Similarly, E_N is not related to E.

If the energy instead of the temperature is held constant in each imaginary replication, the ensemble is called a *microcanonical ensemble*. The canonical ensemble is a constant N, V, T ensemble while the microcanonical ensemble is a constant N, V, E ensemble.

In the canonical ensemble, if the number of the imaginary replicated members in a state with energy E_i is denoted as n_{N_i}, the probability that the number of the members occupy such a state is given by the *canonical distribution* as follows:

$$\frac{n_{N_i}}{N_N} = g_i \frac{e^{-\frac{E_i}{kT}}}{Z} , \qquad (2.11)$$

where g_i is the degeneracy of state i, k is the Boltzmann constant, and

$$Z = \sum_{i=1}^{\infty} g_i e^{-\frac{E_i}{kT}} \quad . \qquad (2.12)$$

The function Z is called the *canonical partition function*[2.3]. All the thermodynamic information about a system can be obtained from the canonical partition function. The canonical partition function can be determined from the *molecular partition function* which can be calculated from spectroscopic data.

The classical form[2.3] of the canonical partition function for N indistinguishable particles is

$$Z = \frac{1}{N!\ h^{3N}} \int \cdots \int e^{-\frac{H(r,p_r)}{kT}}\ dr_1 \ldots dr_N\ dp_{r1} \ldots dp_{rN} \quad , \qquad (2.13)$$

where N! is the correction factor for N indistinguishable particles, and h is Planck's constant. The integration is over the phase space for all N particles. The exponential term in Eq. (2.13) can be written as:

$$\rho(r, p_r) = e^{-\frac{H(r,\, p_r)}{kT}} \quad . \qquad (2.14)$$

The function $\rho(r, p_r)$ is called the *equilibrium distribution function*.

§2.1.3 The Molecular Partition Function and the Boltzmann Distribution

The bridge linking the molecular energy level distribution and bulk thermodynamic properties is the *molecular partition function*. The molecular partition function can be expressed as:

$$z = \sum_{i=1}^{\infty} g_i e^{-\frac{\epsilon_i}{kT}} , \qquad (2.15)$$

where ϵ_i is the i-th energy level of the molecule.

For N indistinguishable molecules, the relation between the canonical partition function and the molecular partition function can be expressed as:

$$Z = \frac{z^N}{N!} . \qquad (2.16)$$

The probability of the molecule being in the i-th energy level, ϵ_i, is

$$\frac{n_i}{N} = g_i \frac{e^{-\frac{\epsilon_i}{kT}}}{z} . \qquad (2.17)$$

This functional form is called the *Boltzmann distribution*.

§2.1.4 Phase Space and Surfaces of Section

The *phase space* is the mathematical space of the dynamical variables of a system[2.4]. The phase space of a dynamical system is described with orthogonal coordinate directions

representing each of the variables needed to specify the instantaneous state of the system. For example, the state of a simple pendulum with small amplitude ($sin\theta \approx \theta$) is specified by its angular displacement, θ, and angular velocity, ω: hence its phase space is planar. On the other hand, a particle moving in three dimensions would have a six-dimensional phase space with three position and three velocity directions. A phase space may be constructed in several different ways. For example, momenta can be used instead of velocities.

Figure 2.B shows the phase space diagram of a simple pendulum with angular displacement, θ, and angular velocity, ω. The amplitude of the motion, a_i, yields a closed orbit of fixed energy. The energy increases with the square of the value of a_i. The orbit is usually called a *phase trajectory*.

An important feature of phase space is that two phase trajectories corresponding to similar energies will pass very close to each other, but the orbits will not cross each other. This non-crossing property derives from the fact that past and future states of a deterministic system are uniquely prescribed by the system state at a given time. If the two trajectories crossed at time t, ambiguity would be introduced into past and future states, thereby rendering the system indeterminate. Such indeterminacy would contradict the uniqueness of the trajectory.

A *surface of section* (also known as a Poincaré section) is a "snapshot" of the motion in the phase space[2,4]. It is a device invented by Henri Poincaré as a means for viewing phase space diagrams of complicated systems. It is particularly useful for a phase space with more than two dimensions. A surface of section is constructed by simplifying the phase space diagram in such a way that motion is observed easily, which consists of cutting or

sectioning the phase trajectory at regular intervals and looking at these sections in a prefered space, usually a plane.

The irregular and unpredictable time evolution of many nonlinear systems has been termed *chaos*[2-4]. Its central characteristic is that the system does not repeat its past behaviour. Periodic, or regular, and chaotic behaviour are contrasted. Despite their lack of regularity, chaotic dynamical systems follow deterministic equations such as the Hamiltonian equations of motion. The necessary conditions for chaotic motion are: (1) the system has at least three independent dynamical variables; (2) the equations of motion contain a nonlinear term that couples several of the variables. Figure 2.C shows a regular r—p_r surface of section corresponding to a one-dimensional motion with constant energy; Fig. 2.D shows a chaotic r—p_r surface of section corresponding to a one-dimensional motion with the energy not constant.

The unique character of the chaotic dynamics is the sensitivity to initial conditions. To understand this, let's imagine the system to be started twice, but from slightly different initial conditions which can be considered to result from measurement error, for example. For non-chaotic systems, this uncertainty leads to an error that grows only linearly with time. However, for a chaotic system, the error grows exponentially in time so that the state of the system is essentially unknown even after a very short time. This phenomenon occurs only when the governing equations are nonlinear.

Ergodic motion is behaviour which is harder to generate than chaotic behaviour. For ergodic systems, the time average of a dynamic variable is the same as the average over a large number of assemblies. It is often assumed that this is the case and this is called the

ergodic hypothesis[2.5]. Most chaotic systems are not ergodic systems.

§2.2 The Nosé Equation Approach

§2.2.1 Molecular Dynamics and Modifications

The Monte Carlo (MC) method and the molecular dynamics (MD) method have become important techniques in the study of fluids. They have been used to simulate the equilibrium and transition properties of fluids.

The Monte Carlo method, as introduced by Metropolis *et al.*[2.6], is based on the idea of importance sampling and has been extended in various ways[2.7]. It is a procedure for evaluating configuration space equilibrium averages for constant temperature ensembles, such as the canonical ensemble and the isothermal-isobaric ensemble. In the canonical ensemble, for example, the number of particles, N, the volume, V, and the temperature, T, are specified in advance, and an algorithm is used to generate a sequence of configurations. The average of any property over this sequence can be compared to the measured value of that property for the thermodynamic state with the specified values of N, V, and T. Similarly, in the isothermal-isobaric ensemble, it is the temperature and pressure, instead of the volume, that is specified in advance. The advantage of the MC method is that the simulation conditions can be the same as the experimental conditions. The disadvantage is that only quantities for a static system can be obtained.

The standard molecular dynamics method is based on an isoergic condition. The Hamiltonian equations of motion for a set of N molecules in a MD cell with fixed volume,

V, and energy, E, are solved numerically. The average of any property over the trajectory is an approximation to the measured value of that property for the thermodynamic state with the specified values of N, V, and E. The ensemble generated by the simulation is the microcanonical, *i.e.*, (N, V, E) ensemble. With the MD method, not only static quantities but also dynamic quantities can be obtained. This is one advantage over the MC method. However, the disadvantage of the MD method is that the simulation conditions are not normally the same as those in the experiments, which are constant temperature or pressure, instead of constant energy. The MD calculations are often more involved to set up the time interval of integrations and run in computer algorithms, while the MC calculations do not involve any time integrations.

Constant temperature MD simulation has been pursued by various means for many years. The original effort was made by Woodcock[2.8]. In order to keep the instantaneous temperature constant, he maintained the total instantaneous kinetic energy at a constant value by rescaling the velocities of the particles at each time step. In this sense, the temperature was a measure of the total instantaneous kinetic energy in a system.

The work done by Hoover[2.9] *et al.* simulated solid-phase shear stress on strain rate at fixed average temperature. The temperature which was averaged over the entire system was enforced while the non-equilibrium shear deformation was directly incorporated into the equations of motion. The steady-state isothermal deformation was obtained using a new velocity-dependent force chosen to satisfy the constraint equation.

Evans[2.10] developed a method to simulate shearing at constant internal energy. The system properties were simulated as functions of the strain rate by keeping the density and

the internal energy constant. A rescaling algorithm was used to calculate a corresponding set of properties as functions of the strain rate with the kinetic temperature and density held constant. Similar work was done by Abraham *et al.*[2.11].

The efforts described so far were based on the idea that the temperature is a measure of the kinetic energy. Therefore, instead of keeping the temperature constant, the kinetic energy was kept constant by rescaling the velocity at each time step. The reference temperature does not appear in the equations of motion and is not truly constant over the whole process.

The constant temperature MD method introduced by Andersen represented a significant breakthrough[2.12]. In his modified MD method, the volume became a variable and was allowed to fluctuate. The average volume was determined by the balance between the internal pressure and an externally applied pressure. The enthalpy of the system was approximately conserved. Therefore, this method generated a constant pressure, P, constant enthalpy, H, (N, P, H) ensemble. For (N, V, T) and (N, P, T) ensembles, Andersen added a stochastic collision term in the equations of motion. Each stochastic collision was an instantaneous event that affected the momentum of one particle. The collisions suffered by a particle occurred according to the Poisson process which is a model for counting random events. The times at which different particles suffered collisions were statistically uncorrelated. Between stochastic collisions, the particles moved in accordance with the Hamiltonian equations of motion. The value of the momentum of molecule i after the collision was chosen randomly from a Boltzmann distribution at temperature T which was the same as the desired temperature of the sample. The change in momentum took place

instantaneously. The Hamiltonian equations of motion for the entire collection of molecules were integrated until the time of the next stochastic collision. The process was repeated until a sufficiently long trajectory was obtained. In this case, the time average of any property calculated from the trajectory was equal to the (N, V, T) or (N, P, T) ensemble average of that property. The equations of motion as modified by Andersen are stochastic in nature, *i.e.*, they are non-deterministic and non-reversible. In addition, the modified equations of motion have been restricted to a system with a large number of molecules.

Haile and Gupta[2.13] introduced a non-holonomic constraint, $\frac{1}{2} m \sum_{i=1}^{N} \dot{r}_i^2$, in the generalized potential or generalized force to couple the external potential or external force to the equations of motion. The constraint is termed non-holonomic since it is not a simple algebraic relation involving the coordinates; instead, it involves the first-order time derivatives. The object of the constraint was to maintain an isothermal system.

Berendsen *et al.*[2.14] inserted stochastic and friction terms in the equations of motion to couple a system to a heat bath with the fixed reference temperature or pressure. These modified equations of motion are also non-deterministic and non-reversible.

§2.2.2 The Idea Proposed by Nosé

In 1984, a method for simulating isothermal conditions was proposed by Nosé[2.15,2.16]. An additional degree of freedom, s, was introduced, which acted as heat bath. Nosé called the real system the *physical system*, and his system, including the physical system and the heat bath, the *extended system*. To simulate isothermal conditions, Nosé considered that the

physical system was put in a large heat bath with constant temperature: there was energy exchange between the physical system and the heat bath. Therefore, the energy of the physical system, E, was allowed to fluctuate while the total energy of the extended system, E_{ES}, was a constant since the extended system was isolated overall. The heat bath acted as a constraint imposed on the physical system. With a special choice of potential for the extended system, it has been proved that the partition function of the extended system is proportional to that of the canonical ensemble. Therefore, the averages of static quantities in the extended system are exactly the same as those in the canonical ensemble, which means that the temperature is truly constant.

The interaction between the physical system and the heat bath is expressed via the scaling of the momentum of the molecules. To perform this, Nosé scaled the differential of time by the factor s. Suppose the variable t is used to represent real time in a physical system: it is transformed to the variable τ in the extended system. The variable τ is called the virtual time of the extended system. The relation between the differential t and the differential τ is

$$dt = \frac{d\tau}{s} \quad . \tag{2.18}$$

The coordinate r_i of molecule i in the physical system is unchanged when it is transformed to the coordinate q_i in the extended system, while the momentum p_n is changed to the momentum p_i, *i.e.*,

$$r_i = q_i \quad , \tag{2.19}$$

$$p_n = s\, p_i \ . \qquad (2.20)$$

This momentum transformation can be interpreted as an exchange of heat between the physical system and the heat bath.

The Hamiltonian of the extended system, H_{ES}, is assumed to have the form

$$H_{ES} = \sum_{i=1}^{N} \frac{p_i^2}{2m_i} + V_N(q) + \frac{p_s^2}{2Q} + (f+1)\ kT\ \ln(s) \ , \qquad (2.21)$$

where k is the Boltzmann constant, and T is the externally set temperature. The first two terms represent the kinetic energy and the potential energy of the molecules in the extended system, respectively. In addition, a new kinetic energy term $p_s^2/2Q$ and a new potential energy term (f+1) kT ln(s) are introduced to represent the effect of the heat bath. If the number of degrees of freedom in the physical system is f, the number of the degrees of freedom in the extended system will be (f+1) since the scaling factor s provides one additional degree of freedom.

The new kinetic energy term looks like the kinetic energy of a particle. The momentum, p_s, is the generalized momentum conjugate to s. The parameter Q behaves as the mass for the motion of s. The special choice of the new potential energy term as a logarithm, (f+1)kTln(s), ensures that the canonical ensemble averages are recovered. The Hamiltonian in the extended system, H_{ES}, is a construct, *i.e.*, it does not necessarily correspond to a real physical system.

§2.2.3 The Partition Function of the Extended System

I now show that the equations of motion derived from Eq. (2.21) produce the configurations in the canonical ensemble at temperature T. For simplicity, I will limit the discussion to the case of an atomic system, but the extension to a molecular system is straightforward. For an N-atom system, the number of degrees of freedom in the physical system is 3N. In simplified form, the Hamiltonian of the extended system in Eq. (2.21) can be written as

$$H_{ES} = H_0(q,p) + \frac{p_s^2}{2Q} + (f+1)\ kT\ \ln(s) \ , \qquad (2.22)$$

where $H_0(q, p)$ represents the Hamiltonian of the N atoms in the extended system, and q and p in parentheses are the general symbols of the configuration for three dimensional motions of all N atoms in the extended system, *i.e.*,

$$H_0(q,p) = \sum_{i=1}^{N} \frac{p_i^2}{2m_i} + V_N(q) \ . \qquad (2.23)$$

Since the extended system is isolated overall, its total energy is a constant and it produces a microcanonical ensemble with (3N+1) degrees of freedom. The distribution function of this ensemble, $\rho(q, p, s, p_s)$, is expressed as the Dirac delta function, $\delta(H_{ES} - E_{ES})$,

$$\rho_{ES} = \delta\ [\ H_0(q, p) + \frac{p_s^2}{2Q} + (f+1)\ kT\ \ln(s) - E_{ES}\ ] \ . \qquad (2.24)$$

The partition function of the extended ensemble is

$$Z_{ES}=\frac{1}{N!h^{3N}}\int dq\int dp\int dp_s\int ds\ s^{3N}\ \delta[H_0(q,p)$$

$$+\frac{p_s^2}{2Q}+(3N+1)kT\ln(s)-E_{ES}] \ , \qquad (2.25)$$

where the integrations go over the phase space for all N atoms. The term s^{3N} comes from three dimensional transformations for all N atoms. For example, for atom i, from Eq. (2.20) there are $dp_{rix} = s\ dp_{ix}$, $dp_{riy} = s\ dp_{iy}$, and $dp_{riz} = s\ dp_{iz}$.

Generally, for any argument f(x) in the Dirac delta function, the following relation exists:

$$\delta(\ f(x)\ ) = \frac{\delta(\ x - x_0\ )}{\left.\frac{df(x)}{dx}\right|_{x=x_0}} \ , \qquad (2.26)$$

where x_0 is a root of f(x), *i.e.*, $f(x_0) = 0$. Moreover, for any argument g(x) and any arbitrary function $\phi(x)$, the integration gives

$$\int dx\ \delta(\ g(x)\ )\ \phi(x) = \frac{\phi(x_0)}{\left.\frac{dg(x)}{dx}\right|_{x=x_0}} \ . \qquad (2.27)$$

In Eq. (2.25), the argument of the Dirac delta function can be considered to be a function of s.

$$f(s) = H_0(q,p) + \frac{p_s^2}{2Q} + (3N+1)\ kT\ \ln(s) - E_{ES} \ . \qquad (2.28)$$

Setting f(s) = 0, the root of f(s) is

$$s_0 = e^{-\frac{(H_0(q,p) + p_s^2/2Q - E_{ES})}{(3N+1)kT}} , \qquad (2.29)$$

with

$$\frac{df(s)}{ds}\Big|_{s=s_0} = \frac{(3N+1)\ kT}{s_0} . \qquad (2.30)$$

Substituting Eqs. (2.28), (2.29) and (2.30) into Eq. (2.26), Eq. (2.25) becomes

$$Z_{ES} = \frac{1}{N!h^{3N}(3N+1)kT}\int dq\int dp\int dp_s\int ds\ s_0\ s^{3N}\ \delta(s - s_0) . \qquad (2.31)$$

In Eq. (2.31), the argument is $g(s) = s - s_0$, and the derivative is $dg(s)/ds = 1$. The arbitrary function in Eq. (2.31) is $\phi(s) = s^{3N}$. Using the relation in Eq. (2.27) as a template to integrate the variable s, Eq. (2.31) becomes

$$Z_{ES} = \frac{1}{N!h^{3N}(3N+1)kT}\int dq\int dp\int dp_s\ s_0^{3N+1} . \qquad (2.32)$$

Using the expression for s_0 in Eq. (2.29), Eq. (2.32) becomes

$$Z_{ES} = \frac{1}{N!h^{3N}(3N+1)kT}\int dq\int dp\int dp_s\ e^{-\frac{(H_0(q,p) + \frac{p_s^2}{2Q} - E_{ES})}{kT}} . \qquad (2.33)$$

Since the total energy in the extended system is constant, the exponent with E_{ES}/kT in Eq. (2.33) is a constant and can be placed in front of the integration. Rearranging Eq. (2.33), we have

$$Z_{ES} = \frac{1}{N!h^{3N}(3N+1)kT}\ e^{\frac{E_{ES}}{kT}}\int dp_s\ e^{-\frac{p_s^2}{2QkT}}\int dq\int dp\ e^{-\frac{H_0(q,p)}{kT}} . \qquad (2.34)$$

In Eq. (2.34), the integration with respect to p_s can be performed, and the integrations with

respect to q and p result in the canonical partition function. Therefore, Eq. (2.34) can be written as

$$Z_{ES} = C(E_{ES},Q,T,N)\ Z\ , \qquad (2.35)$$

where $C(E_{ES},Q,T,N)$ is a calculable constant, and Z is the canonical partition function, *i.e.*,

$$Z = \frac{1}{N!h^{3N}} \int dq \int dp\ e^{-\frac{H_0(q,\ p)}{kT}}\ . \qquad (2.36)$$

As seen in Eq. (2.35), the partition function of the extended system is proportional to the canonical partition function. Since Eq. (2.25) is equivalent to Eq. (2.35), the distribution function of the extended system in Eq. (2.25) is the same as that of the canonical ensemble presented in Eq. (2.36).

Since any ensemble property in the extended system is the function of the configuration (q, p) only, *i.e.*, A(q, p), the ensemble average of any property calculated in the extended system can be expressed as

$$\langle A_{ES} \rangle = \frac{1}{Z_{ES}} \frac{C(E_{ES},Q,T,N)}{N!h^{3N}} \int dq \int dp\ A(q,p)\ e^{-\frac{H_0(q,p)}{kT}}\ . \qquad (2.37)$$

The constant term, $C(E_{ES},Q,T,N)$, can be cancelled with that contained in the Z_{ES} term. Thus, the ensemble average in the extended system is exactly the same as that in the canonical ensemble. The ensemble average in the extended system is also a function of the configuration only.

§2.2.4 Equations of Motion in the Extended System

From the Hamiltonian of the extended system, all the equations of motion can be obtained without introducing any stochastic processes. Using the real configuration (r, p_r), the Hamiltonian of the extended system expressed in Eq. (2.21) can be written as

$$H_{ES} = \sum_{i=1}^{N} \frac{p_{ri}^2}{2m_i s^2} + V_N(r) + \frac{p_s^2}{2Q} + (f+1)\, kT \ln(s) \quad . \qquad (2.38)$$

Applying the Hamiltonian formalism in Eqs. (2.9) and (2.10) to the Hamiltonian of the extended system in Eq. (2.38) with virtual variables, the equations of motion for the extended system are

$$\dot{r}_i = \frac{\partial H_{ES}}{\partial p_{ri}} = \frac{p_{ri}}{m_i s^2} \quad , \qquad (2.39)$$

$$\dot{p}_{ri} = -\frac{\partial H_{ES}}{\partial r_i} = -\frac{\partial V_N(r)}{\partial r_i} = F_i(r) \quad , \qquad (2.40)$$

$$\dot{s} = \frac{\partial H_{ES}}{\partial p_s} = \frac{p_s}{Q} \quad , \qquad (2.41)$$

$$\dot{p}_s = -\frac{\partial H_{ES}}{\partial s} = \sum_{i=1}^{N} \frac{p_{ri}^2}{ms^2} - (f+1)\frac{kT}{s} \quad . \qquad (2.42)$$

These four equations of motion are called the *Nosé equations of motion*. The Nosé equations of motion are actually the modified Hamiltonian equations of motion with the externally fixed temperature appearing in the auxiliary Eq. (2.42). The Nosé equations of motion are deterministic and time-reversible just like the Hamiltonian equations of motion. The

important point is that the Nosé equations of motion can be applied to either a single particle system or any N-particle system with a constant temperature condition. The constant temperature molecular dynamics method which uses Nosé equations of motion to calculate the trajectories is called the *Nosé equation approach*.

In the Nosé equations of motion, the variables r_i and p_{r_i} are the coordinate and the momentum of the particle i, respectively. The variables s and p_s are the non-physical variables. The variable p_s is the generalized momentum conjugate of the variable s. The free parameter, Q, in Eq. (2.41) determines the time scale of the temperature fluctuations. Equation (2.42) is the auxiliary equation with the temperature externally set to ensure the simulation proceeds under constant temperature conditions.

The value of the parameter Q must be chosen reasonably. When the value of the parameter Q is very large, the time derivative, $\dot{s}$, is close to zero, *i.e.*, the variable s stays almost unchanged with time. If the initial value of the variable s is set to be one, *i.e.*, the differential of time is not scaled, the Nosé equations of motion will reduce to the Hamiltonian equations of motion. When the value of the parameter Q is very small, the time derivative, $\dot{s}$, is very large, *i.e.*, the variable s changes greatly with time. As a result, the coordinate of the particle changes very little. Thus, the Nosé equations of motion will become isokinetic equations of motion.

To choose a reasonable value of the parameter Q, one should construct a series of two-dimensional r—p_r surfaces of section when p_s passed through zero with the same initial conditions but different values of the parameter Q, and also plot the kinetic energy distributions corresponding to those surfaces of section. Then, the value of Q for which the

surface of section is most chaotic and for which the corresponding kinetic energy distribution is close to a Boltzmann distribution is selected.

In Table 2-1, I have summarized the variables which are used in the physical system and extended system.

§2.3 Modifications of the Nosé Equation Approach

Nosé achieved a major advance by showing that the distribution function of the extended system is the same as that of the canonical ensemble and that smooth, deterministic, and time-reversible trajectories can be generated. His work has generated a considerable amount of attention since then. Much work has been done to improve the original Nosé equations of motion.

§2.3.1 The Modification Made by Hoover

Hoover[2.17] modified the Nosé equations of motion in order to simplify the dynamics. He defined a new time variable, dt_{new}, so that $dt_{old} \equiv s\, dt_{new}$. With this, the first-order differential Eqs. (2.39), (2.40), (2.41), (2.42) can be expressed in simpler form if their time scale is reduced by s. The differential equations with respect to t_{new} are written as follows:

$$\dot{r}_i = \frac{p_{ri}}{m_i s} , \qquad (2.43)$$

$$\dot{p}_{ri} = s\, F_i(r) \ , \tag{2.44}$$

$$\dot{s} = s\, \frac{p_s}{Q} \ , \tag{2.45}$$

$$\dot{p}_s = \sum_{i=1}^{N} \frac{p_{ri}^2}{ms^2} - (f+1)kT \ . \tag{2.46}$$

The second-order time differential of Eq. (2.43) is

$$\ddot{r}_i = \frac{\dot{p}_{ri}}{m_i s} - \frac{p_{ri}}{m_i s}\,\frac{\dot{s}}{s} \ . \tag{2.47}$$

Substituting Eqs. (2.43), (2.44) and (2.45) into Eq. (2.47), we have

$$\ddot{r}_i = \frac{F_i(r)}{m_i} - \dot{r}_i\,\frac{p_s}{Q} \ . \tag{2.48}$$

Setting $\zeta = p_s/Q$, Eq. (2.48) becomes

$$\ddot{r}_i = \frac{F_i(r)}{m_i} - \zeta\,\dot{r}_i \ . \tag{2.49}$$

The first-order time derivative of ζ is

$$\dot{\zeta} = \frac{\dot{p}_s}{Q} \ . \tag{2.50}$$

Rewriting Eq. (2.43) as $p_{ri} = m_i\, s\, \dot{r}_i$ and substituting it into Eq. (2.46) yields

$$\dot{p}_s = \sum_{i=1}^{N} m_i \dot{r}_i^2 - (f+1)kT \ . \tag{2.51}$$

Then, substituting Eq. (2.51) into Eq. (2.50) yields

$$\zeta = \frac{\left[\sum_{i=1}^{N} m_i \dot{r}_i^2 - (f+1)kT \right]}{Q} \quad . \tag{2.52}$$

To avoid time scaling, $\dot{r}_i$ is redefined as

$$\dot{r}_i = \frac{p_{ri}}{m_i} \quad . \tag{2.53}$$

From Eq. (2.53), $\dot{r}_i = \dot{p}_{ri}/m_i$ is obtained. Substituting $\dot{r}_i$ into Eq. (2.49), we obtain

$$\dot{p}_{ri} = F_i(r) - \zeta \, p_{ri} \quad . \tag{2.54}$$

Since we have set $\zeta = p_\zeta/Q$, Eq. (2.45) can be written as

$$\dot{s} = s \, \zeta \quad . \tag{2.55}$$

In Eq. (2.52), substituting Eq. (2.53) for $\dot{r}_i$, and replacing Nosé's f+1 by f because time scaling is eliminated, yields

$$\zeta = \frac{\left[\sum_{i}^{N} \frac{p_{ri}^2}{m_i} - f \, kT \right]}{Q} \quad . \tag{2.56}$$

Equations (2.53), (2.54), (2.55) and (2.56) are the new equations of motion developed by Hoover. I call them the *Nosé-Hoover equations of motion* and have used them in Chapter 3 and Chapter 5. For consistency, I will use the symbol p_ζ to replace the symbol ζ in the Nosé-Hoover equations of motion in the later chapters.

The Nosé-Hoover equations of motion have all the characteristics of the original Nosé equations of motion. The advantage of the Nosé-Hoover equations of motion over the original Nosé equations of motion is that the inconvenient variable s is eliminated.

It is clear that decreasing the parameter Q will increase the value of the variable p_s and the coupling term $p_s p_r$. Compared with the Hamiltonian equations of motion shown in Eqs. (2.3) and (2.6), the Nosé-Hoover equations of motion includes an additional term, $p_s p_r$. The $p_s p_r$ term behaves as a constraint acting on the particle. However, similar to the discussion about the value of the parameter Q in the original Nosé equations of motion in Subsection §2.2.4, the value of Q in the Nosé-Hoover equations of motion must be chosen neither too large nor too small. When the value of Q is too large, the time derivative, $\dot{p}_s$, is close to zero. If the initial value of the variable p_s is set to be zero, the Nosé-Hoover equations of motion will reduce to the Hamiltonian equations of motion. When the value of Q is too small, the time derivative, $\dot{p}_s$, is very large. As a result, the $p_s p_r$ term is dominant in Eq. (2.54), and the Nosé-Hoover equations of motion will become isokinetic equations of motion. In both cases (Q either very large or very small), the system will not behave the way that the canonical ensemble does. The choice for the value of the parameter Q in the Nosé-Hoover equations of motion is the same as that in the original Nosé equations of motion, as discussed in Subsection §2.2.4.

§2.3.2 The Modification Made by Hamilton

The Nosé-Hoover equations of motion are very useful for the system with a large number of particles, but, for a one-dimensional oscillator, the phase space dynamics is not sufficiently chaotic for a fully statistical description. Hamilton[2.18] proposed a modification of the Nosé-Hoover equations of motion by enforcing the virial theorem. The modified

Nosé-Hoover equations of motion cause the phase space dynamics to be much more chaotic for a one-dimensional oscillator and may be useful for other systems with a small number of particles.

The virial theorem is very general and has many applications in physics and chemistry[2,19]. It states that the average kinetic energy of the system is equal to the average virial of the system, *i.e.*,

$$T_v = \frac{1}{2} r \frac{dV(r)}{dr} , \qquad (2.57)$$

This is the basis for the modified Nosé-Hoover equations of motion. The modified Nosé-Hoover equations of motion are:

$$\dot{r} = \frac{p_r}{m} - s r , \qquad (2.58)$$

$$\dot{s} = -(2 T_v - k T)/Q_1 , \qquad (2.59)$$

$$\dot{p}_r = -\frac{dV(r)}{dr} - p_s p_r , \qquad (2.60)$$

$$\dot{p}_s = (2 E_k - k T)/Q_2 , \qquad (2.61)$$

where the virial term is shown in Eq. (2.57), and the kinetic energy term is

$$E_k = \frac{p_r^2}{2m} . \qquad (2.62)$$

The two parameters, Q_1 and Q_2, and the idea of including the virial energy term, T_v, were

introduced by Hamilton.

The modified Nosé-Hoover equations of motion are still deterministic and reversible, which are the key aspects of the Nosé-Hoover equations of motion. In addition, the modification thermalizes explicitly both the kinetic energy and the virial of the physical system. The time derivative of the variable r is dependent on the variable s. The variables r and s are coupled via the term s r. The variables p_r and p_s are coupled via the $p_s p_r$ term.

Both Q_1 and Q_2 are free parameters. When $Q_1 = Q_2$, the frequencies of the variables s and p_s are equal. Hamilton has provided evidence that the modified Nose-Hoover equations of motion with smaller values of Q_1 and Q_2 cause the phase space dynamics to be much more chaotic than those with the larger values of Q_1 and Q_2, and that it is more difficult to cause the phase space dynamics to be chaotic with $Q_1 = Q_2$ than with $Q_1 \neq Q_2$ for the harmonic oscillator. In Chapter 4, I have used the modified Nosé-Hoover equations of motion to calculate the thermal dissociation of diatomics.

§2.3.3 Other Modifications

There are a few other modifications of either the Nosé or Nosé-Hoover equations of motion proposed in the literature. Jellinek and Berry[12,20] generalized the Hamiltonian mechanics of Nosé by introducing general coordinate-scaling and general momentum-scaling functions to augment the time-scaling variable s of Nosé. Their more generalized equations of motion could improve the ability to simulate systems both at and away from equilibrium, for example, for reproducing transport and time-dependent properties of a physical system.

This generalization was proved within a canonical framework.

Kusnezov[2.21], Winkler[2.22] and Martyna *et al.*[2.23] modified the Nosé-Hoover scheme by thermalizing the kinetic energy of the physical system explicitly. The modifications are successful in producing trajectories that are sufficiently chaotic to calculate average properties of one-dimensional systems, such as a harmonic oscillator.

Further to the work of Hamilton[2.18] and Jellinek and Berry[2.20], L'Heureux and Hamilton[2.24] considered generalized Nosé-Hoover equations of motion which treat the kinetic energy and the virial in an equivalent manner. They modified the Nosé-Hoover equations of motion by explicitly thermalizing the virial independently from the kinetic energy. The resulting equations of motion can thermalize the system by two heat baths independently. The significance of this generalization is that the virial is thermalized explicitly and the scheme is set up within a canonical framework.

With these more generalized Nosé equation approaches, it may be possible to choose the Hamiltonian of the extended system appropriately so that the transport properties and the time-correlated functions of a particular physical system can be produced. It may also be possible to simulate the different parts of a system, such as the different chemical bonds in a compound, with the action of more than one heat bath[2.24].

Chapter 3

The Nosé-Hoover Equation Approach to the Thermal Dissociation of Diatomics in an Inert Gas

In Chapter 2, it has been shown that the simulation method of Nosé[3.1, 3.2] for the extended system creates the canonical ensemble, *i.e.*, the truly isothermal ensemble. Hoover[3.3] modified the Nosé equations of motion by reducing the time scale, which simplified the form of the equations of motion. Until now, the Nosé-Hoover equations of motion have not been applied to any chemical reaction system.

In this theoretical study, I have applied the Nosé-Hoover equation approach to the thermal dissociation of a diatomic molecule in an inert gas[3.4, 3.5]. In the limiting case of infinitely diluted diatomics, the inert gas simply acts as a heat bath. I have selected the hydrogen molecule as the test case because it is simple and experimental data are available. The inert gas can be any molecule as long as it acts only as a heat bath and does not participate in the reaction except by behaving as a collision partner. In this regard, Breshears and Bird[3.6] measured almost identical bimolecular rate constants for the thermal dissociation of hydrogen molecules diluted in argon gas and xenon gas. Both gases have no internal degrees of freedom and do not form long-lived complexes with the hydrogen molecule.

The mechanism for the thermal dissociation of the hydrogen molecule, H_2, (or any other homonuclear diatomic molecule, A_2) in an inert gas, M, environment may be

generalized as follows[13,71]:

$$H_2 - M \underset{k_{-1}}{\overset{k_1}{\rightleftharpoons}} 2H - M \ , \qquad (3.1)$$

$$H_2 - H \underset{k_{-2}}{\overset{k_2}{\rightleftharpoons}} 3H \ , \qquad (3.2)$$

$$H_2 - H_2 \underset{k_{-3}}{\overset{k_3}{\rightleftharpoons}} 2H - H_2 \ . \qquad (3.3)$$

In the case of infinite dilution, the chance that two H_2, or two H atoms, or one H_2 and one H atom, meet together is very small since the concentrations of H_2 and free H atoms are very low. Therefore, the mechanism of thermal dissociation can be simplified to a bimolecular reaction which only involves H_2 and M molecules, *i.e.*,

$$H_2 - M \xrightarrow{k_1} 2H - M \ . \qquad (3.4)$$

Thus, the reaction rate is related to the bimolecular rate constant, k_1, and the concentrations of inert gas and H_2, *i.e.*, rate = k_1 [M] [H_2]. In this bimolecular reaction, if the concentration of the inert gas is considered as a constant, the reaction can be considered as a pseudo-unimolecular reaction in the simplified case. The rate of the pseudo-unimolecular reaction is equal to k_u [H_2], where k_u is the pseudo-unimolecular rate constant, $k_u = k_1$ [M].

In this chapter, I report calculations of the pseudo-unimolecular rate constants and the activation energy for H_2 thermal dissociation, first without considering internal rotation of the hydrogen molecule and then with considering internal rotation of the hydrogen molecule. I compare my results with the available experimental and theoretical data.

The purpose of this work is to show that the Nosé-Hoover equation approach can simulate the thermalization of the H_2 dynamics (that is, to show the H_2 vibrational kinetic energy distribution is close to a Boltzmann distribution). At high temperatures, the thermalization causes H_2 dissociation. I thereby demonstrate the applicability of this approach to model a pseudo-unimolecular reaction. This approach should be able to model the unimolecular or pseudo-unimolecular reaction of polyatomics in an inert gas and to provide data for cases in which experimental or other theoretical approaches may not be feasible. It should also be applicable to the pseudo-unimolecular dissociation of diatomics or desorption of an atom or a molecule from a surface, where the potential energy function is strongly modified by the surface.

§3.1 A Brief Review of the Thermal Dissociation of Diatomics

The thermal dissociation reaction of diatomic molecules in the gas phase is important for several reasons: (1) it may be the initiation step in the mechanism of a complicated reaction; (2) it is a source of bond energy and equilibrium constant data; and (3) it provides tests for theories and the opportunity for rigorous calculation[3,7]. The reverse reaction of dissociation is called recombination.

Thermal dissociation of diatomics in an inert gas has been the subject of numerous experimental and theoretical studies for decades, especially for small molecules such as H_2, O_2, *etc.* Most kinetic measurements for the dissociation reactions of diatomic gases have been made using shock-tube techniques. These results for the dissociation of diatomic

molecules were summarized by Kern[3.7].

In the early 1970's, it was firmly established that in the presence of an inert diluent, the Arrhenius activation energies in the thermal dissociation of diatomics are always less than the spectroscopic dissociation energies of the diatomic molecules[3.8]. For example, the spectroscopic dissociation energy of the hydrogen molecule is 4.47 eV, but the experimental activation energy is much smaller than this value for a broad temperature range. Myerson and Watt[3.9] measured the formation rates of hydrogen atoms in a hydrogen—argon mixture behind shock waves, and found an Arrhenius activation energy of 4.02 eV for dissociating hydrogen over the temperature range 2290—3790K. Breshears and Bird[3.6] measured the bimolecular rate constants of H_2 diluted in argon gas and xenon gas by using incident shock waves over the temperature range 3500—8000K. They obtained an activation energy of 3.86 eV. The discrepancy was attributed to the measurement method and the temperature range presented. The curious deviation of the thermal activation energy from the spectroscopic dissociation energy in the diatomic dissociation reaction has attracted much theoretical research. A variety of theoretical approaches have been proposed for this kind of reaction, including equilibrium and non-equilibrium approaches, master equation approaches, phase space theory and classical trajectory theory, *etc.*. Most calculations have focused on non-equilibrium effects because it has been recognized for a long time that non-equilibrium effects could be important in the dissociation and recombination processes.

There have been two sustained attempts to develop non-equilibrium theories of dissociation and recombination reactions, which are, on the face of them, very different. One is the classical phase space theory of Keck and Carrier[3.10], in which it was argued that

the bound states of most diatomic molecules are so close together near the dissociation limit that the discrete states themselves could be regarded as a continuum. They assumed that motion among the discrete states which are approximated as a continuum is governed by a diffusion equation in which kT/2 of energy is exchanged between the collision partner M and the vibrationally excited diatomic molecule A_2 in each of the collisions. The possibility that a non-equilibrium distribution of bound states existed among the upper bound levels of a molecule was then superimposed on the solution for a trajectory. A suitable choice of the adjustable parameters in the theory led to a satisfactory reproduction of the dissociation rates for a wide range of diatomic molecules. Later, Keck and his co-workers, Shui and Appleton, developed the modified phase space theory of reaction rates[3.11, 3.12, 3.13, 3.14]. They predicted the recombination and dissociation rate constants for a wide range of diatomic molecules in the presence of helium, argon and xenon as collision partners, and found very good agreement with experimental results over a wide temperature range.

The other theoretical method to model thermal dissociation is the master equation approach. It explicitly maintains the discrete nature of every individual energy level, and attempts to solve the chemical kinetic differential equations which have the form of a 'master equation', regarding each individual rotational and/or vibrational state as a distinct species. This approach assumes that the energy level spacings in diatomics are so far apart that they cannot be considered as a continuum even at very high energies. The idea that energy levels can be treated discontinuously is conceptually attractive, but the calculation is time-consuming as there is one differential equation to be included for each bound or quasi-bound state considered, and most diatomic molecules have several thousand such states. Thus,

enormous sets of differential equations have to be solved simultaneously.

The hydrogen molecule is an important test case for diatomic dissociation theory since it has sufficiently few vibration-rotation levels to make it feasible to solve the complete master equation numerically. The hydrogen molecule has only about 350 vibration-rotation levels compared with, for example, about 55,000 levels for the iodine molecule. Dove and Jones[3.15, 3.16] studied H_2 dissociation kinetics by using the master equation approach. Their general conclusion was that rotation as well as vibration of the molecule contributes to the dissociation and lowers the Arrhenius activation energy. Later, Dove and Raynor[3.17, 3.18] studied the collision-induced H_2 dissociation by helium. They solved the master equation by using transition probabilities among bound states and rate constants at (v'_i, J_i) states calculated from the quasi-classical trajectories using the *ab initio* interaction potential of Wilson *et al.*[3.19] in the temperature range from 1000 to 10,000K. In their calculation, the motions were treated classically but the internal energies of the initial states corresponded to the quantized levels. They found that when individual H_2—He collisions were considered, rotational energy was generally less effective than vibrational energy in promoting dissociation. However, in a dissociating gas mixture, this trend would be counteracted to a considerable extent by the greater degeneracy of the upper J states. They predicted that the thermal dissociation reaction was a vibration-rotation ladder climbing process in which molecules whose total internal energy was close to the dissociation limit and which had substantial amounts of both the rotational energy and the vibrational energy would play a major role.

Work on determining major pathways in the thermal dissociation reaction has also

been done by other groups. Kiefer and Hajduk[13.20] used semi-phenomenological, vibrational bias mechanism to calculate the activation energies of thermal dissociation with different models for a few homonuclear molecules diluted in argon. Their results generally supported the experimental phenomena, *i.e.*, the values of the activation energy in the thermal dissociation of diatomics are less than the spectroscopic dissociation energies of the diatomics. They suggested that the steady rate arose from low vibrational energy levels and that high vibrational energy levels were too depleted to contribute to the steady rate. With two adjustable parameters, some of their values were close to the experimental data of Myerson and Watt[13.9] for H_2 dissociation.

Truhlar, Blais and their co-workers[13.21, 3.22, 3.23] studied H_2 dissociation induced by hydrogen molecule and argon collisions with quasi-classical trajectory calculations at a temperature of 4500K. Their conclusions were similar to those of Dove and Raynor[13.17, 3.18]. They calculated an activation energy of 4.22 eV[13.22] for the hydrogen dissociation. This calculated value is 0.26 eV lower than the spectroscopic dissociation energy although it is higher than the experimental values[13.6, 3.9].

Two explanations have been proposed for why the activation energy in the thermal dissociation reaction of a diatomic molecule is lower than its spectroscopic dissociation energy. Kiefer[13.24] suggested v′—v′ transfer. For a mixture in which the diatomic is not highly dilute, the basic form of the rate law is incorrect at high temperature and non-linearity should be introduced into the master equations for the vibrational levels by the inclusion of v′—v′ transfer process. The incorrect rate law is due to the fact that at high temperature, some molecules occupy high vibrational energy levels after gaining energy, but some

molecules remain at low vibrational energy levels. Thus, collisions may occur between a molecule with high vibrational energy and a molecule with low vibrational energy so that energy is transferred from the molecule with high vibrational energy to the molecule with low vibrational energy, and consequently, two molecules with moderate vibrational energy are produced. These molecules dissociate more rapidly than molecules with low vibrational energy. Therefore, the equilibrium condition of detailed balance for the v′—v′ transfer process is violated, the total vibrational energy is noticeably depleted, and there would not be enough number of molecules with high vibrational energies to collision with those molecules with low vibrational energies. As a result, the rate of dissociation seriously depressed by such v′—v′ transfer since the rate is eventually controlled by molecules with low vibrational energies. The rate enhancement is only slight due to the v′—v′ transfer process. In contrast, at low temperature this is not the case. The master equations are so non-linear at high temperature that any procedure which will increase the rate at low temperature will generally produce a much smaller increase in rate at high temperature. The combination of a significant increase in rate at the low temperature range with a slight increase in rate at the high temperature range produces a smaller apparent activation energy.

Another explanation was given by Pritchard, in a detailed discussion in his review article[3,8]. Pritchard postulated the existence of an effective rotational barrier, $U_{max}(J_i)$, for J_i state. Each rotational state has its own effective dissociation energy, $D_0^{eff}(J_i)$, because each rotational state of the diatomic molecule is described by a different effective interatomic potential curve. Figure 3.A shows the effective potential energy curves for H_2 at $v' = 0$ vibrational level and J_i rotational states. Figure 3.B shows the effective potential energy

curves for H_2 at v'_i vibrational level and J = 21 rotational state.

The effective dissociation energy, $D_0^{eff}(J_i)$, is equal to the dissociation energy at the vibrational level $v' = 0$ and the rotational state J_i, $D_0(J_i)$, plus the effective rotational barrier at this state, $U_{max}(J_i)$, *i.e.*, $D_0^{eff}(J_i) = D_0(J_i) + U_{max}(J_i)$. The higher the temperature, the more molecules there are in high rotational states. However, the higher the rotational state, the larger the barrier $U_{max}(J_i)$ that the molecule has to overcome in order to dissociate. Thus, as the temperature increases, the rate of dissociation still increases, but does not increase as rapidly as it would if the dissociation energy was equal to a constant; on the other hand, the Arrhenius activation energy is low since, on average, the molecular energies increase and upward transition probabilities increase faster than do downward transition probabilities.

Teitelbaum[3,25] investigated the non-equilibrium thermal dissociation of ten diatomic molecules diluted in argon using the master equation approach. He predicted that the activation energy of thermal dissociation tends to a limiting value of about 5/6 of the spectroscopic dissociation energy when the temperature becomes infinitely high; and the rate of dissociation is determined by collision-induced dissociation at low temperatures and by energy transfer processes at high temperatures.

§3.2 Hamiltonian Equations of Motion for a Diatomic Molecule

For the thermal dissociation of diatomics infinitely diluted in an inert gas, interactions between the diatomic molecules are ignored. Consequently, only the motion of one molecule needs to be considered. The Hamiltonian equations of motion for a diatomic molecule, AB,

can be obtained from the total Hamiltonian of the molecule. The total Hamiltonian of the molecule AB is equal to its translational and rotational kinetic energies plus the potential energy between the atom A and the atom B. Here, I ignore the rotational motion of the diatomic molecule. The expression of the kinetic energy for a diatomic molecule, AB, is

$$E_k = \frac{p_r^2}{2\mu} , \qquad (3.5)$$

where the variable p_r is the momentum of the centre of mass of the molecule AB. The parameter μ is the reduced mass of the diatomic molecule, calculated as follows:

$$\frac{1}{\mu} = \frac{1}{m_A} + \frac{1}{m_B} , \qquad (3.6)$$

where m_A and m_B are the masses of atom A and atom B, respectively. The total Hamiltonian of a diatomic molecule can be expressed as

$$H = \frac{p_r^2}{2\mu} + V(r) , \qquad (3.7)$$

where the function V(r) is the potential energy of the interatomic A—B, and the variable r is the A—B interatomic distance. Applying the Hamiltonian formalism in Eq. (2.9) and Eq. (2.10) to the Hamiltonian of the molecule AB in Eq. (3.7), I get the Hamiltonian equations of motion for a diatomic molecule as follows:

$$\dot{r} = \frac{p_r}{\mu} \quad , \tag{3.8}$$

$$\dot{p}_r = -\frac{dV(r)}{dr} = F(r) \quad , \tag{3.9}$$

where F(r) is the force acting on the centre of mass of the molecule AB.

The Hamiltonian equations of motion for the diatomic molecule are deterministic and time reversible. The total energy of the molecule AB is constant since the motion is Newtonian. If the potential energy function V(r) is known, the time evolution of the interatomic distance, r, and momentum, p_r, can be obtained by integrating the equations of motion. With the time evolution of r and p_r, the trajectory of diatomic motion is known. When the interatomic distance r is greater than a limit which is much larger than the A—B equilibrium bond distance, the diatomic molecule is considered to be dissociated.

A diatomic molecule can be treated as an anharmonic oscillator, where the interaction potential is a function of the internuclear distance. Accurate description of potential energy functions is obtained by *ab initio* quantum mechanical calculations, such as performed by Wilson *et al*[3.19]. However, such calculations are complicated and are most accurate for relatively small atoms and molecules, *e.g.*, hydrogen and helium.

A number of analytic potential energy functions are available for a variety of diatomic molecules, as described by Wright[3.20]. Simple analytical potential functions are used to reduce the computational requirements. One potential function that closely approximates the experimental potential energy curves for many diatomic molecules was suggested by the American physicist Philip M. Morse in 1929. This function, known as the *Morse potential*

function, has different expressions depending on the selection of the zero point for V(r). Here I use the form:

$$V(r) = D_e(e^{-\alpha(r-R_e)} - 1)^2 , \qquad (3.10)$$

where R_e is the equilibrium bond distance of the molecule AB. The parameter D_e is the depth of the potential energy well, called the *classical dissociation energy*. The parameter α is called the *Morse parameter*. The Morse potential function curve is shown in Fig. 3.C.

As shown in Fig. 3.C, when the interatomic distance r equals R_e, *i.e.*, at the equilibrium bond distance, the potential energy V(r) equals zero; when the interatomic distance r approaches infinity, *i.e.*, the two atoms separate, the potential energy V(r) approaches the value of the classical dissociation energy D_e; when the interatomic distance r is smaller than R_e, *i.e.*, the bond between the two atoms is compressed, the potential energy, V(r), increases quite rapidly.

In the figure, D_0 is the spectroscopic dissociation energy. It can be determined from vibrational spectra by using a graphical technique called the *Birge-Sponer extrapolation*. The value of the classical dissociation energy D_e is equal to the spectroscopic dissociation energy D_0 plus the zero-point vibrational energy of the molecule. The reason that the spectroscopic dissociation energy is smaller than the classical dissociation energy is that the molecule in its ground state possesses zero-point energy so that to dissociate the bond, less energy than the classical dissociation energy is needed. The zero-point energy of a molecule can be obtained from detected $0 \rightarrow 1$ transition in vibrational spectra, and the classical dissociation energy D_e can be found. The Morse parameter α can be calculated from spectroscopic data. The equilibrium bond distance R_e can be obtained experimentally using x-ray diffraction or

the analysis of molecular spectra.

One advantage of the Morse potential function is that all of its parameters can be obtained or calculated from spectroscopic data. However, the disadvantage is that the potential curve is typically too high when it is used to describe the situation close to the dissociation limit since the exponential term tends to zero too rapidly. In addition, the methods of processing data may generate some uncertainty when obtaining the parameters in the Morse potential function.

From the Morse potential curve, we can easily understand that if the kinetic energy of the molecule AB is greater than, or at least equal to, its dissociation energy, the molecule AB will dissociate. In this case, the pseudo-unimolecular rate constant is equal to the collision frequency of AB.

The Hamiltonian equations of motion for the diatomic molecule can simulate thermal dissociation in constant energy conditions, *i.e.*, the total energy of the diatomic molecule remains constant. In order to simulate the H_2 dissociation in experimental conditions, which have constant temperature rather than constant energy, I have used the Nosé-Hoover equations of motion for the hydrogen molecule.

§3.3 Nosé-Hoover Equations of Motion for H_2

The Nosé-Hoover equations of motion for the particle i in an N-particle system have been given in Eqs. (2.53), (2.54), (2.55) and (2.56). For the thermal dissociation of infinitely diluted H_2 in an inert gas, the inert gas is assumed to act simply as a heat bath.

The interactions between the hydrogen molecules are ignored and only a single hydrogen molecule needs to be considered in the equations of motion. Here, I ignore the rotational motion of H_2. The Nosé-Hoover equations of motion for a hydrogen molecule are:

$$\dot{r} = \frac{p_r}{\mu} , \tag{3.11}$$

$$\dot{s} = s\, p_s , \tag{3.12}$$

$$\dot{p}_r = -\frac{dV(r)}{dr} - p_s\, p_r , \tag{3.13}$$

$$\dot{p}_s = (2\, E_k - k\, T)/Q , \tag{3.14}$$

where the vibrational kinetic energy of H_2 is

$$E_k = \frac{p_r^2}{2\mu} , \tag{3.15}$$

and the parameter μ is the reduced mass of H_2, which is equal to half of the mass of one hydrogen atom, *i.e.*, $\mu = m_H/2$. The temperature T is set to be a constant.

The variables r and p_r in the Nosé-Hoover equations of motion are the H—H interatomic distance and the momentum of the centre of mass of H_2, respectively; the function V(r) is the H—H interatomic potential energy. The dimensionless time scale variable, s, and its conjugate momentum, p_s, are the non-physical variables. Equation (3.14) is the auxiliary equation with a free parameter Q. The free parameter Q can be considered as a special mass conjugate to the variable s, and determines the time scale of the temperature fluctuation.

In the Nosé-Hoover equations of motion for H_2, the interatomic distance r and the non-physical variable s are coupled via the $p_s p_r$ term: when E_k is greater than kT/2, p_s is increasing and p_r is decreasing; when E_k is smaller than kT/2, p_s is decreasing and p_r is increasing; on average, p_r is equal to a constant, *i.e.*, the kinetic energy fluctuates and on average kinetic energy is equal to a constant which is directly related to the temperature. The kinetic energy fluctuations mimic the system in contact with a heat bath.

§3.4 Thermal Dissociation of H_2 in an Inert Gas without Considering Molecular Rotation

In this section, I neglect the effect of rotational motion in promoting H_2 dissociation. As known from Section §3.1, rotation, as well as vibration, of the molecule contributes to its dissociation. I will consider the rotational motion of H_2 in Section §3.5. Since the molecular rotation is not considered here, there is no effective potential energy barrier for the dissociation. In this case, it is necessary to define a transition region, outside of which H_2 is deemed to be dissociated. The classical effective dissociation energy, D_e^{cl}, is then equal to the potential energy, V(r), at the outer boundary of the transition region. This has been done in Subsection §3.4.2 by considering the phase space trajectories of H_2.

I have calculated the pseudo-unimolecular rate constants of H_2 thermal dissociation in the temperature range 17,000—22,000K. The temperatures used in the calculation correspond to the energies which are much smaller than the H_2 dissociation energy, but large

enough so that a typical dissociation time is sufficiently short and meaningful numerical integration is feasible. The activation energy of H_2 dissociation has been obtained from an Arrhenius plot for the logarithm of the pseudo-molecular rate constants versus 1/T.

I have chosen the potential energy function for H_2 to be the Morse potential function, as in Eq. (3.10). For H_2, the Morse parameters are D_e = 4.7466 eV, α = 1.04435 a.u.$^{-1}$, and R_e = 1.40023 a.u.[3.27]. Since D_e is the classical dissociation energy, the calculated activation energy is the classical activation energy. The value of the predicted activation energy is equal to the calculated activation energy minus the zero-point energy of H_2. The zero-point energy for H_2 is 0.27 eV[3.28]. The reduced mass of H_2 is equal to 918.5822 a.u.

§3.4.1 Choice of the Parameter Q

In the Nosé-Hoover dynamical system, the H_2 trajectories traverse a four-dimensional phase space which is constructed by r, s, p_r and p_s. Since the extended system of Nosé possesses constant energy, there are only three independent variables. In other words, only three of the four variables, r, s, p_r and p_s, are independent. In order to visualize these trajectories, I constructed two-dimensional r—p_r surfaces of section by plotting points (r, p_r) when p_s passed through zero. If there is a second constant of the motion, these points lie on closed curves and the surface of section is regular. Otherwise, the surface of section is chaotic. Usually, when the surface of section is regular, the phase space trajectory is trapped in a low-order resonance zone.

It was shown by Posch, Hoover and Vesely[3.29] that the Nosé-Hoover equations of

motion can correctly simulate thermalization of oscillator dynamics, *i.e.*, cause the vibrational kinetic energy distribution of the oscillator to be close to a Boltzmann distribution, only if the phase space dynamics is chaotic. As pointed out by Hamilton[13,30], to ensure that this is the case, it is necessary to choose a value of the parameter Q so that the frequency of the auxiliary equation is in low-order resonance with the frequency of H_2 which is a function of the energy and correspondingly, the temperature. Therefore, as the first step, I considered the choice of the parameter Q in the Nosé-Hoover equations of motion.

The procedure to choose the reasonable value of the parameter Q is to compare the surfaces of section and their corresponding kinetic energy distributions, and then to select the Q value for which the surface of section is most chaotic and the corresponding kinetic energy distribution is closest to a Boltzmann distribution. For simplicity, the initial conditions s and p_s were chosen to be 1.0 and 0.0, respectively. Figure 3.1a shows the r—p_r surface of section for a trajectory with the initial conditions r = 3.3 a.u., p_r = 0.0 a.u. and Q = 10. The temperature is 4000K (corresponding to 0.34 eV), where the dissociation events are comparatively rare. Figure 3.1b shows the kinetic energy distribution normalized to 4000K, corresponding to the surface of section in Fig. 3.1a.

Here, I give a brief explanation of the surface of section and the kinetic energy distribution in Fig. 3.1. The points in Fig. 3.1a show the r—p_r motion features for the centre of mass of H_2 when p_s passes through zero. This has been done by recording the variables r and p_r at p_s = 0. Each point shows the H—H interatomic distance r and the corresponding momentum p_r for the centre of mass of H_2 at a particular moment. As seen

in Fig. 3.1a, the surface of section is primarily chaotic. The points on the surface of section are irregular and the location of each point is unpredictable. The (r,p_r) points can only be determined by the equations of motion.

In Fig. 3.1b, the bars indicate the probabilities corresponding to the kinetic energy ranges. There is no unit for E_k' shown in the figure since the value of E_k' has been normalized to 4000K (*i.e.*, 0.34 eV). *e.g.*, $E_k' = 1$, corresponding to 0.34 eV; $E_k' = 2$, corresponding to 0.68 eV, *etc.*

The kinetic energy range throughout (b) figures in the thesis is shown only for 0—5, corresponding to the actual energy value which depends on the temperature used for the normalization. Any probabilities beyond this range were not shown.

As seen in Fig. 3.1b, the first bar shows that the probability for the kinetic energy being in the range from 0 to 1 (corresponding to 0—0.34 eV) is about 0.84; the second bar shows that the probability for the kinetic energy being in the range from 1 to 2 (corresponding to 0.34—0.68 eV) is about 0.10. The solid curve on the plot indicates a continuous exact Boltzmann distribution. The exact Boltzmann distribution[3.31] for the vibrational kinetic energy is:

$$P(E_k') = \frac{1}{\sqrt{\pi\ E_k'}} \exp(-E_k') \quad , \qquad (3.16)$$

where E_k' is the normalized kinetic energy value.

I used the middle value of E_k' in each bar to calculate the exact Boltzmann distribution. For example, the middle value of E_k' is 0.5 for the first bar, the probability by Eq. (3.16) is 0.48; the middle value of E_k' is 1.5 for the second bar, the probability is

0.10. Then, these probabilities corresponding to middle values of E_x' were linked together to be the solid curve shown in Fig. 3.1b. As seen in Fig. 3.1b, the tendency of the histogram is close to the Boltzmann distribution. Since the surface of section is chaotic and the corresponding kinetic energy distribution is close to the exact Boltzmann distribution, this indicates that the H_2 dynamics is thermalized.

Similarly, Figs. 3.2a, 3.3a, 3.4a, 3.5a, 3.6a and 3.7a show the r—p_r surface of section for trajectories at 4000K with the same initial conditions, r = 3.3 a.u. and p_r = 0.0 a.u., but with different values of the parameter Q. The parameter Q is set to be 17, 20, 25, 30, 35 and 40, respectively. Figures 3.2b, 3.3b, 3.4b, 3.5b, 3.6b and 3.7b show the kinetic energy distribution normalized to 4000K, corresponding to their respective surfaces of section.

Comparing Figs. 3.1a through 3.7a, it can be seen that all these figures are primarily chaotic and symmetric with respect to reflection across the p_r = 0. The reason of the symmetry with respect to reflection across the p_r = 0 is that the same absolute values of p_r (positive or negative) correspond to the same value of kinetic energy. There are four blank areas in Fig. 3.1a, (1.5, 8), (1.5, -8), (1.3, 0) and (1.7, 0). This is due to the fact that the value of the parameter Q is small so that the Nosé-Hoover dynamical system does not behave in a canonical way, as discussed in Subsection §2.3.1. Phase space trajectories are trapped in these areas. As the value of Q increases, the boundaries of the blank areas become less clear in the surfaces of section. When the value of Q is equal to 25, Fig. 3.4a shows that the boundaries of the blank areas are very unclear and the whole surface of section is most chaotic. As the value of Q continues to increase, the boundaries of the blank areas become

clear again since the Nosé-Hoover dynamical system also does not behave in a canonical way when the value of Q is large.

Comparing Figs. 3.1b through 3.7b, it can be seen that the kinetic energy distribution normalized to 4000K (*i.e.*, the histogram) in each figure is close to the exact Boltzmann distribution (shown as a solid curve in each figure). The kinetic energy in these figures is not bounded as the variable p_r in the corresponding surfaces of section is not bounded. Combined with the fact that their corresponding surfaces of section are primarily chaotic, it can be concluded that the H_2 dynamics is primarily thermalized in all these cases.

The hydrogen molecule dissociates easily if it has a large probability of having a high kinetic energy. Figures 3.1b, 3.3b, 3.4b and 3.7b show distributions with relatively larger probabilities for E_k' at high values, *e.g.*, $E_k' = 5$, than Figs. 3.2b, 3.5b and 3.6b. On the other hand, Fig. 3.4a is more chaotic than Figs. 3.1a, 3.3a and 3.7a. I therefore chose the optimum value of the parameter Q for this case, that is, $Q = 25$. This trajectory could dissociate at some long enough time. However, a typical dissociation time is so long at 4000K that accurate numerical integration of the equations of motion for such a chaotic phase space trajectory is prohibitive.

To verify that the value of Q cannot be chosen too small or too large, I calculated H_2 trajectories with the parameter $Q = 5$ and $Q = 125$, respectively, while the other conditions were kept the same as those in Figs. 3.1 through 3.7. The results are shown in Figs. 3.8 and 3.9, respectively. Comparing Figs. 3.8 and 3.1, the boundaries of the blank areas in Fig. 3.8a are more clear than those in Fig. 3.1a; the first bar of the histogram in Fig. 3.8b is higher than that in Fig. 3.1b and the second bar of the histogram in Fig. 3.8b is lower

than that in Fig. 3.1b, which indicates that there is greater probability for having low kinetic energy. The same applies to Figs. 3.9 and 3.7. These results indicate that the H_2 dynamics is not fully thermalized when the value of Q is very small or very large, and thus the behavior of the dynamical system deviates from that of a canonical ensemble.

§3.4.2 Thermalization of H_2 Dynamics without Rotation

In Subsection §3.4.1, I have shown that for non-dissociating H_2, where the dissociation events are comparatively rare, the Nosé-Hoover equations of motion can thermalize the H_2 dynamics when the surface of section is chaotic. I now show the case of non-dissociating H_2 where the surface of section is regular. I chose the initial conditions r = 1.5 a.u. and p_r = 0.0 a.u., and kept other conditions the same as those in Fig. 3.4. The results are shown in Fig. 3.10.

In Fig. 3.10a, the surface of section is regular and the shape is symmetric with respect to the reflection along the p_r = 0 axis. The phase space trajectory is trapped in a low-order resonance zone and the variable p_r is bounded. Correspondingly, Fig. 3.10b shows the kinetic energy distribution normalized to 4000K. As seen in the figure, the kinetic energy is also bounded, and the upper bound is 3.0 (corresponding to 1.02 eV, which is much smaller than the dissociation energy of H_2). The kinetic energy distribution obviously deviates from the exact Boltzmann distribution (shown as a solid curve) because it is lacking the high kinetic energy distribution. The H_2 dynamics is not thermalized in this case, whereas in Fig. 3.4, the surface of section is chaotic and the corresponding kinetic energy

distribution is close to the exact Boltzmann distribution, and the H_2 dynamics is thermalized.

Thus, I conclude that for non-dissociating H_2, only when the phase space dynamics is chaotic do the fluctuations of kinetic energy correspond to a thermal distribution. Only then can the Nosé-Hoover equations of motion thermalize the H_2 dynamics: the Nosé-Hoover equations of motion cannot thermalize the H_2 dynamics when the phase-space dynamics is regular. The former case is illustrated in Fig. 3.4. The latter case is illustrated in Fig. 3.10.

I now show that for dissociating H_2, the Nosé-Hoover equations of motion can thermalize the H_2 dynamics in the strong-coupling region. I considered H_2 at 17,000K (corresponding to 1.46 eV), where dissociation events are comparatively common. Figure 3.11 shows the surface of section and the corresponding kinetic energy distribution normalized to 17,000K for a dissociating trajectory at 17,000K with the same initial conditions as those in Fig. 3.4.

In Fig. 3.11a, it can be seen that for $r < 3$, the surface of section is chaotic. For $r > 5$, the surface of section is regular: there are positive values of p_r only, as expected for separated H + H. The values of p_r look paired between 5 and 10. This is due to the fact that two hydrogen atoms still oscillate when they separate although the H—H bond is very weak, and thus the values of p_r fluctuate.

As shown in Fig. 3.11b, the kinetic energy distribution, normalized to 17,000K for this segment of the trajectory, deviates from the exact Boltzmann distribution as it is bounded, and the upper bound is around 3.0 (corresponding to 4.38 eV, which is very close to the dissociation energy of H_2). The reason for this deviation is that the values of p_r

change very little when two hydrogen atoms separate despite fluctuations, and thus the kinetic energy is bounded.

I conclude that for dissociating H_2, the Nosé-Hoover equations of motion can thermalize the H_2 dynamics in the strong-coupling region ($r < 3$), but they cannot thermalize the separated H + H dynamics ($r > 5$). However, to calculate the rate of the H_2 dissociation, it is unnecessary to thermalize the separated H + H dynamics because, as in Fig. 3.11b, there is significant probability of kinetic energy very close to the value of the H_2 dissociation energy normalized to 17,000K, which is around 3. This indicates that dissociation events are quite common at this temperature.

For r between 3 a.u. and 5 a.u., I somewhat arbitrarily define a transition region which is designed to incorporate the highest vibrational energy. This region of the phase space is depleted since the rate of H_2 dissociation competes with the rate of phase space redistribution. The Nosé-Hoover equation approach cannot adequately control the rate of phase space redistribution since the practical range of Q is small. Thus, I deem H_2 to be dissociated when $r > 5$. Using $r = 5$ a.u. in Eq. (3.10), the classical effective dissociation energy, D_e^{eff}, is equal to 4.53 eV. Subtracting the zero-point energy of H_2, the effective dissociation energy, D_0^{eff}, is therefore equal to 4.26 eV.

§3.4.3 Calculation of the Lifetime Distribution for H_2 Dissociation

Since the thermal dissociation of H_2 in an inert gas is considered a pseudo-unimolecular reaction, the plot for the logarithm of the number of dissociated H_2 versus

dissociation time should be linear at a fixed temperature. The negative slope of the line is equal to the rate constant of the dissociation reaction at that temperature. Thus, as an intermediate step towards calculating the rate constant, I considered the calculated lifetime distribution, *i.e.*, the distribution of dissociation times, where dissociation is defined as reaching the outer boundary of the transition region, *i.e.*, $r > 5$. To make sure that reaction has taken place (*i.e.*, H—H is separated), I defined $r > 10$ as the separation distance for the calculation. I chose the first 500 (r, p_r) values from the surface of section points at T = 4000K with initial conditions $r = 3.3$ a.u. and $p_r = 0.0$ a.u. (as seen in Fig. 3.4a).

The calculated lifetime distribution for T = 17,000K is shown in Fig. 3.12. In the figure, each bar shows the number of dissociated H_2 corresponding to the time range. For example, the first bar shows that there are about 260 H_2 dissociated at 0 to 10000 a.u. time range. The solid curve on the plot indicates a purely exponential decay distribution. I calculated the exponential decay as: $N_{diss} = 500 \times \exp(-t')$, where t' was chosen to be the middle value of coordinate on time axis at each bar, *i.e.*, $t' = 0.5, 1.5, 2.5$, *etc.* (see App. C for formula derivation). Thus, the exponential dissociated numbers are 303, 111, 41, *etc.*, corresponding to the middle values of the dissociation time ranges. Then, these numbers corresponding to middle values of t' were linked together to form the solid curve shown in Fig. 3.12.

As seen in Fig. 3.12, the number of dissociated H_2 is less than the exponential dissociated number at the shortest time range (refer to the first bar), and is approximately exponential at the middle time ranges. In addition, there is a tail at the long time ranges (refer to the sixth bar and beyond); that is, a component of the lifetime distribution for

which the decay is slower than exponential. Moreover, of the 500 trajectories considered, only 400 dissociated, so I infer that a fair fraction of the trajectories is trapped in resonance zones. Some of these trajectories would never dissociate, and would not affect the calculated rate constants. However, if some of these trajectories *do* dissociate, then the calculated rate constants *will* be affected. These complications are discussed in Subsection §3.4.5. The fraction of the trajectories trapped in the resonance zones decreases as the temperature goes up.

§3.4.4 Calculation of Rate Constants and Activation Energy for H_2 Dissociation

In order to avoid the long-time tail effect in the lifetime distribution, I calculated the dissociation rate constant from the initial parts of the lifetime distribution. I considered the first five numbers of dissociated H_2 (*i.e.*, the first five bars in the histogram) up to the dissociation time in Fig. 3.12. From a least-squares fit to the logarithm of the numbers versus time, I found $k_d = 3.52 \pm 0.48 \times 10^{12}$ sec^{-1} for T = 17,000K, as seen in Fig. 3.13. Similarly, $k_d = 4.33 \pm 0.39 \times 10^{12}$ sec^{-1} for T = 19000K, as seen in Fig. 3.14. For T = 18000, 20000 and 22000K, I found $k_d = 4.07 \pm 0.16 \times 10^{12}$ sec^{-1}, $5.58 \pm 0.50 \times 10^{12}$ sec^{-1} and $6.20 \pm 0.53 \times 10^{12}$ sec^{-1}, respectively.

Here, to improve the statistics, the number of trajectories was increased to 1000. There are slight increases for the calculated values of the rate constants themselves; for example, I found $k_d = 3.80 \pm 0.19 \times 10^{12}$ sec^{-1} for T = 17,000K, and $k_d = 4.62 \pm 0.21$

$\times 10^{12}$ sec^{-1} for T = 19,000K. However, as expected, the value of the pseudo-unimolecular rate constant increases as the temperature increases.

From an Arrhenius plot, *i.e.*, a least-squares fit to the logarithm of the pseudo-unimolecular rate constant versus the reciprocal of the temperature, the classical activation energy was found to be 3.82 $\pm$ 0.48 eV. This value minus the zero-point energy of H_2, leads to a predicted activation energy E_a = 3.55 $\pm$ 0.48 eV over the temperature range 17,000—22,000K. The Arrhenius plot is shown in Fig. 3.15. My calculated result is close to the experimental value of 3.86 eV measured by Breshears and Bird[3.61]. As in the other studies[3.20, 3.22, 3.25], my calculated activation energy of the H_2 dissociation is significantly smaller than the spectroscopic dissociation energy of 4.47 eV, and even smaller than the effective dissociation energy which is 4.26 eV.

§3.4.5 Discussion

I have shown that the Nosé-Hoover equations of motion can thermalize the H_2 dynamics for both non-dissociating and dissociating H_2 in the temperature range 4000—22,000K when the phase space dynamics is chaotic. I have also calculated the pseudo-unimolecular rate constants for H_2 dissociation in the temperature range 17,000—22,000K. From an Arrhenius plot, I have predicted the activation energy of H_2 dissociation. My conclusions are as follows:

(1) The Nosé-Hoover equations of motion can thermalize the H_2 dynamics only if the phase space dynamics is chaotic. The Nosé-Hoover equation approach cannot thermalize

the separated H + H dynamics. However, to some extent, it can thermalize the H_2 dynamics in the transition region.

(2) As noted in Subsection §3.4.3, a fair fraction of the trajectories is trapped in resonance zones. Some of these trajectories will never dissociate. As discussed by DeLeon and Berne[3.32], the calculated rate constants could be simply corrected for these trajectories by a factor equal to the fraction of the chaotic phase space. However, the fraction of the chaotic phase space is approximately constant over the temperature range considered here, and this correction would therefore not affect my calculated activation energy.

Some trajectories that are trapped in the resonance zones *do* dissociate. As discussed by Dumont and Brumer[3.33], these trajectories cause a long-time tail in the lifetime distribution (as seen in Fig. 3.12). Unfortunately, the calculated rate constants cannot be simply corrected for these trajectories. My prescription for calculating the rate constants from the initial parts of the lifetime distribution is an approximate procedure that tries to avoid this problem. To examine the possible sensitivity of the results to these phase space transients, I have calculated k_d at 17.000K and 19.000K for the second 1000 (r, p_r) values, respectively. The results are $k_d = 3.68 \pm 0.19 \times 10^{12}$ sec^{-1} and $4.47 \pm 0.20 \times 10^{12}$ sec^{-1}, respectively, which are comparable to the values reported in Subsection §3.4.4.

(3) I cannot, at present, obtain the bimolecular rate constants for the H_2—M collision dissociation from the pseudo-unimolecular rate constants for the H_2 dissociation since the concentration of the inert gas is unknown. The concentration of the inert gas is related to the rate of phase space redistribution, which the Nosé-Hoover equation approach is not able to adequately control. However, this problem does not noticeably affect the calculation of

the activation energy for the real bimolecular H_2—M collision dissociation reaction. For a two-degree-of-freedom system, such as the Nosé-Hoover equations of motion for H_2, the rate of the phase space redistribution is directly related to the K entropy. Thus, it may be possible to relate the concentration of the inert gas to the K entropy.

The *K entropy*, which is named after Russian mathematician A. N. Kolmogorov, is a special quantity to describe the local instability of the motion[3,34]. For non-chaotic time evolution, the motion is regular, and the K entropy is equal to zero; for chaotic evolution, the motion is chaotic, and the K entropy is greater than zero; for random evolution, the motion is random, and the K entropy is large[3,35]. In the case of the H_2—M collision dissociation, the phase space dynamics is approximately equally chaotic, which indicates that the K entropy is approximately constant. Therefore, the concentration of the inert gas can be considered constant. The bimolecular rate constant for the H_2—M collision dissociation is approximately equal to the pseudo-unimolecular rate constant for the H_2 dissociation multiplied by a constant. Consequently, my calculated activation energy can be considered approximately equal to that of the real bimolecular reaction.

(4) In Table 3-1, I have listed the activation energies of H_2 dissociation from different sources. As seen in the table, my calculated result agrees, within the uncertainty limits, with the experimental value of 3.86 eV measured by Breshears and Bird. It is also very close to the theoretical value predicted by Teitelbaum since the temperature used in my calculation is so high that it can be considered as infinite. My calculated value is smaller than the experimental result of Myerson and Watt yet still agrees, within the uncertainty. It is significantly smaller than the theoretical prediction of Blais and Truhlar. The

discrepancy is probably due to the fact that the temperature range selected by Blais and Truhlar is comparatively low. As may be seen, not only my result but also those of Breshears and Bird, and Teitelbaum are smaller than theirs.

(5) The temperature used in my calculation is so high that it is impossible to reach by any current experiment. The reason that I used such a high temperature is due to the computation time. In order to obtain accurate numerical integration, a typical dissociation time must be sufficiently short. At lower temperature, for example T = 4000K, a typical dissociation time is too long to permit accurate numerical integration of the equations of motion.

(6) The Nosé-Hoover equations of motion can deal with a single particle as well as an N-particle system. During my calculation, I only considered a single H_2 molecule. As H_2 dissociation was assumed under the condition of infinite dilution, the interactions of H_2—H_2 were ignored, and yet the interactions of H_2—M existed. However, these H_2—M interactions should be very unimportant since H_2 is a non-polar, non-dipole molecule. Thus, the approximation is acceptable.

§3.5 Inclusion of Rotation in the Nosé-Hoover Equation Approach for H_2 Dissociation

In Section §3.4, I have considered the Nosé-Hoover equation approach to the thermal dissociation of the non-rotating diatomic molecule, H_2. I showed that, with significant qualifications, the Nosé-Hoover equation approach could thermalize the H_2 dynamics for the

temperature range 4000—22,000K, and that I could calculate the pseudo-unimolecular rate constants for the H_2 dissociation in the temperature range 17,000—22,000K. One of the problems observed was that the Nosé-Hoover equation approach is not ergodic and consequently, there is a long-time tail in the lifetime distribution.

In this section, I have extended my work to the rotating diatomic molecule, H_2. The purpose of this work is twofold. First, quasiclassical calculations[3.17, 3.21, 3.22, 3.23] have shown that rotation is effective in promoting the dissociation of diatomics. I wish to see if this is the case for the Nosé-Hoover equation approach. Second, with regard to the long-time tail problem noted in the previous section, I wish to examine the extent to which the inclusion of the rotation causes the Nosé-Hoover dynamics to be more ergodic.

§3.5.1 The Rotational Kinetic Energy For a Diatomic Molecule

The diatomic molecule, AB, can be considered as a linear rigid rotor as shown in the Fig. 3.D.

By definition, the moment of inertia, I, is equal to

$$I = m_A r_A^2 + m_B r_B^2 , \qquad (3.17)$$

where the parameters m_A and m_B are the masses of atoms A and B, while the variables r_A and r_B represent the distances of atoms A and B to the centre of mass, respectively.

To determine r_A and r_B, Eq. (3.18) and (3.19) can be solved simultaneously:

$$m_A r_A = m_B r_B , \tag{3.18}$$

$$r_A - r_B = r , \tag{3.19}$$

$$r_A = \frac{m_B r}{m_A - m_B} , \quad r_B = \frac{m_A r}{m_A - m_B} , \tag{3.20}$$

where the variable r is the interatomic distance of A—B. Substituting the r_A and r_B expressions into Eq. (3.17), I get

$$I = \mu r^2 , \tag{3.21}$$

where the parameter μ is the reduced mass of AB.

The angular momentum for the one-dimensional rotation of a linear rigid rotor, L_1, can be expressed as

$$L_1 = I \omega , \tag{3.22}$$

where the variable ω is the angular velocity.

The rotational kinetic energy for one-dimensional rotational motion is

$$E_{1r} = \frac{L_1^2}{2I} = \frac{I\omega^2}{2} . \tag{3.23}$$

The angular velocity, ω, can be converted to the linear velocity, v, as $\omega = v/r$. Obviously, there are two rotational dimensions for a linear rigid rotor. Therefore, the total rotational kinetic energy should be doubled.

$$E_r = I\omega^2 = I\frac{v^2}{r^2} \quad . \tag{3.24}$$

For simplicity, I chose the moment of inertia equal to its average value, *i.e.*, $I = \mu R_e^2$, where the parameter R_e is the equilibrium bond distance between atom A and atom B: According to the equipartition theorem[3.28], the average of quadratic velocity, v^2, is related to the temperature as

$$<\frac{1}{2}\mu v^2> = \frac{1}{2}kT \quad . \tag{3.25}$$

Thus, Eq. (3.24) can be re-written as

$$E_r = \mu R_e^2 \frac{kT}{r^2 \mu} = \frac{R_e^2}{r^2} kT \quad . \tag{3.26}$$

The average value of the squared interatomic distance, r^2, is equal to R_e^2, *i.e.*, $<r^2> = R_e^2$. Therefore, the average value of E_r in Eq. (3.26) is equal to kT, which indicates that the formula of E_r shown in Eq. (3.26) conforms to the equipartition theorem. This theorem states that the average rotational kinetic energy for each rotational degree of freedom should be equal to half of kT, and here E_r is the total rotational energy for the rotational motion in two dimensions.

§3.5.2 Nosé-Hoover Equations of Motion for H_2 Including Rotation

The Nosé-Hoover equations of motion for rotating H_2 should be similar to those for the non-rotating H_2 in Section §3.3. I give the equations as follows:

$$\dot{r} = \frac{p_r}{\mu} , \tag{3.27}$$

$$\dot{s} = s\, p_s , \tag{3.28}$$

$$\dot{p}_r = -\frac{dV(r)}{dr} + 2\frac{R_c^2}{r^3} k T - p_s p_r , \tag{3.29}$$

$$\dot{p}_s = (2 E_k - k T)/Q_1 - (E_r - k T)/Q_2 , \tag{3.30}$$

where the vibrational and rotational kinetic energies are

$$E_k = \frac{p_r^2}{2\mu} , \quad E_r = \frac{R_c^2}{r^2} k T , \tag{3.31}$$

respectively, and the reduced mass is $\mu = m_H/2$.

I have added a term, $2 R_c^2 k T / r^3$, which represents centrifugal force, in Eq. (3.29). This term is obtained from the negative derivative of E_r with respect to r, *i.e.*, $-dE_r/dr$ (see Subsection §2.1.1, the Hamiltonian formalism). Equation (3.30) is the auxiliary equation. In Eq. (3.30), I have included the separate terms E_k and E_r because the time scales for vibration and rotation are very different. Reflecting this difference, I chose $Q_2 = 10^4 Q_1$ since the rotational spacings are much smaller than the vibrational ones so that the contribution of rotational motion should be much smaller than that of vibrational motion.

In the Nosé-Hoover equations of motion including rotation for H_2, both rotation and vibration were seen to be significant. For short times (relative to the period of rotation), the rotational effect is dominant. As seen in Eq. (3.30), when E_r is greater than kT, p_s is increasing, and p_r is decreasing through the coupling term $p_s p_r$ in Eq. (3.29); on the other hand, when E_r is smaller than kT, p_s is decreasing, and p_r is increasing; on average, E_r is equal to kT and p_r is equal to a constant. For long times, the vibrational effect is dominant in Eq. (3.30), and the rotational effect is contributed by the $2R_e^2kT/r^3$ term in Eq. (3.29).

As in Section §3.4, I chose the potential energy function to be the Morse potential function (as seen in Eq. (3.10)). The parameters are also the same as those used in Section §3.4, *i.e.*, D_e = 4.7466 eV, α = 1.04435 a.u.$^{-1}$, R_e = 1.40083 a.u.[3.27]. The zero-point energy for H_2 is 0.27 eV[3.28]. The reduced mass μ = 918.5822 a.u.

§3.5.3 Choice of the Parameter Q_t

As the first step in calculating H_2 dissociation with the Nosé-Hoover equations of motion including rotation, I considered the choice of the parameter Q_t. To choose a reasonable value of the parameter Q_t, I constructed a series of two-dimensional r—p_r surfaces of section with the same initial conditions but different values of the parameter Q_t when p_s passed through zero. I also plotted the kinetic energy distributions corresponding to those surfaces of section. I then selected the value of Q_t for which the surface of section is most chaotic and for which the corresponding kinetic energy distribution is close to the exact Boltzmann distribution with the largest probability for kinetic energy close to the

dissociation energy of H_2.

As in Subsection §3.4.1, the temperature was chosen to be 4000K (corresponding to 0.34 eV), where the dissociation events are comparatively rare; for simplicity, the initial conditions s and p_s were chosen to be 1.0 and 0.0, respectively; and the initial conditions r and p_r were still chosen to be 3.3 a.u. and 0.0 a.u., respectively. The reason that I chose the initial r = 3.3 a.u., which is comparatively large, is that for non-dissociating H_2, when the value of the initial r is close to the H—H equilibrium bond distance (R_e = 1.40083 a.u.), the phase space trajectory is trapped in a low-order resonance zone and the surface of section is regular (as seen in Fig. 3.10a). Therefore, the H_2 dynamics cannot be thermalized. When the value of the initial r is away from the equilibrium bond distance, the phase space dynamics is chaotic (as seen in Fig. 3.4a). I therefore retained the choice of the initial r which was used in Subsection §3.4.1 for the current subsection. The r—p_r surfaces of section and the kinetic energy distributions normalized to 4000K, for trajectories with the same initial conditions but different values of the parameter Q_1, are shown in Figs. 3.16, 3.17, 3.18, 3.19, 3.20 and 3.21, respectively. In these figures, the parameter Q_1 is 17, 20, 25, 30, 35 and 40, respectively.

Generally, all the surfaces of section are primarily chaotic, and the kinetic energy distribution normalized to 4000K (*i.e.*, the histogram) in each (b) figure is close to the exact Boltzmann distribution (shown as a solid curve in each (b) figure), which means that the H_2 dynamics is primarily thermalized in all these cases. However, there are some blank areas on the surfaces of section, and these blank areas change with the value of Q_1. As seen in Fig. 3.16a, where the value of Q_1 is small, there are two blank areas near the centre of the

figure, which indicate that phase space trajectories are trapped there. As the value of Q_t increases, the size of the blank areas become smaller in Fig. 3.17a; in Fig. 3.18a, only one blank area is left; the blank area becomes smaller in Fig. 3.19a; and the size of the blank area stays small but the boundary becomes clearer in Figs. 3.20a and 3.21a.

Comparing Figs. 3.16b through 3.21b, Figs. 3.16b, 3.17b, 3.19b and 3.20b show their distributions with relatively larger probabilities for E_x' at high values, *e.g.*, $E_x' = 5$, than Figs. 3.18b and 3.21b. The hydrogen molecule dissociates easily if it has a large probability of having a high kinetic energy. On the other hand, Fig. 3.19a is more chaotic than Figs. 3.16a, 3.17a and 3.20a. I therefore chose the optimum value of the parameter Q_t to be 30 as in Fig. 3.19.

The value of the parameter Q_t is slightly larger than the value of Q chosen in Subsection §3.4.1, probably due to the fact that the rotation term in the auxiliary Eq. (3.30) increases the frequency of p_s so that the value of the parameter Q_t has to be increased in order to ensure that the frequency of the auxiliary equation is in low-order resonance. The results are not sensitive to the particular choice of Q_t in the range 25—35, but for much larger or smaller values of Q_t there are large regions of regular dynamics in the phase space since the Nosé-Hoover dynamics deviates from the canonical dynamics.

§3.5.4 Thermalization of H_2 Dynamics Including Rotation

In Subsection §3.5.3, I have shown that for non-dissociating H_2, the Nosé-Hoover equations of motion including rotation can thermalize the H_2 dynamics when the surface of

section is chaotic. I now show the case of non-dissociating H_2 where the surface of section is regular. I changed the initial conditions to be r = 1.5 a.u. and p_r = 0.0 a.u. and kept other conditions the same as those in Fig. 3.19. The result is shown in Fig. 3.22. Both Figs. 3.19 and 3.22 show cases for non-dissociating H_2. In Fig. 3.22a, the surface of section is regular: the phase-space trajectory is trapped in a low-order resonance zone; and the variable p_r is bounded. In Fig. 3.22b, it can be seen that the kinetic energy is also bounded, and the upper bound is around 3.0 (corresponding to 1.02 eV, which is much smaller than the dissociation energy of H_2). The kinetic energy distribution normalized to 4000K deviates from the Boltzmann distribution (shown as a solid curve) as it is lacking the high kinetic energy distribution. These phenomena are similar to those shown in Fig. 3.10. Therefore, I conclude that for non-dissociating H_2, the Nosé-Hoover equations of motion including rotation, as well as excluding rotation, thermalize the H_2 dynamics only when the phase space dynamics is chaotic.

The inclusion of rotation causes the phase space dynamics of H_2 to be more chaotic than when rotation is excluded. To show this, I compare Fig. 3.4a and Fig. 3.18a whose trajectories were run under exactly the same initial conditions, but the latter trajectory was calculated with the inclusion of rotation. It can be seen that the boundaries for the blank areas in Fig. 3.18a are not as clear as those in Fig. 3.4a, especially at r greater than the H—H equilibrium bond distance, for example, at r between 1.8 and 2.2. This indicates that the equations of motion with the rotational modification cause the phase space dynamics of H_2 to be more chaotic. Comparison of the other pairs of figures, for example, Figs. 3.3a and 3.17a, shows similar results. The reason that the inclusion of rotation causes the phase

space dynamics to be more chaotic is that the rotation term in Eq. (3.30) increases the value of the variable p_θ so that the coupling term $p_\theta p_r$ in Eq. (3.29) is increased, and the time derivative, $\dot{p}_r$, is larger. Although the $2 R_e^2 k T / r^3$ term in Eq. (3.29) decreases the coupling effect of $p_\theta p_r$, such a decrease reaches a minimum at large values of r.

For dissociating H_2, for example, at T = 17,000K, I calculated the surface of section and the kinetic energy distribution for the initial conditions r = 3.3 a.u., p_r = 0.0 a.u. and Q = 30. The result is shown in Fig. 3.23. Figure 3.23a is quite similar to Fig. 3.11a, which means that including rotation thermalizes the H_2 dynamics in the strong-coupling region, but it cannot thermalize the separated H + H dynamics. As discussed in §3.4.2, it is unnecessary to thermalize the separated H + H to calculate the rate of H_2 dissociation. Figure 3.23b shows that the upper bound of E_k' is around 2.0 (corresponding to 2.92 eV), which is lower than that in Fig. 3.11b. This indicates that rotation contributes to dissociation. Due to the rotation contribution, the kinetic energy needed in the dissociation is not as high as that when rotation is excluded.

§3.5.5 Calculation of the Lifetime Distribution for H_2 Dissociation Including Rotation

To examine whether the inclusion of rotation causes the Nosé-Hoover dynamics to be more ergodic, I calculated the distribution of dissociation times. Again, to ensure H—H separation, I defined r > 10 as the separated distance during the calculation. I chose the first 500 (r, p_r) values from the surface of section points at T = 4000K, Q_1 = 30 with the

initial conditions r = 3.3 a.u. and p_r = 0.0 a.u. (as seen in Fig. 3.19a).

The calculated lifetime distribution for T = 17,000K is shown in Fig. 3.24. In the figure, the bars show the number of dissociated H_2 corresponding to the time range. For example, the first bar shows that there are about 315 H_2 dissociated at 0 to 10000 a.u., *etc.* The solid curve on the plot shows a purely exponential decay. As calculated in Subsection §3.4.3, the exponential decay numbers are 303, 111, 41, *etc.*, corresponding to the middle values of the dissociation time range.

As seen in Fig. 3.24, the histogram is approximately exponential. Comparing Fig. 3.24 with Fig. 3.12, whose dissociation times were calculated excluding rotation, it can be seen that although Fig. 3.24 shows that there are more H_2 molecules which dissociate at the shortest time (refer to the first bar), a long-time tail still exists at long times, as expected from the existence of boundaries in resonance zones. I therefore conclude that although the inclusion of rotation can cause the Nosé-Hoover dynamics to be more chaotic, it cannot cause the Nosé-Hoover dynamics to be more ergodic.

In addition, of the 500 trajectories considered in this subsection, 436 dissociated. Compared with 400 dissociated trajectories observed in Subsection §3.4.3, the number of the dissociated trajectories increased significantly. I infer that the inclusion of rotation in the Nosé-Hoover equations of motion is effective in promoting the dissociation of diatomics.

§3.5.6 Calculation of Rate Constants and Activation Energy for H_2 Dissociation Including Rotation

As stated in Subsection §3.4.3, the negative slope of the line which is plotted as the logarithm of number of dissociated H_2 versus dissociation time at a fixed temperature is equal to the pseudo-unimolecular rate constant for H_2 dissociation at that temperature. To avoid the long-time tail effect in the lifetime distribution, I again used the prescription introduced in Subsection §3.4.4 to calculate the dissociation rate constant from the initial parts of the lifetime distribution. I considered the first five numbers of dissociated H_2 (*i.e.*, the first five bars in the histogram) up to the dissociation time in Fig. 3.24. From a least-squares fit to the logarithm of the number versus time, I found $k_d = 4.88 \pm 0.44 \times 10^{12}$ sec^{-1} for T = 17,000K (shown in Fig. 3.25). Similarly, for T = 16000, 18000, 19000, 20000K, I found $k_d = 3.55 \pm 0.83 \times 10^{12}$ sec^{-1}, $5.41 \pm 0.41 \times 10^{12}$ sec^{-1}, $5.58 \pm 0.53 \times 10^{12}$ sec^{-1} and $5.90 \pm 0.28 \times 10^{12}$ sec^{-1}, respectively.

From an Arrhenius plot of a least-squares fit to the logarithm of the pseudo-unimolecular rate constants versus 1/T (see Fig. 3.26), the classical activation energy is found to be 3.27 ± 0.77 eV. This value minus zero-point energy of 0.27 eV[13.23], leads to an activation energy $E_a = 3.0 \pm 0.77$ eV in the temperature range 16,000 - 20,000K. This predicted activation energy is about 16% lower than that of non-rotating H_2 in Subsection §3.4.4. Consequently, I conclude that rotation is indeed effective in promoting H_2 dissociation.

§3.5.7 Discussion

I have shown that the Nosé-Hoover equations of motion including rotation, as well as excluding rotation, can thermalize the H_2 dynamics only when the phase space dynamics is chaotic. Moreover, the inclusion of rotation can cause the phase space dynamics to be a little more chaotic than the rotation exclusion approach. I have also calculated pseudo-unimolecular rate constants for H_2 dissociation and predicted the activation energy of H_2 dissociation. The conclusions are as follows:

(1) With regard to the problem of the long-time tail, I have proved that the inclusion of rotation cannot cause the Nosé-Hoover dynamics to be more ergodic. However, I have shown that including rotation in the Nosé-Hoover equation approach can cause the phase space dynamics of H_2 to be a little more chaotic.

(2) I have shown that the inclusion of the rotation in the Nosé-Hoover equations of motion is effective in promoting the dissociation of diatomics. In Table 3-2, I list rate constants with and without rotation at three different temperatures.

As seen in Table 3-2, all the rate constants which include H_2 rotation are larger than those without including H_2 rotation, but the percentage of increase drops as the temperature increases. This means that the rate constant does not increase as rapidly as the temperature increases. As discussed by Pritchard[3.8], the effective rotational barrier, $U_{max}(J_i)$, which the molecule has to overcome in order to dissociate, increases with temperature. Therefore, at high temperature, rate constant does not increase as rapidly as that at low temperature. However, at higher temperature, there are more molecules populating the higher rotational

energy states, so the Arrhenius activation energy is lowered. In my calculation, the result shows that the Arrhenius activation energy for H_2 dissociation is 16% lower when H_2 rotation is considered.

(3) The pseudo-unimolecular rate constants should be insensitive to the value of Q_2. The reason is that the value of Q_2 itself is very large so that the rotation term in Eq. (3.30) contributes very little to the frequency of this auxiliary equation. Thus, most of the increase in k_d is due to the $2R_c^2kT/r^3$ term in Eq. (3.29).

On the other hand, the rotation term in Eq. (3.30) couples the r and s variables through the $p_s p_r$ term, and for large values of Q_2, introduces a low-frequency component in the s variable, which should increase the ergodicity of the Nosé-Hoover dynamics. However, although this term greatly affects trajectories in the irregular regions of the phase space, trajectories in the regular regions are only slightly affected and the resonance zones remain essentially unchanged. Therefore, the inclusion of rotation can only cause the Nosé-Hoover dynamics to be more chaotic, but it does not cause the Nosé-Hoover dynamics to be significantly more ergodic.

Chapter 4

Modified Nosé-Hoover Equation Approach to Thermal Dissociation of Diatomics in an Inert Gas

In Chapter 3, I have used the Nosé-Hoover equations of motion with and without rotational modification to calculate the thermal dissociation of a homonuclear diatomic molecule, H_2, in an inert gas. The Nosé-Hoover equation approach can adequately thermalize a multidimensional system with a large number of particles. However, it is known[14,11] that for many one-dimensional potentials, such as that for a diatomic molecule, H_2, the phase space dynamics is not sufficiently chaotic for a fully statistical description. The reason is that the Nosé-Hoover equation approach is actually a forced one-degree-of-freedom system, and the parameter Q, which is associated with the bath degree of freedom, can only be chosen in a certain range.

To improve this shortcoming, Hamilton[14,21] modified the original Nosé-Hoover scheme by enforcing the virial theorem, and the resulting phase space dynamics is much more chaotic. I call the modification the modified Nosé-Hoover equations of motion. The modified Nosé-Hoover equations of motion thermalize explicitly both the kinetic energy and the virial of the physical system.

In this chapter, I have applied the modified Nosé-Hoover equations of motion to the thermal dissociation of both homonuclear and heteronuclear diatomic molecules in an inert gas. I chose H_2 as an example of a homonuclear diatomic and HCl as an example of a

heteronuclear diatomic. As assumed in Chapter 3, the inert gas can be any molecule as long as it only acts as a heat bath. Again, I approximated the thermal dissociation of diatomics as a pseudo-unimolecular reaction. In this chapter, I neglected the rotational motion of the molecule.

The purpose of this work was threefold. First, I wished to show that the modified Nosé-Hoover equations of motion can cause the phase space dynamics to be more chaotic than without the modification. Secondly, I calculated the activation energy of the H_2 dissociation to see if the value is closer to the experimental value. Thirdly, I calculated the activation energy of the HCl dissociation to see if the modified Nosé-Hoover equation approach could also be applied to a heteronuclear diatomic pseudo-unimolecular reaction.

§4.1 Modified Nosé-Hoover Equations of Motion for a Diatomic Molecule

For a diatomic molecule, the modified Nosé-Hoover equations of motion[14,21] introduced in Subsection §2.3.2 are:

$$\dot{r} = \frac{p_r}{\mu} + s\,(r - R_e)\ , \qquad (4.1)$$

$$\dot{s} = -(2\,T_v - k\,T)/Q_1\ , \qquad (4.2)$$

$$\dot{p}_r = -\frac{dV(r)}{dr} - p_s\,p_r\ , \qquad (4.3)$$

$$\dot{p}_s = (2\,E_k - k\,T)/Q_2\ , \qquad (4.4)$$

where the virial term and the kinetic energy term are

$$T_v = \frac{1}{2}\,(r - R_e)\,\frac{dV(r)}{dr}\ ,\quad E_k = \frac{p_r^2}{2\mu}\ , \qquad (4.5)$$

respectively, the parameter μ is the reduced mass, and the parameter R_e is the equilibrium bond distance of the diatomic.

The modified Nosé-Hoover equations of motion are still deterministic and time reversible, which are the key aspects of the Nosé-Hoover equation approach. Similar to the original Nosé-Hoover equations of motion, the modified Nosé-Hoover equations of motion can correctly thermalize the oscillator dynamics only if the phase space dynamics is chaotic.

The idea of this modification is based on the virial theorem[4.3] which states that the time averages of the virial term T_v and the kinetic energy term E_k are equal. In this set of equations, the p_r and p_s variables are coupled via the $p_s p_r$ term just as they are in the original Nosé-Hoover equations of motion. The variables r and s are coupled via the $p_s p_r$ term indirectly, and also via the s (r-R_e) term in Eq. (4.1). When T_v is greater than half of kT, s is decreasing and r is decreasing, too; when T_v is smaller than half of kT, s is increasing

and r is increasing as well. The time development of the variable r depends on the variable s. Both s and r variables fluctuate and, on average, both of them are equal to constants. There is no direct relationship between the variables s and p_s in the modified Nosé-Hoover equations of motion. Instead, the s and p_s variables are coupled through the r and p_r variables.

The modified Nosé-Hoover equations of motion include two auxiliary equations, Eq. (4.2) and Eq. (4.4), with two free parameters, Q_1 and Q_2. With $Q_1 = Q_2$, the frequencies of the s and p_s variables are equal. It has been shown by Hamilton[4.2] that for an anharmonic oscillator, the phase space dynamics is chaotic for both $Q_1 = Q_2$ and $Q_1 \neq Q_2$; but for a harmonic oscillator, it is difficult for the modified Nosé-Hoover equations of motion with $Q_1 = Q_2$ to cause the phase space dynamics to be chaotic.

§4.2 Thermal Dissociation of H_2 in an Inert Gas

As in Section §3.4, I again chose the potential energy function to be the Morse potential function (shown in Eq. 3.10). The parameters are also the same as those used in Section §3.4, *i.e.*, $D_e = 4.7466$ eV, $\alpha = 1.04435$ a.u.$^{-1}$, and $R_e = 1.40083$ a.u.[4.4] The zero-point energy for H_2 is 0.27 eV[4.5]. The reduced mass μ is equal to 918.5822 a.u.

§4.2.1 Choices of the Parameters Q_1 and Q_2

The modified Nosé-Hoover equations of motion can thermalize the H_2 dynamics only if the phase-space dynamics is chaotic. To ensure this, I considered the choices of the parameters Q_1 and Q_2 in the modified Nosé-Hoover equations of motion. I constructed a series of two-dimensional r—p_r surfaces of section by plotting points (r, p_r) with the same initial conditions but different values of Q_1 and Q_2 when p_s passed through zero. I also plotted the kinetic energy distributions corresponding to those surfaces of section. I then selected the values of Q_1 and Q_2 for which the surface of section was most chaotic and the corresponding kinetic energy distribution was closest to the exact Boltzmann distribution with the largest probability for kinetic energy close to the dissociation energy of H_2.

As in Chapter 3, the temperature was chosen to be 4000K (corresponding to 0.34 eV), where the dissociation events are comparatively rare: for simplicity, the initial conditions s and p_s were again chosen to be 1.0 and 0.0, respectively; and the initial conditions r and p_r were chosen to be 3.3 a.u. and 0.0 a.u., respectively. Figures 4.1, 4.2, 4.3, 4.4, 4.5, 4.6 and 4.7 show the r—p_r surfaces of section and the kinetic energy distributions normalized to 4000K, for trajectories with the same initial conditions but different values of the parameters Q_1 and Q_2. Among these, Figs. 4.1, 4.2, 4.3, 4.4 and 4.5 show situations for which the parameters Q_1 and Q_2 are both equal to 15, 25, 35, 45 and 55, respectively. Figure 4.6 shows the situation for which $Q_1 = 15$ and $Q_2 = 55$; and Fig. 4.7 shows the situation for which $Q_1 = 55$ and $Q_2 = 15$.

As seen in the (a) figures, all the surfaces of section are primarily chaotic no matter

whether $Q_1 = Q_2$ or $Q_1 \neq Q_2$. Although there are some blank areas near $p_r = \pm 3$, the boundaries for the blank areas are not clear, especially compared to the plots in Chapter 3 (see Figs. 3.1a through 3.7a). This indicates that the modified Nosé-Hoover equations of motion cause the phase space dynamics to be more chaotic than the original Nosé-Hoover equations of motion do. The existence of blank areas on surfaces of section is due to the insufficient thermalization of H_2 dynamics.

As seen in the (b) figures, the kinetic energy distribution normalized to 4000K in each histogram is close to the exact Boltzmann distribution (shown as a solid curve in each (b) figure), which means that the H_2 dynamics is primarily thermalized in all these cases. Figures 4.3b, 4.5b and 4.6b show their distributions with relatively larger probabilities for E_x' at high value, *e.g.*, $E_x' = 5$, than Figs. 4.1b, 4.2b, 4.4b and 4.7b. The hydrogen molecule dissociates easily if it possesses a large probability of being at a high kinetic energy. On the other hand, the blank areas at $p_r = \pm 3$ in Fig. 4.5a and at $r = 1.7$, $p_r = \pm 3$ in Fig. 4.6a are clearer than those in Fig. 4.3a. Therefore, I chose the optimum values of the parameters Q_1 and Q_2 for this case: $Q_1 = Q_2 = 35$.

To compare with the choice of $Q_1 = Q_2 = 35$, I now show two extreme cases with very small and very large values of Q_1 and Q_2, $Q_1 = Q_2 = 3.5$ and $Q_1 = Q_2 = 700$, respectively. I constructed two-dimensional r—p_r surfaces of section by plotting points (r, p_r) with the same initial conditions except for Q_1 and Q_2 as those in Fig. 4.3 when p_r passed through zero. I also plotted the kinetic energy distributions corresponding to the surfaces of section. The results are shown in Figs. 4.8 and 4.9, respectively.

I first consider the case with $Q_1 = Q_2 = 3.5$. Comparing Fig. 4.8 with Fig. 4.3, it

can be seen that the surface of section in Fig. 4.8a is as chaotic as that in Fig. 4.3a, but it seems to be divided into three parts, top, middle and bottom: the corresponding kinetic energy distribution normalized to 4000K is close to the exact Boltzmann distribution. This indicates that the modified Nosé-Hoover equations of motion can thermalize the H_2 dynamics at very small values of Q_1 and Q_2 although the low-order resonance zones are becoming clearer. The reason is that when the values of Q_1 and Q_2 are very small, the frequencies of the s and p_s variables become very large. The $s\,(r - R_e)$ term in Eq. (4.1) and the $p_s p_r$ term in Eq. (4.3) are dominant. However, the p_r/μ in Eq. (4.1) and the $dV(r)/dr$ term in Eq. (4.3) are still affected because of the coupling between the r and p_r variables. Overall, all four equations (Eqs. (4.1) through (4.4)) are affected. Consequently, there is no major difference between the choices of the very small values and the chosen values of Q_1 and Q_2, as shown by the surface of section and the kinetic energy distribution.

Next, I consider the case with very large values of Q_1 and Q_2. As seen in Fig. 4.9, the whole surface of section looks chaotic, and although the (r, p_r) points tend to lie on a curve, the boundary of the curve is not very clear. The corresponding kinetic energy distribution normalized to 4000K is close to the Boltzmann distribution except that the second bar is a little lower than the Boltzmann distribution. The result shown in Fig. 4.9 indicates that the modified Nosé-Hoover equations of motion can also thermalize the H_2 dynamics at very large values of Q_1 and Q_2. The reason is that when the values of Q_1 and Q_2 are very large, the frequencies of the s and p_s variables are close to zero at the beginning of the integration. Thus, only Eqs. (4.1) and (4.3) are affected. Since the energy of the extended system is constant, the variable p_r can be considered to be a function of the variable r.

Therefore, there is a tendency for (r, p_r) points lying on a curve on the r—p_r surface of section. However, as stated previously, there are couplings between the variables r and s, and between the variables p_r and p_s. Thus, as the variables r and p_r change, Eqs. (4.2) and (4.4) would eventually be affected during the calculation, the r and p_r function under the constant energy condition would be eliminated, and eventually the trajectory will cover the whole surface of section.

To explore the Q_1 and Q_2 dependence further, I also considered two extreme cases where $Q_1 \neq Q_2$. I chose: (1) $Q_1 = 3.5$, $Q_2 = 700$, and (2) $Q_1 = 700$, $Q_2 = 3.5$. I constructed two-dimensional r—p_r surfaces of section by plotting points (r, p_r) with the same initial conditions otherwise as those in Fig. 4.3 when p_s passed through zero. I also plotted the kinetic energy distributions corresponding to the surfaces of section. The results are shown in Figs. 4.10 and 4.11, respectively.

Comparing Fig. 4.10a with Fig. 4.11a, the (r, p_r) points are more dense in Fig. 4.11a. The reason is that when Q_1 is very large and Q_2 is very small, the frequency of the s variable is close to zero while the frequency of the p_s variable becomes very large. The $p_s p_r$ term in Eq. (4.3) is dominant and the frequency of the p_r variable is very large. The large frequency of the p_r variable, $\dot{p}_r$, will affect the frequency of the r variable, $\dot{r}$, by p_r/μ term and eventually the frequency of the s variable, $\dot{s}$, because of the coupling between the r and s variables. Overall, all four equations (Eqs. (4.1) through (4.4)) are affected.

On the contrary, when Q_1 is very small and Q_2 is very large (as seen in Fig. 4.10a), the frequency of the s variable becomes very large while the frequency of the p_s variable is close to zero. The s $(r - R_e)$ term in Eq. (4.1) is dominant and the frequency of the r

variable is very large. Although the large frequency of the r variable, $\dot{r}$, will affect the frequency of the p_r variable, $\dot{p}_r$, by dV(r)/dr term, the variable r changes rapidly, and thus there are fewer (r, p_r) points in the strong coupling region.

Combining all the cases observed in this subsection, I conclude that the modified Nosé-Hoover equations of motion cause the phase space dynamics to be more chaotic than the original Nosé-Hoover equations of motion do, and the modified Nosé-Hoover equations of motion can thermalize the H_2 dynamics over a wide range of values of Q_1 and Q_2.

§4.2.2 Uniform Thermalization of Non-dissociating H_2 Dynamics

Since the boundaries for the blank areas on the surfaces of section are not as clear as those in Chapter 3, I note that the modified Nosé-Hoover equation approach causes the phase space dynamics of H_2 to be more chaotic than the original Nosé-Hoover equation approach. To explore further, I considered the cases at other initial conditions.

I first changed the initial conditions to r = 1.5 a.u. and p_r = 0.0 a.u. and kept other conditions the same as those in Fig. 4.3, where the initial condition of the interatomic distance is larger than the H_2 equilibrium bond distance (the H_2 equilibrium bond distance R_e = 1.40083 a.u.). The initial condition of the interatomic distance, r = 1.5 a.u., is close to the H_2 equilibrium bond distance. The results are shown in Fig. 4.12.

Comparing Fig. 4.12 and Fig. 4.3, it can be seen that the surface of section is chaotic and the kinetic energy distribution normalized to 4000K is close to the Boltzmann distribution

(shown as a solid curve) in Fig. 4.12, as well as in Fig. 4.3. This indicates that the H_2 dynamics is thermalized for the initial value of r close to the H—H equilibrium bond distance. However, this is not the case in Chapter 3, where the surface of section is regular and the kinetic energy distribution shows deviation from the Boltzmann distribution for the initial value of r close to the H—H equilibrium bond distance, as seen in Fig. 3.10.

I then chose the initial conditions to be r = 1.3 a.u. and p_r = 0.0 a.u. and kept other conditions the same as those in Fig. 4.3. The initial condition of the interatomic distance, r = 1.3, is smaller than the H_2 equilibrium bond distance. The results are shown in Fig. 4.13, which shows that the surface of section is also chaotic and the kinetic energy distribution is also close to a Boltzmann distribution. This indicates that the H_2 dynamics is also thermalized for the initial value of r smaller than the H—H equilibrium bond distance.

Comparing Figs. 4.3a, 4.12a and 4.13a, the surfaces of section appear different although all of them are chaotic. This is due to sensitivity to the initial conditions, which is unique characteristic of chaotic dynamics. The slight difference in initial conditions, for example, in r, results in totally different trajectories so that the surfaces of section shown in Figs. 4.3a, 4.12a and 4.13a are different.

For $Q_1 \neq Q_2$, I tested the initial conditions: (1) r = 1.5 a.u., p_r = 0.0 a.u., and (2) r = 1.3 a.u., p_r = 0.0 a.u., respectively, while the other conditions were kept the same as those in Fig. 4.6. The results are shown in Figs. 4.14 and 4.15, respectively. As seen, the surfaces of section are chaotic and the kinetic energy distributions are close to a Boltzmann distribution in both Figs. 4.14 and 4.15, just as observed in Fig. 4.6. These results indicate that in the case $Q_1 \neq Q_2$, the H_2 dynamics can be thermalized for the initial values of r close

to and smaller than the H—H equilibrium bond distance, as well as for the initial value of r larger than the H—H equilibrium bond distance.

Summarizing all above cases, the H_2 dynamics was observed to be thermalized for different initial conditions, no matter $Q_1 = Q_2$ or $Q_1 \neq Q_2$. Therefore, I infer that the modified Nosé-Hoover equations of motion thermalize non-dissociating H_2 dynamics uniformly.

§4.2.3 Calculation of the Lifetime Distribution for H_2 Dissociation Using Modified Nosé-Hoover Equations of Motion

To compare the lifetime distribution in the present case with those in Chapter 3, I next determined the lifetime distribution calculated with the modified Nosé-Hoover equations of motion. I chose the first 500 (r, p_r) values from the surface of section points at T = 4000K with the initial conditions $r = 3.3$ and $p_r = 0.0$, as seen in Fig. 4.3a.

The calculated lifetime distribution for T = 7250K is shown in Fig. 4.16. In this figure, the bars show the number of dissociated H_2 corresponding to time ranges. For example, the first bar shows that there are about 150 H_2 dissociated at 0 to 10000 a.u., *etc.* Comparing the histogram in Fig. 4.16 to those in Figs. 3.12 and 3.24, the decay shown in Fig. 4.16 is apparently slower, for example, Fig. 4.16 shows that there are about 150 H_2 dissociated at 0 to 10000 a.u. time range, while Figs 3.12 and 3.24 show that there are about 260 and 315 H_2 dissociated, respectively, in the same time range. Therefore, I used another exponential to fit the histogram in Fig. 4.16: $N_{diss} = 150 \times \exp(-0.3\ t')$, where t' was

chosen to be the middle value of dissociation time at each bar, *i.e.*, t' = 0.5, 1.5, 2.5, 3.5, *etc.* (see App. C for formula derivation). Thus, the exponential dissociated numbers are 129, 96, 71, 52, 39, 29, *etc.*, corresponding to the middle values of the dissociation time ranges. These numbers corresponding to middle values of t' were linked together to be the solid curve shown in Fig. 4.16.

As seen in Fig. 4.16, the dissociation decay is approximately as fast as exponential, and there no long time tail exists. Also, of the 500 trajectories considered, 496 dissociated, which indicates that almost no trajectories are trapped in resonance zones. On the contrary, there is a long time tail in the lifetime distributions in Chapter 3, as seen in Figs. 3.12 and 3.24, and a fair fraction of trajectories is trapped in resonance zones. These differences show that the modified Nosé-Hoover equations of motion thermalize the H_2 dynamics more efficiently than without the modification. The reason that the decay shown in Fig. 4.16 is slower than those in Figs. 3.12 and 3.24 is due to the lower temperature used.

§4.2.4 Calculation of Rate Constants and Activation Energy for H_2 Dissociation Using Modified Nosé-Hoover Equations of Motion

I calculated the pseudo-unimolecular rate constant of H_2 dissociation from the lifetime distribution. To avoid the possible non-exponential effect at longer times, I again used the prescription of calculating the dissociation rate constant from the initial parts of the lifetime distribution. I considered the first five numbers of dissociated H_2 (*i.e.*, the first five bars in the histogram) up to the dissociation time in Fig. 4.16. From a least-squares fit to the

logarithm of the number versus time, the negative slope of the line is equal to the dissociation rate constant at the temperature 7250K (shown in Fig. 4.17). The calculated rate constants at different temperatures are summarized in Table 4-1.

As seen in Table 4-1, there is an aberration (k_f is larger for T = 8750K than for 9000K). The reason for the aberration is that the dissociation decay is fast at high temperature so that number of dissociated H_2 is large at short times, but very small even at intermediate times. These small dissociation numbers may cause a non-exponential effect in the prescription used for calculating the dissociation rate constant so that a relatively big uncertainty is involved. As seen in the table, the uncertainty is larger at high temperatures than that at low temperatures. However, despite the aberration, as expected, the pseudo-unimolecular rate constant increases rapidly as the temperature increases.

From an Arrhenius plot of a least-squares fit to the logarithm of the pseudo-unimolecular rate constants versus 1/T (shown in Fig. 4.18), I obtained the classical activation energy of 4.05 ± 0.33 eV. Correcting for the zero-point energy of H_2, 0.27 eV[4.5], I obtain an activation energy for H_2 dissociation of 3.78 ± 0.33 eV in the temperature range 7250—9500K. This predicted value is very close to the experimental value, 3.86 eV, which was measured by Breshears and Bird[4.6].

§4.2.5 Effect of the Parameters Q_1 and Q_2 on the Activation Energy of H_2 Dissociation

The predicted activation energy for H_2 dissociation of E_a = 3.78 ± 0.33 eV in Subsection §4.2.4 is calculated using parameters $Q_1 = Q_2 = 35$. In order to investigate the effect of the parameters Q_1 and Q_2 on the activation energy of the H_2 dissociation, I calculated the activation energy at very small and very large values of Q_1 and Q_2 in this subsection. I selected $Q_1 = Q_2$ for all the cases considered here. I abbreviate Q_1 and Q_2 as Q in the current subsection.

I first calculated the pseudo-unimolecular rate constants of H_2 dissociation at different values of Q and obtained the corresponding classical activation energies. Subtracting the zero-point energy from the classical activation energies, I obtained the predicted activation energies, which are listed in Table 4-2 for different values of Q.

It can be seen that there is no significant difference for the values of the activation energy in the range of Q from 30 to 40 if the uncertainties are considered; the deviations become big when the values of Q are fairly small or fairly large. At the small value of Q, the frequencies of the s and p_s variables are high. The couplings between r and s variables and between p_r and p_s variables are strong. The s (r - R_e) term in Eq. (4.1) and the $p_s p_r$ term in Eq. (4.3) are dominant and act as constraints. The calculated activation energy is high.

For a large value of Q, the frequencies of the s and p_s variables are low. The s (r - R_e) term in Eq. (4.1) and the $p_s p_r$ term in Eq. (4.3) have little effect. The modified Nosé-Hoover equations of motion are reduced to the Hamiltonian equations of motion. Under the

constant energy condition of the Newtonian system, all the kinetic energy of the H_2 molecule can be converted into the potential energy when the two hydrogen atoms separate, *i.e.*, the kinetic energy is efficiently used. The calculated activation energy is therefore low.

At more extreme values of Q, for example, Q = 350, there are so many aberrations of the calculated pseudo-unimolecular rate constant versus temperature that the activation energy for H_2 dissociation cannot be obtained.

§4.2.6 Discussion

I have demonstrated that the modified Nosé-Hoover equation approach thermalizes the H_2 dynamics more uniformly, and causes the phase space dynamics to be more chaotic than the original Nosé-Hoover equation approach does. I have also calculated the pseudo-unimolecular rate constants and predicted the activation energy of H_2 dissociation. The conclusions are as follows:

(1) The modified Nosé-Hoover equation approach thermalizes the H_2 dynamics more uniformly, and causes the phase space dynamics to be more chaotic than the original Nosé-Hoover equation approach does.

(2) The dissociation decay in the lifetime distribution for H_2 dissociation calculated with the modified Nosé-Hoover equations of motion approximately obeys exponential behaviour. The long time tail is eliminated.

(3) The modified Nosé-Hoover equations of motion can thermalize the phase space dynamics over a wide range of values of Q_1 and Q_2.

(4) The calculated activation energy of the H_2 dissociation is not sensitive to the particular choices of Q_1 and Q_2 in the range 30—40. However, with a very small or very large values of Q_1 and Q_2, the result is affected. The calculated activation energy decreases as the values of Q_1 and Q_2 increase.

(5) In Table 4-3, I have compared my calculated values of the activation energy for H_2 dissociation with the result of Breshears and Bird[4.6] and with the prediction of Teitelbaum[4.7], respectively. Compared to the value of the activation energy calculated by the original Nosé-Hoover equation approach, the modified Nosé-Hoover equation result is closer to both the experimental and the theoretical values. The temperature range chosen for the modified Nosé-Hoover equations of motion was much lower than that chosen for the original Nosé-Hoover equations of motion. The former range is comparable to the temperature range used in the experiment, but high enough to be considered as infinitely large to match the theoretical prediction carried out for $T \rightarrow \infty$.

(6) The reason that I could choose a reasonable temperature range for the modified Nosé-Hoover equations of motion is that the modified Nosé-Hoover equations of motion can thermalize the H_2 dynamics efficiently due to the two free parameters, Q_1 and Q_2, introduced, and thus a typical dissociation time is short enough to obtain an accurate numerical integration of the equations of motion even at relatively low temperature.

§4.3 Thermal Dissociation of HCl in an Inert Gas

In this section, I applied the modified Nosé-Hoover equations of motion to the thermal dissociation of a heteronuclear diatomic molecule, HCl, in an inert gas. I again chose the Morse potential function (shown in Eq. (3.10)) to describe the potential energy of the H—Cl. For the HCl molecule, the Morse parameters are D_e = 4.613 eV, α = 0.9868964 a.u.$^{-1}$, and R_e = 2.414 a.u.[4.51] The zero-point energy for HCl is 0.19 eV[4.51]. The reduced mass μ is equal to 1786.3544 a.u.

§4.3.1 Choices of the Parameters Q_1 and Q_2

To calculate HCl dissociation, I first considered the choices of the parameters Q_1 and Q_2 in the modified Nosé-Hoover equations of motion. To choose reasonable values of the parameters Q_1 and Q_2, I constructed a series of two-dimensional r—p_r surfaces of section by plotting points (r, p_r) with the same initial conditions but different values of Q_1 and Q_2 when p_s passed through zero. I also plotted the kinetic energy distributions corresponding to those surfaces of section. I then selected the values of Q_1 and Q_2 for which the surface of section is most chaotic and the corresponding kinetic energy distribution is closest to the exact Boltzmann distribution with the largest probability for kinetic energy close to the dissociation energy of HCl.

As previously, the temperature was chosen to be 4000K (corresponding to 0.34 eV), where dissociation events of HCl are comparatively rare; for simplicity, the initial

conditions of s and p_s were still chosen to be 1.0 and 0.0, respectively; and the initial conditions r and p_r were chosen to be 2.6 a.u. and 0.0 a.u., respectively. Figures 4.19, 4.20, 4.21 and 4.22 show the results with $Q_1 = Q_2 = 10$, $Q_1 = Q_2 = 20$, $Q_1 = Q_2 = 30$, $Q_1 = Q_2 = 40$, respectively. Figure 4.23 shows the results with $Q_1 = 10$ and $Q_2 = 40$. Figure 4.24 shows the results with $Q_1 = 40$ and $Q_2 = 10$.

Comparing Figs. 4.19a through 4.24a, although there are some blank areas at around $r = 2.5$ and $p_r = \pm 5$ due to the insufficient thermalization of HCl dynamics, the boundaries are very unclear and overall, the surfaces of section look chaotic. As seen in the (b) figures, the kinetic energy distribution normalized to 4000K is close to the exact Boltzmann distribution (shown as a solid curve in each (b) figure), which indicates that the HCl dynamics is primarily thermalized in all cases.

Comparing the probabilities of E_k' in the (b) figures, Figs. 4.20b, 4.23b and 4.24b show their distributions with larger probabilities at $E_k' = 5$ than Figs. 4.19b, 4.21b and 4.22b, which means that HCl dissociation is easier. Moreover, Fig. 4.20b has a smaller probability at $E_k' = 1$ than Figs. 4.23b and 4.24b, *i.e.*, there is smaller probability for low kinetic energy. Therefore, I chose the optimum values of the parameters $Q_1 = Q_2 = 20.0$ in this case.

§4.3.2 Calculation of Rate Constants and Activation Energy for HCl Dissociation Using Modified Nosé-Hoover Equations of Motion

In order to calculate the pseudo-unimolecular rate constants for HCl dissociation, I used the same procedure as before. I first calculated the lifetime distribution. I again chose the first 500 (r, p_r) values from the surface of section points at T = 4000K with initial conditions r = 2.6 a.u. and p_r = 0.0 a.u. (as seen in Fig. 4.20a). The calculated lifetime distribution for T = 7250K is shown in Fig. 4.25. The solid curve shows a purely exponential decay. Here, I used $N_{diss} = 250 \exp(-t'/2)$ to fit the histogram in Fig. 4.25 (see Appendix C for N_{diss} formula). It may be seen that the decay is approximately exponential and, of the 500 trajectories considered, all of them have dissociated.

I then calculated the pseudo-unimolecular dissociation rate constant from the lifetime distribution. To avoid the possible non-exponential effect at longer times, I again used the prescription of calculating the dissociation rate constant from the initial parts of the lifetime distribution. I considered the first five numbers of dissociated HCl (*i.e.*, the first five bars in the histogram) up to the dissociation time in Fig. 4.25. From a least-squares fit to the logarithm of number versus time, the negative slope of the line is equal to the HCl dissociation rate constant at the temperature of 7250K (shown in Fig. 4.26). The calculated rate constants at different temperatures are summarized in Table 4-4. As seen in the table, the pseudo-unimolecular rate constant increases rapidly with increasing temperature in the range 6750—9500K, as expected. The rate constant at T = 10000K remains almost unchanged, compared to that at T = 9500K. This is due to the rotation effect, as discussed

in §3.1. The effective rotational barrier, $U_{max}(J_t)$, which the molecule has to overcome in order to dissociate, increases with temperature. Therefore, at high temperature, the rate constant does not increase as rapidly as that at low temperature.

From an Arrhenius plot of a least squares fit to the logarithm of the pseudo-unimolecular rate constants versus 1/T (shown in Fig. 4.27), I obtained the classical activation energy 4.08 ± 0.23 eV. Subtracting the zero-point energy of HCl, which is 0.19 eV[14,51], I found the activation energy of HCl dissociation to be E_a = 3.89 ± 0.23 eV in the temperature range 6750—10,000K. This predicted value is very close to the experimental value of 3.59 eV measured by Breshears and Bird[14,91], and it is lower than the spectroscopic dissociation energy of HCl, which is 4.42 eV.

§4.3.3 Discussion

In Section §4.3, I have applied the modified Nosé-Hoover equations of motion to the thermal dissociation of a heteronuclear diatomic molecule, HCl, in an inert gas. I have calculated the pseudo-unimolecular rate constants of HCl dissociation, and also have predicted the activation energy of HCl dissociation. The conclusions are as follows:

(1) The modified Nosé-Hoover equations of motion can thermalize a heteronuclear diatomic molecule, HCl, as well as a homonuclear diatomic molecule.

(2) The dissociation decay in the lifetime distribution for HCl dissociation calculated with the modified Nosé-Hoover equations of motion is approximately exponential. There is no long time tail.

(3) In Table 4-5, I have listed the experimental results and the theoretical predictions of the activation energy for HCl dissociation from different sources.

As seen in the table, my calculated value of the activation energy for HCl dissociation is a little high but close to two of the three sets of shock tube results and the other theoretical prediction. The activation energy measured by Jacobs and co-workers is low, compared to the other two experimental values. The reason for this is that their activation energy was actually an estimated value from their rate constant expression which was not written in an Arrhenius form.

In addition, the temperature range used in my calculation is comparable to that observed experimentally, especially to that observed by Breshears and Bird. It indicates that the modified Nosé-Hoover equation can be confidently applied to a heteronuclear diatomic dissociation reaction.

(4) In Table 4-6, I have compared the experimental results and my calculated values of the activation energies for H_2 and HCl dissociation. The experimental results show that the activation energy of HCl dissociation is significantly lower than that of H_2 dissociation. My results calculated using the modified Nosé-Hoover equations of motion are almost the same if the uncertainties are considered. However, the discrepancy between theory and experiment is greater for HCl than for H_2. This is probably due to the interactions between the HCl and inert gas molecules being ignored during the calculation of HCl dissociation. The HCl molecule is strongly polar so that its long-range interactions are significant and should not be ignored. In the case of the non-polar H_2 molecule, however, the interactions between the H_2 and inert gas molecules are weak enough to be ignored.

Chapter 5

The Nosé-Hoover Equation Approach to Thermal Desorption of Atoms from a Surface

In previous chapters, I studied the thermal dissociation of diatomics, H_2 and HCl, in an inert gas, using the Nosé-Hoover equation approach and the modified Nosé-Hoover equation approach. I calculated the activation energies of thermal dissociation for both molecules, and found them to be quite close to the experimental values. In this chapter, I have extended my work to the reaction between atoms and a solid surface. The purpose of this work is to see if the Nosé-Hoover equations of motion can correctly thermalize atom/surface dynamics and provide reasonable results for the thermal desorption of atoms from a surface.

§5.1 Introduction

A plane that separates two phases is known as a *surface* or an *interface*[5.11]. Surfaces show special properties that are different from those of the phases themselves. For example, the surface of a solid often shows a strong affinity for molecules that come into contact with it, or become *adsorbed* onto it. The accumulation of particles at a surface is called *adsorption*. The substance that adsorbs is the *adsorbate*. The underlying material is the *adsorbent* or *substrate*. The reverse of adsorption is *desorption*. Basically, adsorption can

be classified as *physisorption* or *chemisorption*. Chemical reactions may occur predominantly on certain sites, which are called *active centres*[5.2].

In the physisorption process, atoms or molecules adsorb on an insulator surface, and the interactions between adsorbate and substrate are van der Waals intermolecular forces, which are relatively weak. The energy of physisorption is small, usually less than 200 meV. The equilibrium is very rapid and it is reversible. The adsorbate may be removed without any change of the adsorbate or surface by lowering the pressure.

In the chemisorption process, atoms or molecules adsorb on a metallic surface, and adsorbate is held to the surface by strong covalent forces. An important consequence is that after a surface has become covered with a single layer of adsorbed molecules, it is saturated. Langmuir[5.3] emphasized that chemisorption involves the formation of an unimolecular layer. It has been shown that additional adsorption can occur only on the top of the existing layer, and that the forces in this next layer of adsorption are generally weak. The chemical nature of the chemisorbed adsorbate may be significantly different when it is adsorbed on a surface. Chemisorption is frequently associated with an appreciable activation energy and may therefore be a relatively slow process. It may be difficult to remove molecules which are chemisorbed, and desorption may be accompanied by chemical changes.

It may be possible for a molecule to be physisorbed at first and then to enter into some chemical reaction with the solid surface on a longer time scale. At low temperatures, chemisorption may be so slow that for practical purposes only physisorption is observed. At high temperatures, physisorption is insignificant because adsorbate desorbs as easily as it adsorbs, and only chemisorption occurs[5.4].

The distinction between physisorption and chemisorption is sometimes blurred. Qualitatively, chemisorption is distinguishable from physisorption in that chemical specificity is higher and the energy of adsorption is large. One experimental distinction is that in chemisorption systems, the energy of adsorption in the first layer is ordinarily much greater than that in the succeeding layers since the adsorption is physisorption in the succeeding layers. However, solid surfaces are never completely smooth and adsorbed molecules may be attached more strongly to active centres than to others.

Thermal adsorption and desorption are important elementary processes in surface-catalyzed reactions, and have attracted much research[5.5]. In a theoretical study of thermal adsorption and desorption, it is practical to investigate a small atom/surface system or a simple molecule/surface system since it is easy to set up the model and hence to study the basic phenomena, and then to extend it to more complex systems. For this reason, I have chosen hydrogen atoms desorbing from the LiF (001) surface in my study.

The interactions between hydrogen atoms and the LiF (001) surface are long-range induced dipole—ionic interactions. The hydrogen atom is polarized under the ionic potential of LiF so that it produces an induced dipole. If the hydrogen atom is assumed to interact with the surface only along an axis perpendicular to the plane of the surface, the atom/surface potential energy averaged over the surface can be described by a simple potential function, such as the Morse potential or the exponential-3 potential. Figure 5.A shows the Morse potential and the exponential-3 potential curves for the H/LiF (001) system. The expression of the Morse potential used is[5.6]

$$V(r) = D_e \left[e^{-2\alpha(r-R_e)} - 2\, e^{-\alpha(r-R_e)} \right] . \qquad (5.1)$$

Here $R_e = 0$ as in reference [5.6]: the usual choice of R_e is the equilibrium distance which would simply result in displacing the plot in Fig. 5.A.

The expression of the exponential-3 potential is[5.6]

$$V(r) = \frac{\alpha R_e D_e}{\alpha R_e - 3} \left[\frac{3}{\alpha R_e} e^{-\alpha(r-R_e)} - \left(\frac{R_e}{r}\right)^3 \right] . \qquad (5.2)$$

In Eqs. (5.1) and (5.2), the variable r is the perpendicular distance between the H atom and the plane of the LiF (001) surface: R_e is the minimum perpendicular distance between the H atom and the plane of the LiF (001) surface: α is the potential parameter: and D_e is the depth of the potential well.

As seen in Fig. 5.A, when r approaches infinity, both the Morse potential energy and the exponential-3 potential energy are equal to zero. However, the exponential-3 potential function tends to zero more slowly than the Morse potential function as its curve is wider at the desorption limit, which indicates that the exponential-3 potential describes the situation close to the desorption limit better than the Morse potential. The depth of the potential well, D_e, in both potentials is very small, which indicates that hydrogen atoms are very easy to desorb from the LiF (001) surface.

Finzel *et al.*[5.7] measured the binding energies of hydrogen and deuterium atoms scattering from LiF (001) and NaF (001) surfaces. The parameters of the Morse potential function for gas/surface interactions were determined from the binding energies of any two energy levels. Le Roy[5.8] studied the interactions of atomic hydrogen and helium with LiF (001) and NaF (001) surfaces. The parameters of the inverse-power potential were estimated

by using a simple graphical method with appropriate available data. Chow and Thompson[5,6] introduced a complex potential model to handle the inelastic and diffuse scattering effect for atomic hydrogen and deuterium from LiF (001) and NaF (001) surfaces. They used the Morse potential and the exponential-3 potential to calculate the bound state resonances and the intensity curve.

Despite all the work done, the kinetic data, such as the rate constant and the activation energy for thermal desorption of H atoms from the LiF (001) surface, are unknown. There is no simple technique to obtain the kinetic data for an atom/surface or a molecule/surface system with such a small desorption energy either experimentally or theoretically.

In the following work, I have applied the Nosé-Hoover equations of motion to the thermal desorption of H atoms from the LiF (001) surface. I used the Morse potential and the exponential-3 potential to describe the interaction of the H atom with the LiF (001) surface. I calculated the rate constants and the activation energy of the thermal desorption.

§5.2 Thermal Desorption of H Atoms from a LiF (001) Surface

The adsorption of H atoms on the LiF (001) surface is classified as physisorption since the depth of the potential well, D_e, in either the Morse potential or the exponential-3 potential is very small, less than 20 meV. In order to use a simple potential function which is averaged over the surface for the H/LiF interaction as discussed in Section §5.1, I assumed that hydrogen atom interacts with the surface only along an axis perpendicular to

the plane of the surface. I also made the assumptions: (1) H atoms are infinitely diluted in an inert gas or under ultra-high vacuum condition so that there are no interactions between H atoms both on the surface and in the gas phase (in this case, the LiF (001) surface acts as a heat bath); (2) the LiF (001) surface is perfectly smooth so that every site is equally active.

The Nosé-Hoover equations of motion for a hydrogen atom on a surface are:

$$\dot{r} = \frac{p_r}{m_H} , \tag{5.3}$$

$$\dot{s} = s\, p_s , \tag{5.4}$$

$$\dot{p}_r = -\frac{dV(r)}{dr} - \tag{5.5}$$

$$\dot{p}_s = (2\, E_k - kT)/Q \tag{5.6}$$

where

$$E_k = \frac{p_r^2}{2m_H} . \tag{5.7}$$

The variable r is the perpendicular distance between the H atom and the plane of the LiF (001) surface; the variable p_r is the momentum possessed by the H atom. The variables s and p_s are non-physical variables. The parameter Q is a free parameter. The function V(r) is chosen to be an averaged H/LiF interaction potential, for which I first chose the Morse potential function.

The form of the Morse potential is expressed in Eq. (5.1), where the Morse

parameters are D_e = 17.8 meV, α = 0.55033368 a.u.$^{-1}$, and R_e = 0 a.u.[15,61] The zero point energy of the Morse potential for H/LiF (001) is equal to 5.8 meV[15,61]. The mass of a hydrogen atom is 1837.1645 a.u.

§5.2.1 Choice of the Parameter Q

I first considered the choice of the parameter Q in the Nosé-Hoover equations of motion. I constructed a series of two-dimensional r—p_r surfaces of section with the same initial conditions but different values of the parameter Q for the cut p_s = 0. I also plotted the kinetic energy distributions of the H atom corresponding to those surfaces of section. I then selected the value of Q for which the surface of section was most chaotic and the corresponding kinetic energy distribution was closest to the exact Boltzmann distribution with the largest probabilities for kinetic energy at high values.

Since the H atom is physisorbed on the LiF (001) surface, the desorption energy is very small. To ensure that the desorption events are comparatively rare, I chose the temperature to be 20K (corresponding to 1.72 meV, which is much lower than D_e). Again, for simplicity, the initial conditions of s and p_s were chosen to be 1.0 and 0.0, respectively; and the initial conditions r and p_r were chosen to be 1.5 a.u. and 0.0 a.u., respectively. Figures 5.1a, 5.2a, 5.3a, 5.4a and 5.5a show the r—p_r surfaces of section for a trajectory with the parameter Q = 15, 25, 35, 45 and 55, respectively. Figures 5.1b, 5.2b, 5.3b, 5.4b and 5.5b show their corresponding kinetic energy distribution normalized to 20K. The solid curve on each (b) figure is the exact Boltzmann distribution obtained from Eq. (3.16).

It may be seen that Figs. 5.1a and 5.2a show regular surfaces of section: and Figs. 5.1b and 5.2b show that the kinetic energy distributions deviate from the exact Boltzmann distribution as E_t' is bounded at 3. As Q increases. Fig. 5.3a and 5.4a show chaotic surfaces of section although there are some blank areas. *e.g.*. (0.5. 0.3). Figures 5.3b and 5.4b show that the kinetic energy distributions are close to the exact Boltzmann distribution. Figure 5.5a shows that the surface of section is less chaotic than Figs. 5.3a and 5.4a although its corresponding kinetic energy distribution is still close to the exact Boltzmann distribution. Comparing Figs. 5.1a through 5.5a. the appearance of the surface of section is sensitive to the parameter Q. This is probably due to the weak potential so that the $p_r p_r$ term is dominant in Eq. (5.5). which is affected by Q.

Comparing Fig. 5.3a with Fig. 5.4a. the surface of section shown in Fig. 5.3a is more chaotic. Therefore. I chose the optimum value of the parameter Q equal to 35.

§5.2.2 Calculation of the Activation Energy for Thermal Desorption

In order to calculate the activation energy for the thermal desorption of H atoms from the LiF (001) surface. I first calculated the rate constants. assuming it to be a pseudo-unimolecular reaction. To improve the reliability. I increased the number of (r. p_r) points for the calculation of rate constants. I chose the first 700 (r. p_r) values from the surface of section points at T = 20K with the initial conditions r = 1.5 a.u. and p_r = 0.0 a.u. (as seen in Fig. 5.3a). I considered the temperatures T = 85. 90. 95 and 120K. I calculated the lifetime distributions (not shown). *i.e.*. the distribution of desorption times. To avoid non-

exponential effects in the lifetime distributions. I again used the prescription of calculating the desorption rate constants from the initial parts of the lifetime distribution. I then found rate constants from a least-squares fit to the logarithm of the number of desorbed H atoms versus desorption time. $k_d = 0.48 \pm 0.16 \times 10^{12}$ sec^{-1}, $0.50 \pm 0.13 \times 10^{12}$ sec^{-1}, $0.59 \pm 0.14 \times 10^{12}$ sec^{-1} and $0.76 \pm 0.07 \times 10^{12}$ sec^{-1}, corresponding to the temperatures considered, respectively. Figure 5.6 shows a least-squares fit for the rate constant at a temperature of 120K.

From an Arrhenius plot of a least-squares fit to the logarithm of rate constants versus 1/T (shown in Fig. 5.7), I obtained the classical activation energy for the thermal desorption $E_a = 11.86 \pm 1.33$ meV. Subtracting the zero point energy of 5.8 meV[15.01], I predict an activation energy of 6.06 ± 1.33 meV.

§5.2.3 Alternate Calculation of the Activation Energy for Thermal Desorption

There are functions other than the Morse potential that may be used to describe the interactions between an adsorbed atom and a surface. In order to compare the results calculated with different potential functions, in this subsection I calculated the activation energy for the thermal desorption of H atoms from the LiF (001) surface using the exponential-3 potential function.

The Nosé-Hoover equations of motion for the H atom are the same as those used in Section §5.2, which are shown in Eqs. (5.3) through (5.7). The exponential-3 potential

function is expressed in Eq. (5.2), where the potential parameters are D_e = 19.7 meV, α = 1.9420429 a.u.$^{-1}$, and R_e = 4.5354302 a.u.[5.6] The zero point energy of the exponential-3 potential for H/LiF (001) is equal to 7.6 meV[5.6]. The mass of a hydrogen atom is 1837.1645 a.u.

Following the same procedure used for the choice of Q in the Nosé-Hoover equations of motion in Subsection §5.2.1, I chose the temperature to be 20K, and the initial conditions of s, p_s, r and p_r to be 1.0, 0.0, 5.5 a.u. and 0.0 a.u., respectively. I found the optimum value of the parameter Q to be 30 in this subsection.

I then used the procedure in Subsection §5.2.2 to calculate the activation energy for the thermal desorption of H atoms from the LiF (001) surface. I first calculated the rate constants. I chose the first 700 (r, p_r) values from the surface of section (not shown) at T = 20K with the initial conditions r = 5.5 a.u., p_r = 0.0 a.u., s = 1.0, p_s = 0.0 and the parameter Q = 30 to calculate the lifetime distributions. I considered the temperatures T = 95, 105, 110 and 125K. To avoid the non-exponential effect in the lifetime distributions (not shown), I again used the prescription of calculating the desorption rate constants from the initial parts of the lifetime distribution. From a least-squares fit to the logarithm of the number of desorbed H atoms versus desorption time, I found $k_d = 0.45 \pm 0.21 \times 10^{12}$ sec^{-1}, $0.54 \pm 0.13 \times 10^{12}$ sec^{-1}, $0.60 \pm 0.17 \times 10^{12}$ sec^{-1} and $0.67 \pm 0.18 \times 10^{12}$ sec^{-1}, corresponding to the temperatures considered.

From an Arrhenius plot of a least-squares fit to the logarithm of rate constants versus 1/T (shown in Fig. 5.8), I obtained the classical activation energy of the thermal desorption E_a = 13.92 ± 1.53 meV. Subtracting the zero point energy of 7.6 meV[5.6], I predict an

activation energy of 6.32 ± 1.53 meV.

§5.3 Discussion

I have applied the Nosé-Hoover equations of motion to the thermal desorption of H atoms from the LiF (001) surface. I used both a Morse potential function and an exponential-3 potential function to describe the H/LiF interactions which are averaged over the surface. I predicted the activation energy for the thermal desorption of H atoms from the LiF (001) surface. The conclusions are as follows:

(1) The Nosé-Hoover equations of motion can thermalize the H/LiF dynamics when the phase space dynamics is chaotic.

(2) With the Morse potential function, I predict the activation energy for the thermal desorption of H atoms from the LiF (001) surface to be 6.06 ± 1.33 meV in the temperature range 85—120K. With the exponential-3 potential function, I predict the activation energy to be 6.32 ± 1.53 meV in the temperature range 95—125K. The results calculated with different potential functions are quite close in my study although the uncertainties in both calculations are relatively large.

The large uncertainty in the activation energy comes from the uncertainties in the rate constants, which are caused by possible non-exponential effects in the lifetime distributions. Since the interactions between the H atom and the LiF (001) surface are very weak, the desorption time is very sensitive to the temperature. However, the non-exponential effect should be improved by choosing a large number of samples, *i.e.*, (r, p_r) points. On the other

hand, my calculated values of the activation energy for the thermal desorption are in reasonable agreement since the desorption energy, D_e, for both the Morse potential function and the exponential-3 potential function, is very low.

(3) The temperature range used in my calculations is very low, but still in the range which can be handled by experiments. Compared to another alkali chloride surface, Iannotta[5,9] indicated that for the adsorption of H atoms on the NaCl (001) surface, no steady-state adsorption had been observed at a surface temperature of 80K. In other words, H atoms desorbed from the NaCl (001) surface at a temperature of 80K and up. The temperature observed in the experiment of Iannotta[5,9] is comparable with that at which I saw substantial H/LiF desorption. Although different surfaces are involved, both are ionic. Therefore, I believe that my calculation is reasonable.

(4) I have assumed that the LiF (001) surface is perfectly smooth so that every site is equally active, which means that the adsorption of H atoms on the LiF (001) surface is not site-specific. Actually, H atoms should be adsorbed more strongly on top of F^- than on top of Li^+. However, my calculated values of the activation energy for the thermal desorption of H atoms from the LiF (001) surface use only the averaged effect. This will tend to underestimate the activation energy since the averaged interactions are weaker than the actual interactions between the H atom and the F^- ion.

(5) I have demonstrated by example that the Nosé-Hoover equations of motion can be applied to the thermal desorption of atoms from a surface. My results show that with the Nosé-Hoover equations of motion, calculations are feasible where experiment or other approaches may not be possible. I predict that the Nosé-Hoover equation approach or its

modification could also be applied to molecular desorption or reaction on the surface.

Chapter 6

Conclusions and Predictions

In this theoretical study, I have applied the Nosé-Hoover equations of motion[6.1, 6.2, 6.3] with and without rotational modification[6.4, 6.5] to the thermal dissociation of a diatomic molecule, H_2, in an inert gas which simply acts as a heat bath. I approximated the thermal dissociation of diatomics as a pseudo unimolecular reaction. The results show that the Nosé-Hoover equations of motion can thermalize the H_2 dynamics. I have also calculated the pseudo-unimolecular rate constants and the activation energy of H_2 dissociation. The activation energy calculated in this work agrees with the values measured by incident shock wave experiment[6.6] quite well.

The fact that the activation energy of the thermal dissociation is significantly smaller than the dissociation energy is attributed to non-equilibrium effects, in particular, a non-Boltzmann vibrational-energy distribution. The rate of diatomic dissociation competes with the rate of vibrational-energy redistribution for the highest vibrational energies and these vibrational energies become depleted. However, the Nosé-Hoover equations of motion cannot control the rate of phase-space redistribution (or vibrational-energy redistribution), and thus it is not possible to control the degree to which the vibrational-energy distribution is non-Boltzmann. In this regard, it may be helpful to consider generalizations of the Nosé equation studied by Jellinek and Berry[6.7] for which it is possible, in principle, to incorporate non-equilibrium effects, and thus to control the rate of phase-space redistribution.

The Nosé-Hoover equation cannot thermalize the separating H + H dynamics, but, to the extent that it can thermalize the H_2 dynamics in the transition region, it is legitimate to employ a statistical model to predict the product distributions. Of the statistical models that have been proposed, one is directly applicable: the thermal model of Herschbach and other workers[10,31]. In this model, it is assumed that there is thermal equilibrium between a particular degree of freedom and a bath consisting of the other degrees of freedom. If the Nosé-Hoover equation approach is applicable to the pseudo-unimolecular reaction of polyatomics in an inert gas, then it could be used in conjunction with the thermal model to predict product distributions.

My results suggest that the Nosé-Hoover equation approach should be applicable to the pseudo-unimolecular reaction of polyatomics in an inert gas where other approaches may not be feasible. It has the advantage of flexibility, in that only some (for example, the low frequency) vibrational modes need to be thermalized. Other vibrational modes could then be dynamically coupled to these and, if desired, to external degrees of freedom.

The generalized Nosé equations of motion combined with a statistical model to predict product distributions should be applicable to bimolecular reactions.

The inclusion of rotation does not cause the Nosé-Hoover equations of motion to be more ergodic. However, my calculations have shown that rotation is effective in promoting dissociation. I have included separate terms for the vibrational kinetic energy, E_v, and the rotational kinetic energy, E_r, in the Nosé-Hoover equations of motion including rotation because the time scales for vibration and rotation are very different. This modification can be used to thermalize the vibrational and rotational modes at different scales via Q_1 and Q_2.

I have also applied the modified Nosé-Hoover equations of motion[10,9] to the thermal dissociation of homonuclear and heteronuclear diatomic molecules, H_2 and HCl, in an inert gas. The modified Nosé-Hoover equations of motion can cause the phase-space dynamics to be more chaotic. The activation energy of H_2 dissociation calculated using the modified Nosé-Hoover equations of motion is closer to the experimental value than that calculated using the original Nosé-Hoover equations of motion. For the heteronuclear diatomic, the interactions between the diatomic molecule and the inert gas should be considered.

Finally, I have applied the original Nosé-Hoover equations of motion to the thermal desorption of H atoms from the LiF (001) surface. My results show that Nosé-Hoover equations of motion can thermalize atom/surface dynamics when the phase space dynamics is chaotic. My results suggest that the Nosé-Hoover equation approach or a modification thereof could also be applied to molecular desorption or reaction on the surface. In any case, the interatomic potential energy function will be strongly modified by the surface, and the inclusion of temperature effects will lead to a much more realistic modelling of surface phenomena.

References

Chapter 1

[1.1] See, for example, a) L. V. Woodcock, Chem. Phys. Lett., 10, 257—261 (1971); b) H. C. Andersen, J. Chem. Phys., 72, 2384—2393 (1980).

[1.2] S. Nosé, Mol. Phys., 52, 255—268 (1984).

[1.3] See, for example, a) D. J. Evans and B. C. Holian, J. Chem. Phys., 83, 4069—4074 (1985); b) I. L'Heureux and I. P. Hamilton, Phys. Rev. E, 47, 1411—1414 (1993); c) F. D. Ditolia and M. Ronchetti, Phys. Rev. E, 48, 1726—1737 (1993).

[1.4] W. G. Hoover, Phys. Rev. A, 31, 1695—1697 (1985).

[1.5] I. P. Hamilton, Phys. Rev. A, 42, 7467—7470 (1990).

[1.6] See, for example, H. O. Pritchard, Specialist Periodical Reports, Reaction Kinetics, Vol. 1, 243—290 (The Chemical Society, London, 1975).

[1.7] I. P. Hamilton and L. Liu, J. Chem. Phys., 93, 5616—5620 (1990).

[1.8] L. Liu and I. P. Hamilton, J. Chem. Phys., 95, 3859—3860 (1991).

[1.9] W. D. Breshears and P. F. Bird, Symposium (International) on Combustion, 14th, 211—218 (Combustion Institute, Pittsburgh, 1973).

[1.10] W. D. Breshears and P. F. Bird, J. Chem. Phys., 56, 5347—5351 (1972).

Chapter 2

[2.1] P. W. Atkins, Physical Chemistry, 4th Ed. (W. H. Freeman and Company, New York, 1990).

[2.2] For detailed discussion, see books on the topic of statistical thermodynamics, *e.g.*, D. A. McQuarrie, Statistical Thermodynamics, Harper's Chemistry, edited by Stuart A. Rice (1973).

[2.3] For detailed discussion, see books on the topic of statistical mechanics or statistical thermodynamics, *e.g.*, T. L. Hill, An Introduction to Statistical Thermodynamics (Addison-Wesley, Reading, Mass., 1960).

[2.4] G. L. Baker and J. P. Gollub, Chaotic Dynamics: An Introduction (Cambridge University Press, Cambridge, 1990).

[2.5] See, for example, I. E. Farquhar, Ergodic Theory in Statistical Mechanics (John Wiley, New York, 1964).

[2.6] N. Metropolis, A. W. Rosenbluth, M. N. Rosenbluth, A. H. Teller and E. Teller, J. Chem. Phys., 21, 1087—1092 (1953).

[2.7] See, for example, a) J. P. Valleau and S. G. Whittington, Statistical Mechanics, Part A: Equilibrium Techniques, p.137, edited by B.J. Berne (1977); b) J. P. Valleau and G. M. Torrie, *ibid.*, p. 169.

[2.8] L. V. Woodcock, Chem. Phys. Lett., 10, 257—261 (1971).

[2.9] W. G. Hoover, A. J. C. Ladd and B. Moran, Phys. Rev. Lett., 48, 1818—1820 (1982).

[2.10] D. J. Evans, J. Chem. Phys., 78, 3297—3302 (1983).

[2.11] F. F. Abraham, S. W. Koch and R. C. Desai, Phys. Rev. Lett., 49, 923—926 (1982).

[2.12] H. C. Andersen, J. Chem. Phys., 72, 2384—2393 (1980).

[2.13] J. M. Haile and S. Gupta, J. Chem. Phys., 79, 3067—3076 (1983).

[2.14] H. J. C. Berendsen, J. P. M. Postma, W. F. van Gunsteren, A. DiNola and J. R. Haak, J. Chem. Phys., 81, 3684—3690 (1984).

[2.15] S. Nosé, Mol. Phys., 52, 255—268 (1984).

[2.16] S. Nosé, J. Chem. Phys., 81, 511—519 (1984).

[2.17] W. G. Hoover, Phys. Rev. A, 31, 1695—1697 (1985).

[2.18] I. P. Hamilton, Phys. Rev. A, 42, 7467—7470 (1990).

[2.19] See, for example, G. Marc and W. G. McMillan, Adv. Chem. Phys., 58, 209—361 (1985).

[2.20] J. Jellinek and R. S. Berry, Phys. Rev. A, 38, 3069—3072 (1988).

[2.21] D. Kusnezov, A. Bulgac and W. Bauer, Ann. Phys. (N.Y.), 204, 155 (1990).

[2.22] R. G. Winkler, Phys. Rev. A, 45, 2250—2255 (1992).

[2.23] G. J. Martyna, M. L. Klein and M. Tuckerman, J. Chem. Phys., 97, 2635—2643 (1992).

[2.24] I. L'Heureux and I. P. Hamilton, Phys. Rev. E, 47, 1411—1414 (1993).

Chapter 3

[3.1] S. Nosé. Mol. Phys., 52, 255—268 (1984).

[3.2] S. Nosé. J. Chem. Phys., 81, 511—519 (1984).

[3.3] W. G. Hoover. Phys. Rev. A, 31, 1695—1697 (1985).

[3.4] I. P. Hamilton and L. Liu. J. Chem. Phys., 93, 5616—5620 (1990).

[3.5] L. Liu and I. P. Hamilton. J. Chem. Phys., 95, 3859—3860 (1991).

[3.6] W. D. Breshears and P. F. Bird. Symposium (International) on Combustion, 14th, 211—218 (Combustion Institute, Pittsburgh, 1973).

[3.7] R. D. Kern. Compr. Chem. Kinet., 18, 1—37 (1976).

[3.8] See, for example, H. O. Pritchard. Specialist Periodical Reports, Reaction Kinetics, Vol. 1, 243—290 (The Chemical Society, London, 1975).

[3.9] A. L. Myerson and W. S. Watt. J. Chem. Phys., 49, 425—433 (1968).

[3.10] J. C. Keck and G. F. Carrier. J. Chem. Phys., 43, 2284—2298 (1965).

[3.11] V. H. Shui, J. P. Appleton and J. C. Keck. J. Chem. Phys., 53, 2547—2558 (1970).

[3.12] V. H. Shui and J. P. Appleton. J. Chem. Phys., 55, 3126—3132 (1971).

[3.13] V. H. Shui, J. P. Appleton and J. C. Keck. Symposium (International) on Combustion, 13th, 19—33 (Combustion Institute, Pittsburgh, 1971).

[3.14] V. H. Shui. J. Chem. Phys., 58, 4868—4879 (1973).

[3.15] J. E. Dove and D. G. Jones. J. Chem. Phys., 55, 1531—1540 (1971).

[3.16] J. E. Dove and D. G. Jones. Chem. Phys. Lett., 17, 134—136 (1972).

[3.17] J. E. Dove and S. Raynor. Chem. Phys., 28, 113—124 (1978).

[3.18] J. E. Dove and S. Raynor, J. Phys. Chem., 83, 127—133 (1979).

[3.19] C. W. Wilson Jr., R. Kapral and G. Burns, Chem. Phys. Lett., 24, 488—491 (1974).

[3.20] J. H. Kiefer and J. C. Hajduk, Chem. Phys., 38, 329—339 (1979).

[3.21] N. C. Blais and D. G. Truhlar, J. Chem. Phys., 65, 5335—5356 (1976).

[3.22] N. C. Blais and D. G. Truhlar, J. Am. Chem. Soc., 99, 8108—8109 (1977).

[3.23] D. G. Truhlar, N. C. Blais, J.-C. J. Hajduk and J. H. Kiefer, Chem. Phys. Lett., 63, 337—343 (1979).

[3.24] J. H. Kiefer, J. Chem. Phys., 57, 1938—1956 (1972).

[3.25] H. Teitelbaum, Chem. Phys., 124, 55—76 (1988).

[3.26] J. S. Wright, J. Chem. Soc., Faraday Trans. 2, 84, 219—226 (1988).

[3.27] R. N. Porter and M. Karplus, J. Chem. Phys., 40, 1105—1115 (1964).

[3.28] P. W. Atkins, Physical Chemistry, 4th Ed. (W. H. Freeman and Company, New York, 1990).

[3.29] H. A. Posch, W. G. Hoover and F. J. Vesely, Phys. Rev. A, 33, 4253—4265 (1986).

[3.30] I. P. Hamilton, Phys. Rev. A, 38, 3120—3123 (1988).

[3.31] I. L'Heureux and I. P. Hamilton, Phys. Rev. E, 47, 1411—1414 (1993).

[3.32] N. DeLeon and B. J. Berne, J. Chem. Phys., 75, 3495—3509 (1981).

[3.33] R. S. Dumont and P. Brumer, J. Chem. Phys., 90, 96—104 (1989).

[3.34] G. M. Zaslavskii and B. V. Chirikov, Sov. Phys. Usp., 14, 549—567 (1972) [Usp. Fiz. Nauk, 105, 3 (1971)].

[3.35] G. L. Baker and J. P. Gollub, Chaotic Dynamics: An Introduction (Cambridge University Press, Cambridge, 1990).

Chapter 4

[4.1] H. A. Posch, W. G. Hoover and F. J. Vesely, Phys. Rev. A, 33, 4253—4265 (1986).

[4.2] I. P. Hamilton, Phys. Rev. A, 42, 7467—7470 (1990).

[4.3] See, for example, G. Marc and W. G. McMillan, Adv. Chem. Phys., 58, 209—361 (1985).

[4.4] R. N. Porter and M. Karplus, J. Chem. Phys., 40, 1105—1115 (1964).

[4.5] P. W. Atkins, Physical Chemistry, 4th Ed. (W. H. Freeman and Company, New York, 1990).

[4.6] W. D. Breshears and P. F. Bird, Symposium (International) on Combustion, 14th, 211—218 (Combustion Institute, Pittsburgh, 1973).

[4.7] H. Teitelbaum, Chem. Phys., 124, 55—76 (1988).

[4.8] S. Ron, Y. Shima and M. Baer, Chem. Phys., 101, 45—54 (1986).

[4.9] W. D. Breshears and P. F. Bird, J. Chem. Phys., 56, 5347—5351 (1972).

[4.10] T. A. Jacobs, N. Cohen and R. R. Giedt, J. Chem. Phys., 46, 1958—1968 (1967).

[4.11] D. J. Seery and C. T. Bowman, J. Chem. Phys., 48, 4314—4317 (1968).

Chapter 5

[5.1] K. J. Laidler and J. H. Meiser, Physical Chemistry (The Benjamin/Cummings Publishing Company, Inc., Menlo Park, California, 1982).

[5.2] P. W. Atkins, Physical Chemistry, 4th Ed. (W. H. Freeman and Company, New York, 1990).

[5.3] I. Langmuir, J. Amer. Chem. Soc., 38, 2221—2238 (1916).

[5.4] A. W. Adamson, Physical Chemistry of Surfaces, 5th Ed. (John Wiley & Sons, Inc., New York, 1990).

[5.5] See, for example, S. J. Lombardo and A. T. Bell, Surface Science Reports, 13, 1-72 (1991).

[5.6] H. Chow and E. D. Thompson, Surface Science, 82, 1—21 (1979).

[5.7] H.-U. Finzel, H. Frank, H. Hoinkes, M. Luschka, H. Nahr, H. Wilsch and U. Wonka, Surface Science, 49, 577—605 (1975).

[5.8] R. J. Le Roy, Surface Science, 59, 541—553 (1976).

[5.9] S. Iannotta, Faraday Discussions, 96, 191 (1993).

Chapter 6

[6.1] S. Nosé, Mol. Phys., 52, 255—268 (1984).

[6.2] S. Nosé, J. Chem. Phys., 81, 511—519 (1984).

[6.3] W. G. Hoover, Phys. Rev. A, 31, 1695—1697 (1985).

[6.4] I. P. Hamilton and L. Liu. J. Chem. Phys.. 93. 5616—5620 (1990).

[6.5] L. Liu and I. P. Hamilton. J. Chem. Phys.. 95. 3859—3860 (1991).

[6.6] W. D. Breshears and P. F. Bird. Symposium (International) on Combustion. 14th. 211—218 (Combustion Institute. Pittsburgh. 1973).

[6.7] J. Jellinek and R. S. Berry. Phys. Rev. A. 38. 3069—3072 (1988).

[6.8] W. B. Miller. S. A. Safron. and D. R. Herschbach. J. Chem. Phys.. 56. 3581—3592 (1972). For examples of application. see. a) D. Wardlaw. P. Brumer and T. A. Osborn. J. Chem. Phys.. 76. 4916—4924 (1982); b) I. P. Hamilton and P. Brumer. J. Chem. Phys.. 82. 595—597 (1985).

[6.9] I. P. Hamilton. Phys. Rev. A. 42. 7467—7470 (1990).

Table 2-1 Summary of Variables Used.

	Variable in the physical system	Variable in the extended system	Relationship of the variables
Coordinate	r_i	q_i	$r_i = q_i$
Momentum	p_{ri}	p_i	$p_{ri} = s\, p_i$
Time	t	τ	$dt = d\tau/s$
Additional variables		s and p_s	

Table 3-1 Comparison of Activation Energies (H_2).

Source	Method	Temperature Range (K)	Activation Energy (eV)
Myerson and Watt[3.9]	incident shock waves	2290—3790	4.02 ± 0.21
Breshears and Bird[3.6]	incident shock waves	3500—8000	3.86 ± 0.21
Blais and Truhlar[3.22]	quasi-classical trajectory	4500	4.22 ± 0.04
Teitelbaum[3.25]	master equation	∞	3.73
present work	Nosé-Hoover equations	17,000—22,000	3.55 ± 0.48

Table 3-2 Comparison of Rate Constants with and without H_2 Rotation.

Temperature (K)	with H_2 rotation, k_d ($\times 10^{12} sec^{-1}$)	without H_2 rotation, k_d ($\times 10^{12} sec^{-1}$)	% of increase in rate due to including rotation
17,000	4.88 ± 0.44	3.52 ± 0.48	40
18,000	5.41 ± 0.41	4.07 ± 0.16	33
20,000	5.90 ± 0.28	5.58 ± 0.50	5

Table 4-1 Calculated Rate Constants for H_2 Dissociation at Different Temperatures.

Temperature (K)	Rate Constant ($\times 10^{12} sec^{-1}$)
7250	1.36 ± 0.04
7500	2.28 ± 0.18
7750	2.89 ± 0.22
8000	3.22 ± 0.25
8250	3.72 ± 0.21
8500	4.43 ± 0.21
8750	5.29 ± 0.54
9000	5.05 ± 0.72
9500	7.84 ± 0.88

Table 4-2 Predicted Activation Energies for Different Values of Q (H_2).

Values of Q	Temperature Range (K)	Activation Energy (eV)
7	6500—8500	4.13 ± 0.23
20	6500—9000	3.99 ± 0.31
30	7000—9500	3.75 ± 0.46
35	7250—9500	3.78 ± 0.33
40	7500—9500	3.81 ± 0.48
50	7250—10,000	3.66 ± 0.17
175	7000—10,000	3.51 ± 0.37

Table 4-3 Comparison of Activation Energies (H_2).

Source	Method	Temperature Range (K)	Activation Energy (eV)
Breshears and Bird[4.6]	incident shock waves	3500—8000	3.86 ± 0.21
Teitelbaum[4.7]	master equation approach	∞	3.73
present work	Nosé-Hoover Eqs.	17,000—22,000	3.55 ± 0.48
present work	modified Nosé-Hoover Eqs.	7250—9500	3.78 ± 0.33

Table 4-4 Calculated Rate Constants for HCl Dissociation at Different Temperatures.

Temperature (K)	Rate Constant ($\times 10^{12}$sec^{-1})
6750	1.34 ± 0.14
7000	1.90 ± 0.09
7250	2.59 ± 0.09
7500	3.09 ± 0.22
7750	4.45 ± 0.26
8000	5.90 ± 0.43
8500	6.83 ± 0.19
9000	8.65 ± 1.00
9500	12.72 ± 0.61
10000	12.82 ± 3.12

Table 4-5 Comparison of Activation Energies (HCl).

Source	Method	Temperature Range (K)	Activation Energy (eV)
Jacobs, *et al.*[4.10]	incident shock waves	2800—4600	3.04 ± 0.21
Seery and Bowman[4.11]	incident shock waves	2900—4000	3.51 ± 0.21
Breshears and Bird[4.9]	incident shock waves	3500—7000	3.59 ± 0.21
Teitelbaum[4.7]	master equation approach	∞	3.69
present work	modified Nosé-Hoover Eqs.	6750—10,000	3.89 ± 0.23

Table 4-6 Comparison of Activation Energies for H_2 and HCl dissociation.

Source	Method	Activation energy of H_2 dissociation (eV)	Activation energy of HCl dissociation (eV)
Breshears and Bird[4.6, 4.9]	incident shock waves	3.86 ± 0.21	3.59 ± 0.21
present work	modified Nosé-Hoover Eqs.	3.78 ± 0.33	3.89 ± 0.23

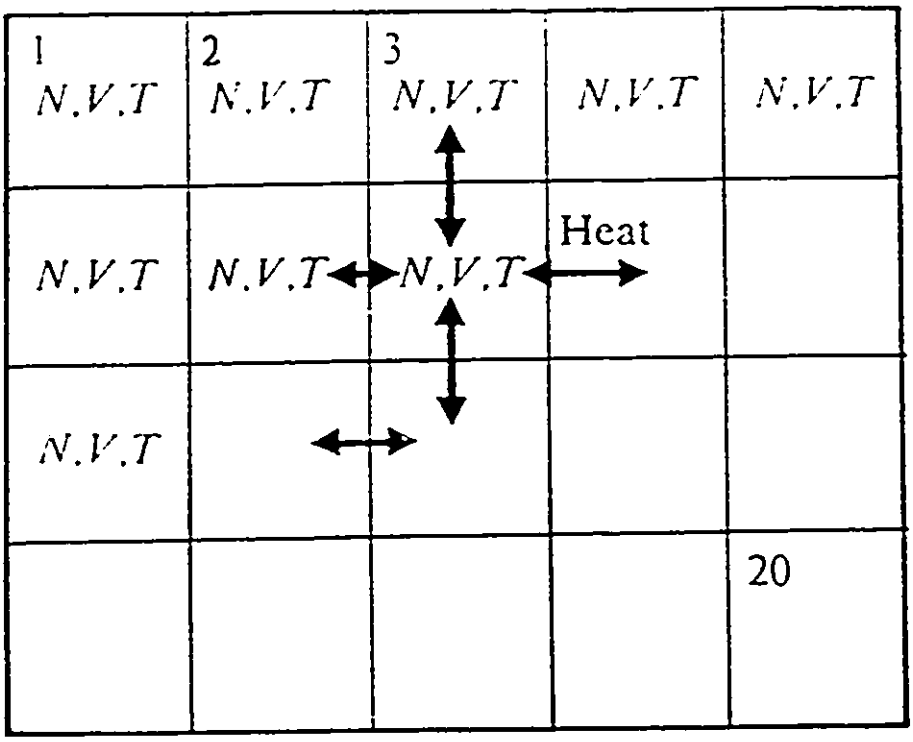

Fig. 2.A Representation of the canonical ensemble with 20 imaginary replications.

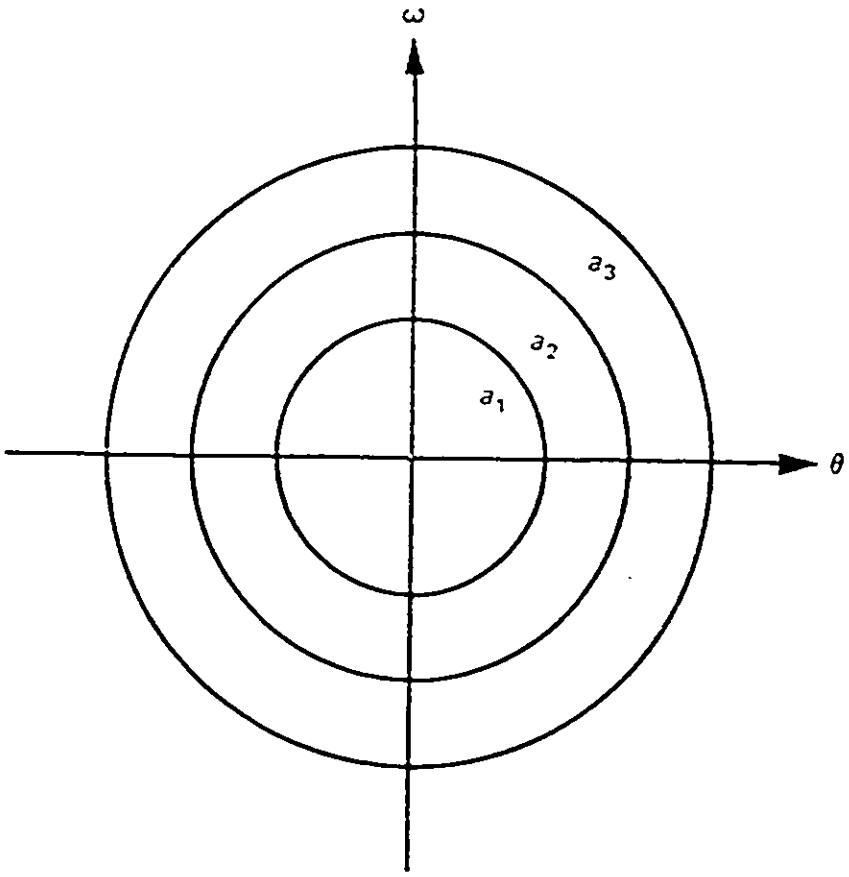

Fig. 2.B Phase space diagram of a simple pendulum.

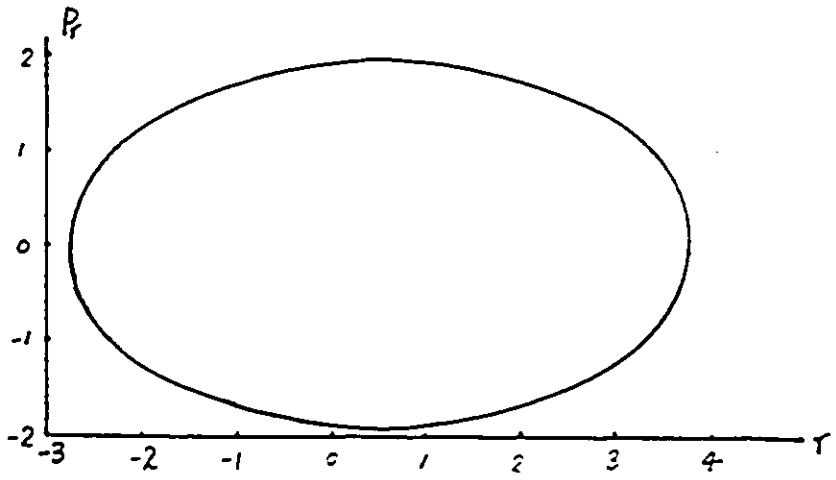

Fig. 2.C A regular r—p_r surface of section corresponding to one-dimensional motion with constant energy.

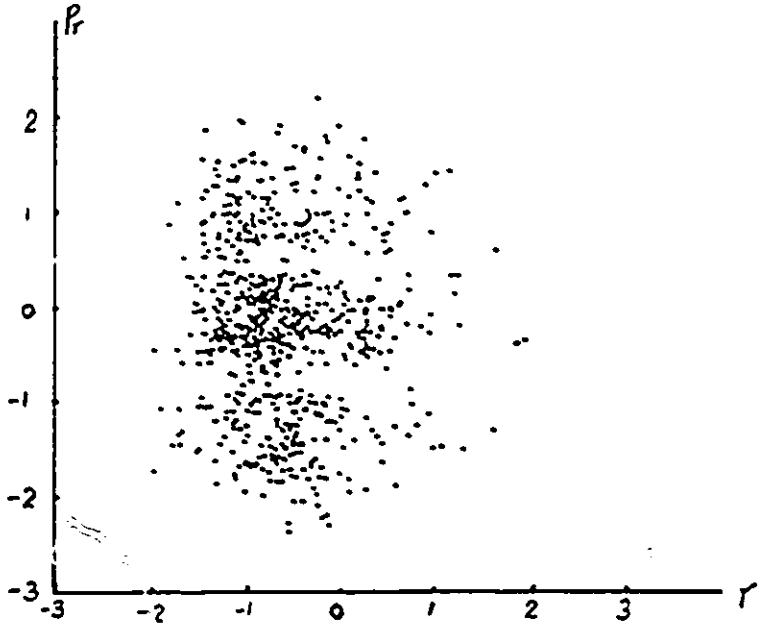

Fig. 2.D A chaotic r—p_r surface of section corresponding to one-dimensional motion with energy not constant.

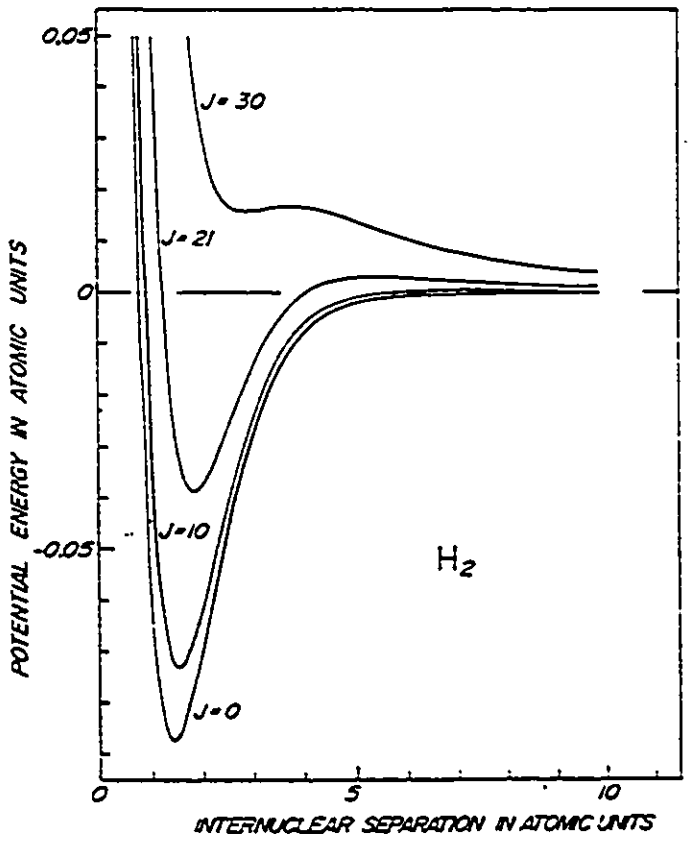

Fig. 3.A Effective potential energy curves for H_2 at $v' = 0$ vibrational level and rotational states, J, as noted.

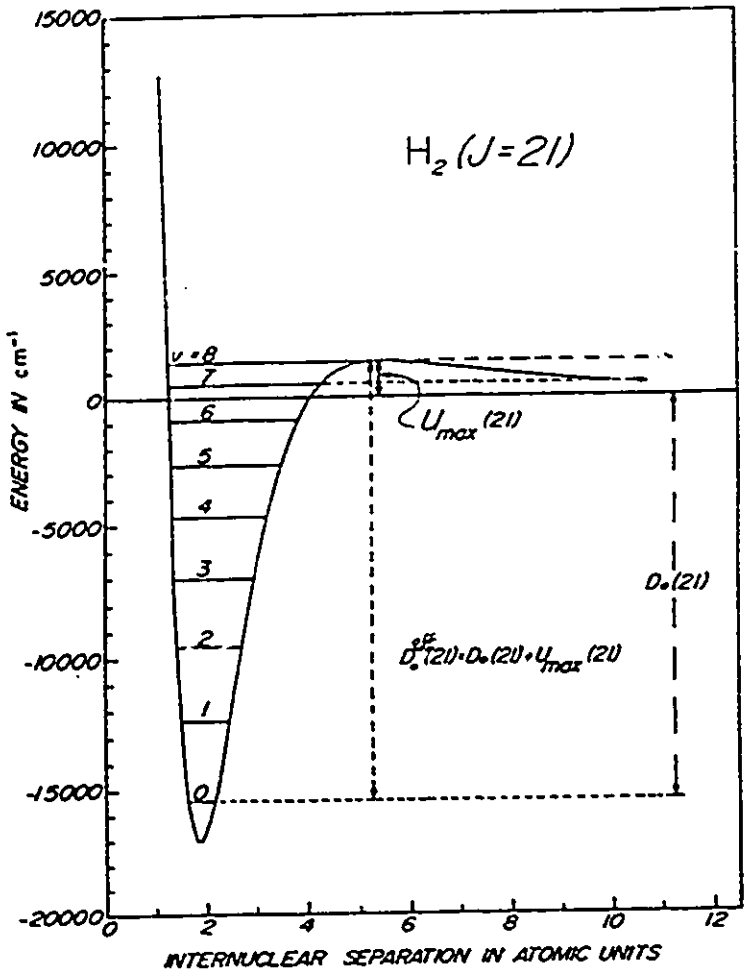

Fig. 3.B Effective potential energy curve for H_2 at vibrational levels, v', as noted and J = 21 rotational state.

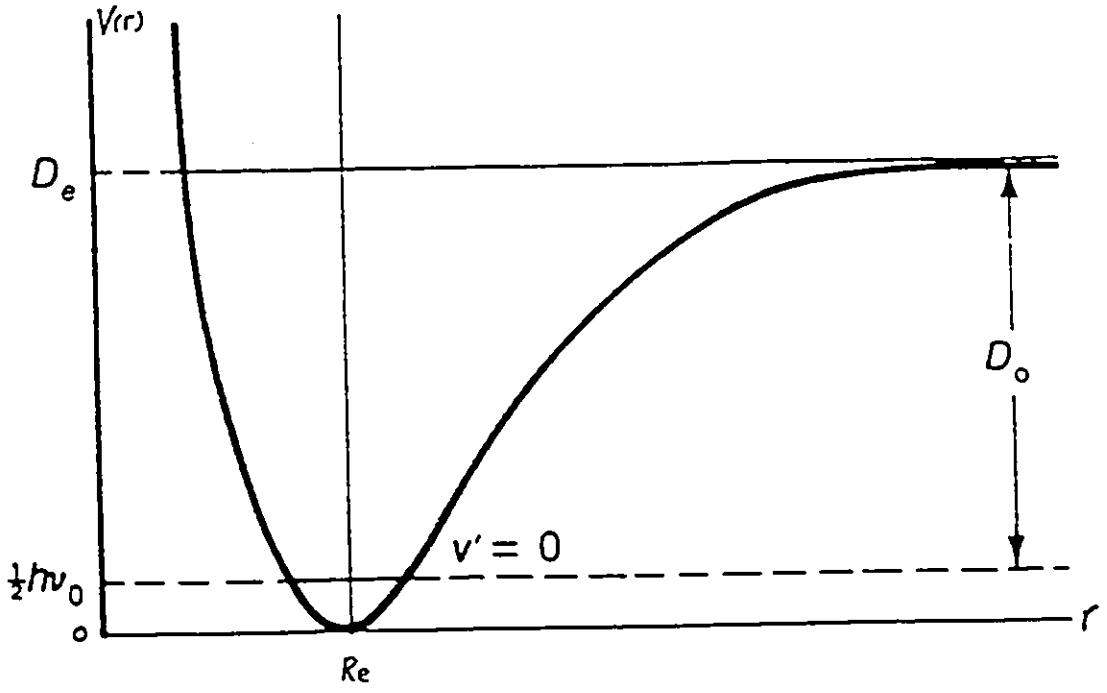

Fig. 3.C Morse potential curve for a diatomic molecule.

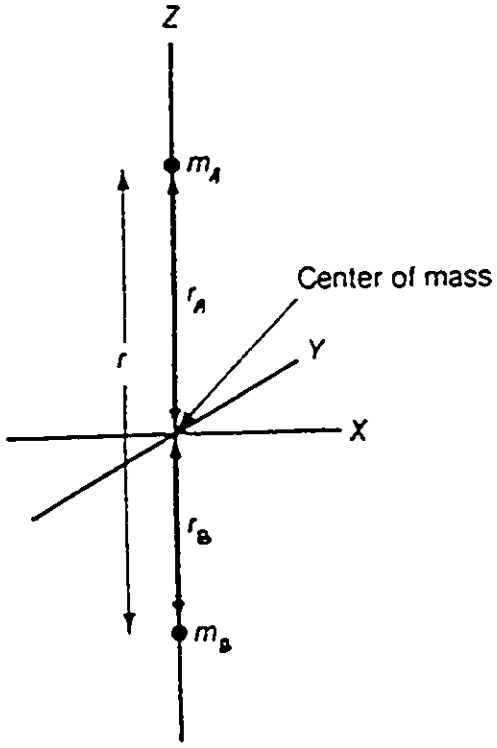

Fig. 3.D A rigid rotor representing a diatomic molecule AB.

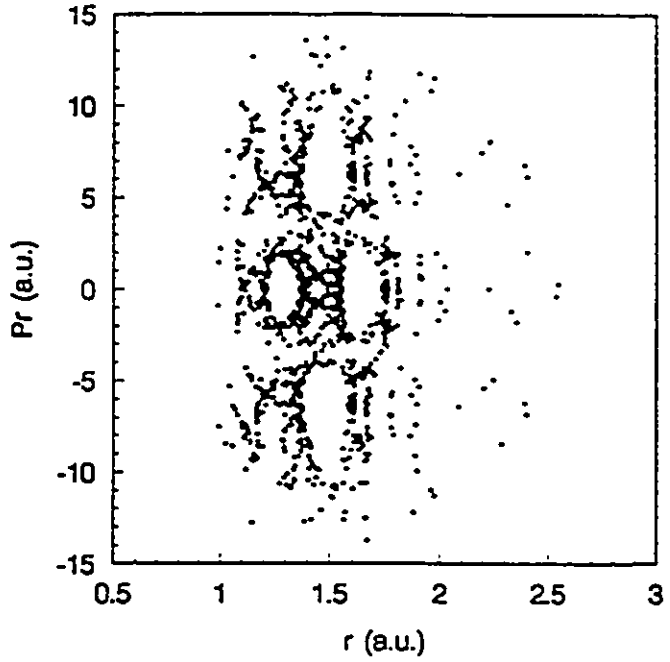

Fig. 3.1a The surface of section for H_2 dynamics generated using Nosé-Hoover equations. Q = 10, T = 4000K, initial conditions r = 3.3 a.u. and p_r = 0.0 a.u.

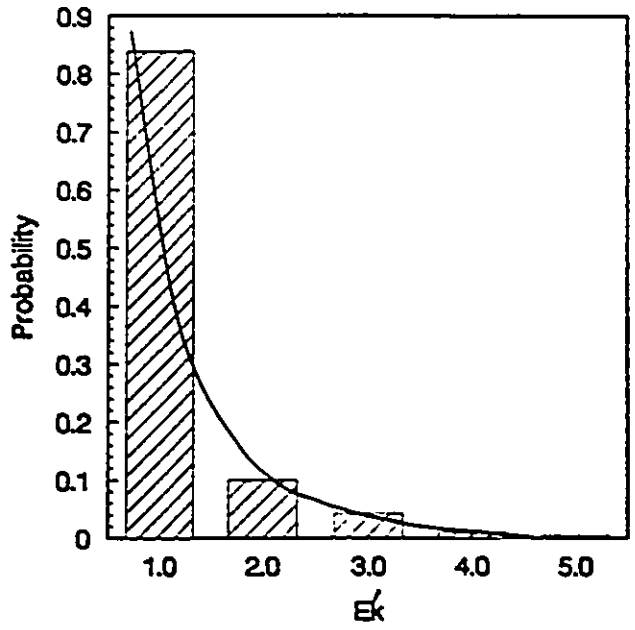

Fig. 3.1b The kinetic energy distribution, normalized to 4000K, corresponding to Fig. 3.1a.

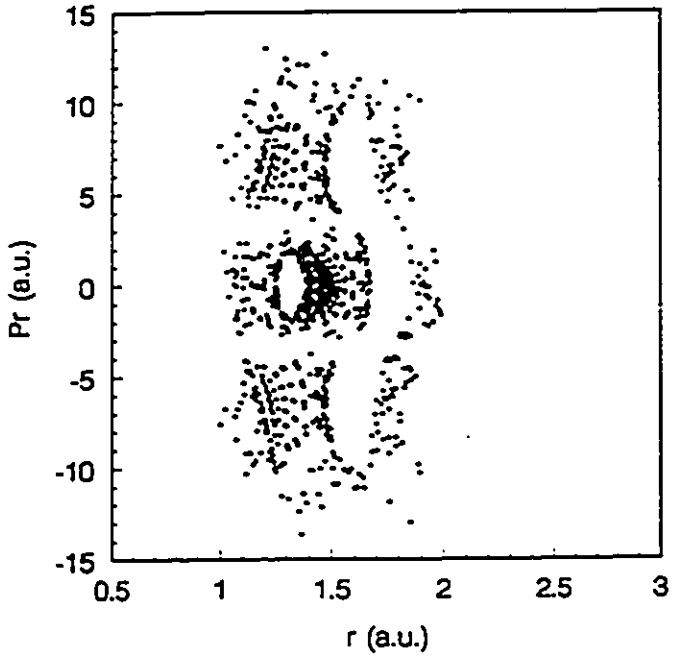

Fig. 3.2a The surface of section for H_2 dynamics generated using Nosé-Hoover equations. Q = 17, T = 4000K, initial conditions r = 3.3 a.u. and p_r = 0.0 a.u.

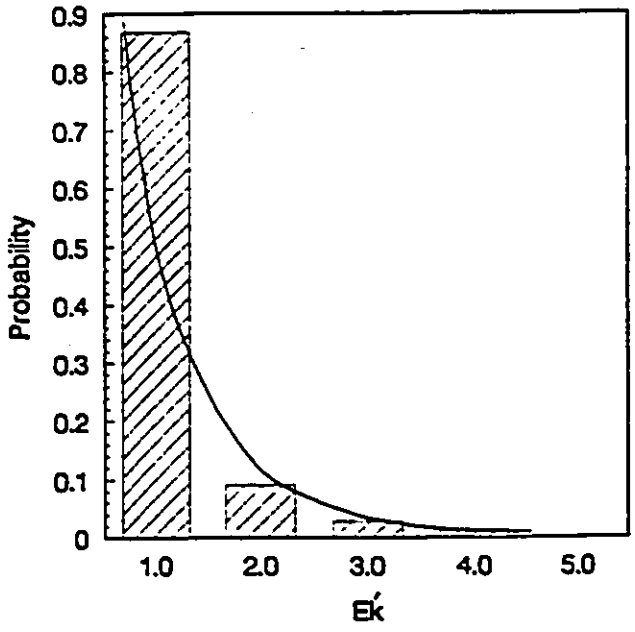

Fig. 3.2b The kinetic energy distribution, normalized to 4000K, corresponding to Fig. 3.2a.

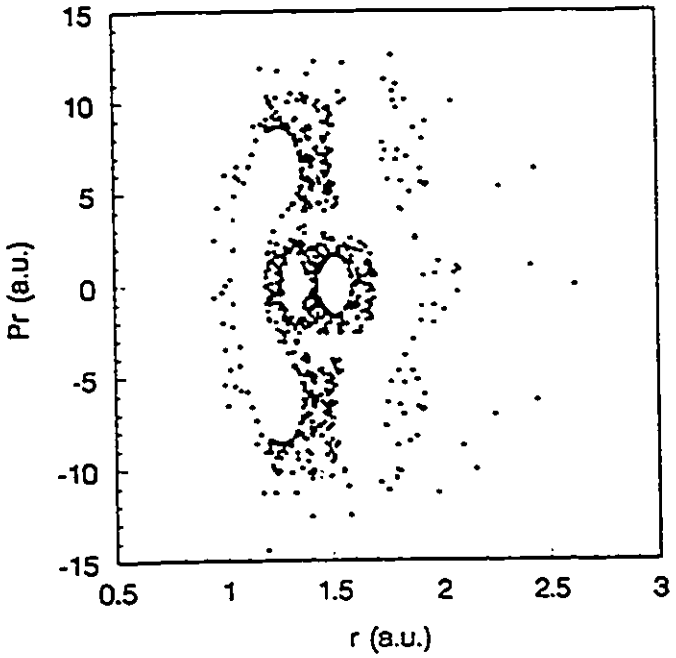

Fig. 3.3a The surface of section for H_2 dynamics generated using Nosé-Hoover equations. Q = 20, T = 4000K, initial conditions r = 3.3 a.u. and p_r = 0.0 a.u.

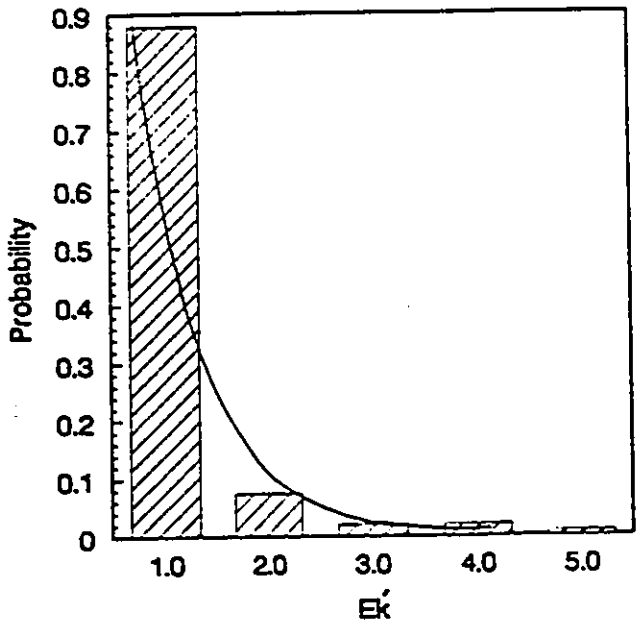

Fig. 3.3b The kinetic energy distribution, normalized to 4000K, corresponding to Fig. 3.3a.

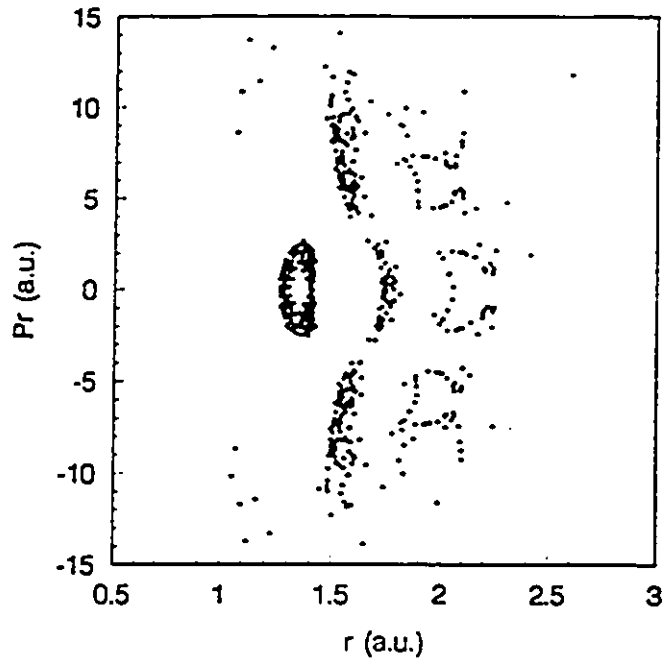

Fig. 3.4a The surface of section for H_2 dynamics generated using Nosé-Hoover equations. Q = 25, T = 4000K, initial conditions r = 3.3 a.u. and p_r = 0.0 a.u.

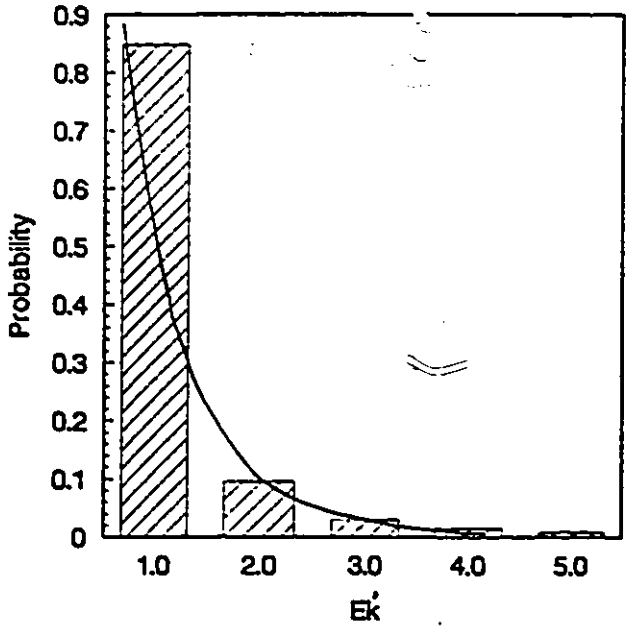

Fig. 3.4b The kinetic energy distribution, normalized to 4000K, corresponding to Fig. 3.4a.

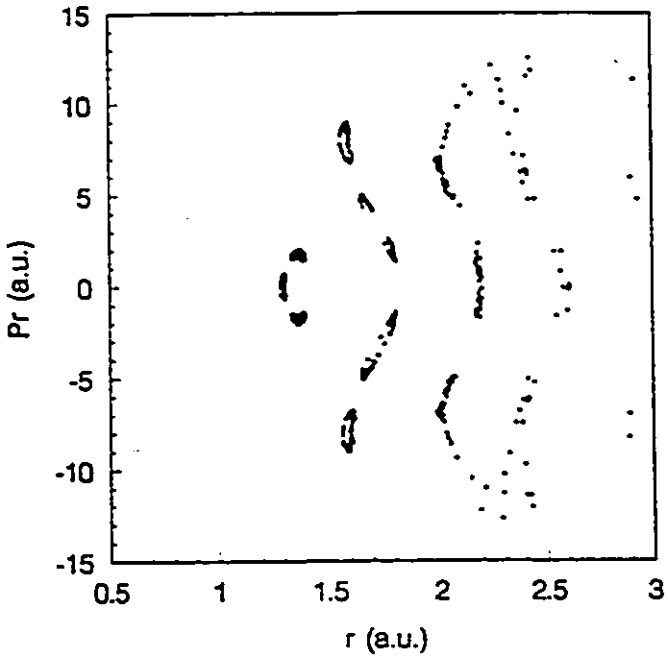

Fig. 3.5a The surface of section for H_2 dynamics generated using Nosé-Hoover equations. Q = 30, T = 4000K, initial conditions r = 3.3 a.u. and p_r = 0.0 a.u.

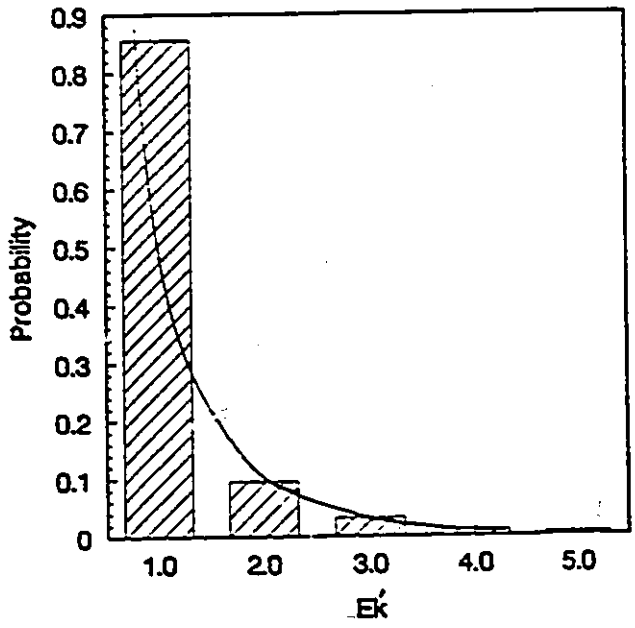

Fig. 3.5b The kinetic energy distribution, normalized to 4000K, corresponding to Fig. 3.5a.

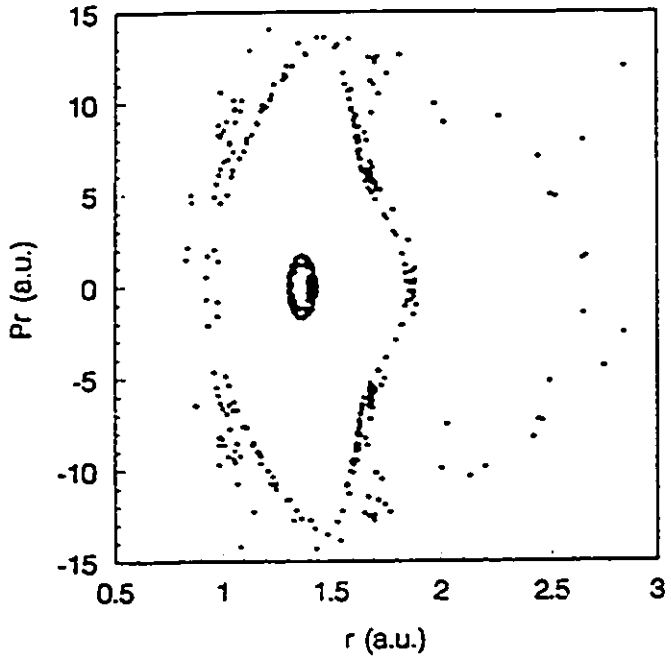

Fig. 3.6a The surface of section for H_2 dynamics generated using Nosé-Hoover equations. Q = 35, T = 4000K, initial conditions r = 3.3 a.u. and p_r = 0.0 a.u.

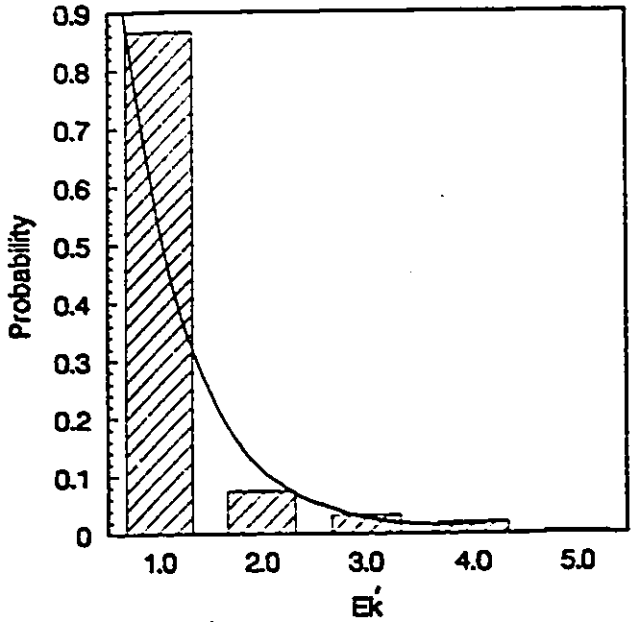

Fig. 3.6b The kinetic energy distribution, normalized to 4000K, corresponding to Fig. 3.6a.

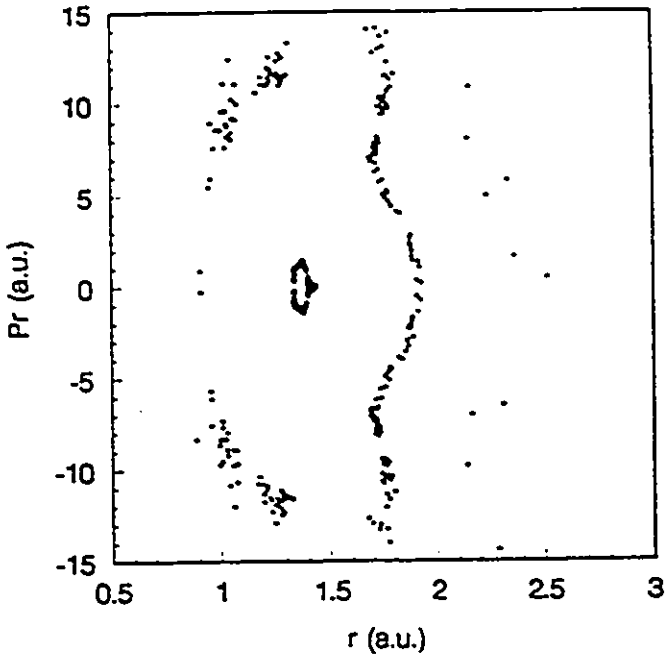

Fig. 3.7a The surface of section for H_2 dynamics generated using Nosé-Hoover equations. Q = 40, T = 4000K, initial conditions r = 3.3 a.u. and p_r = 0.0 a.u.

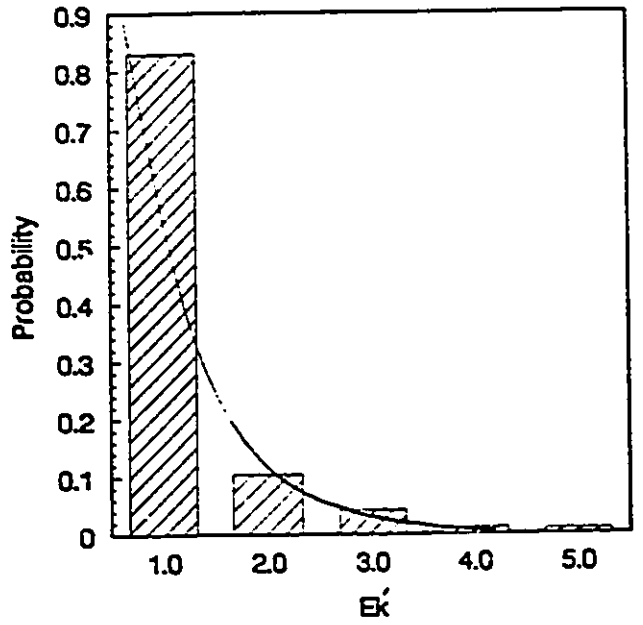

Fig. 3.7b The kinetic energy distribution, normalized to 4000K, corresponding to Fig. 3.7a.

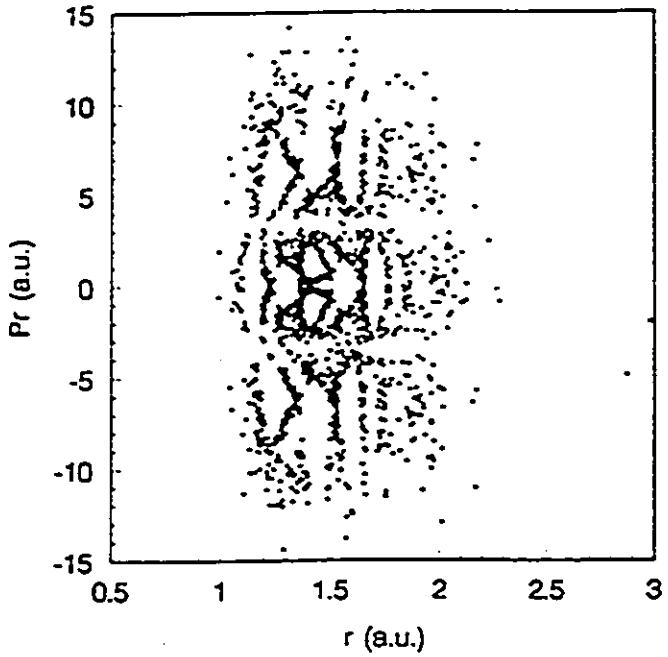

Fig. 3.8a The surface of section for H_2 dynamics generated using Nosé-Hoover equations. Q = 5, T = 4000K, initial conditions r = 3.3 a.u. and p_r = 0.0 a.u.

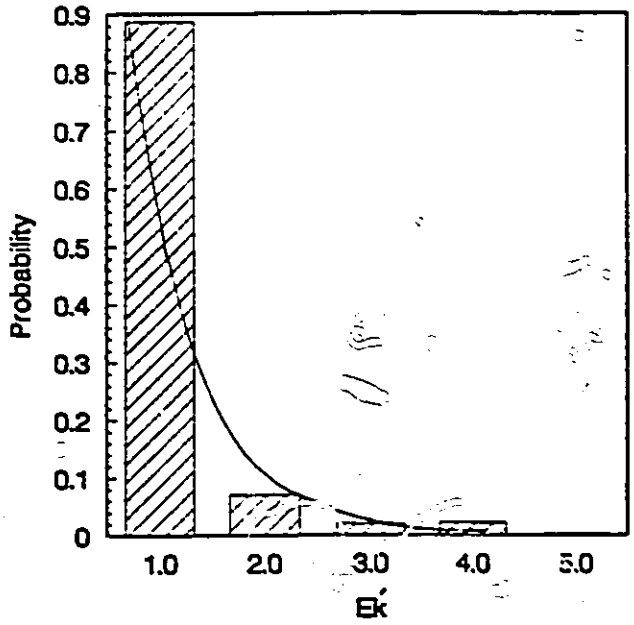

Fig. 3.8b The kinetic energy distribution, normalized to 4000K, corresponding to Fig. 3.8a.

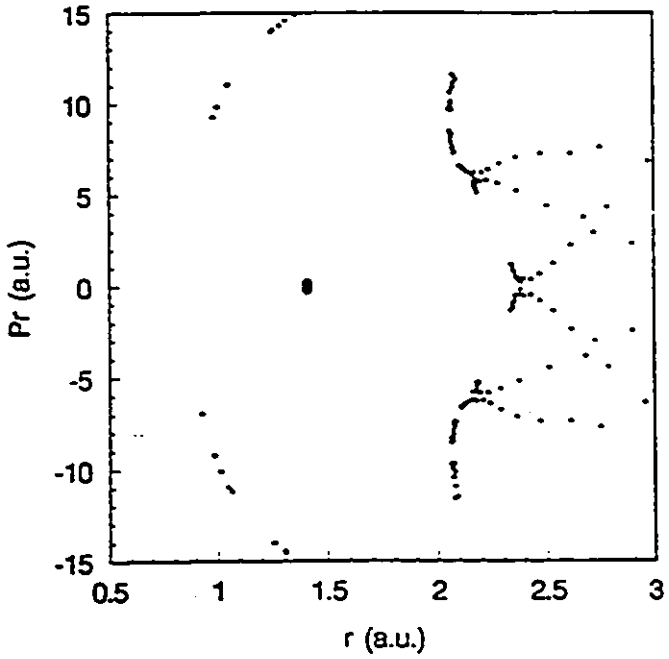

Fig. 3.9a The surface of section for H_2 dynamics generated using Nosé-Hoover equations. Q = 125, T = 4000K, initial conditions r = 3.3 a.u. and p_r = 0.0 a.u.

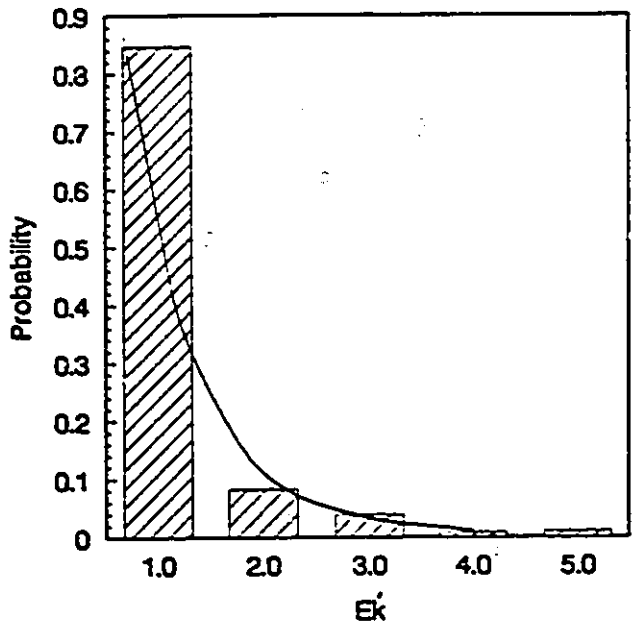

Fig. 3.9b The kinetic energy distribution, normalized to 4000K, corresponding to Fig. 3.9a.

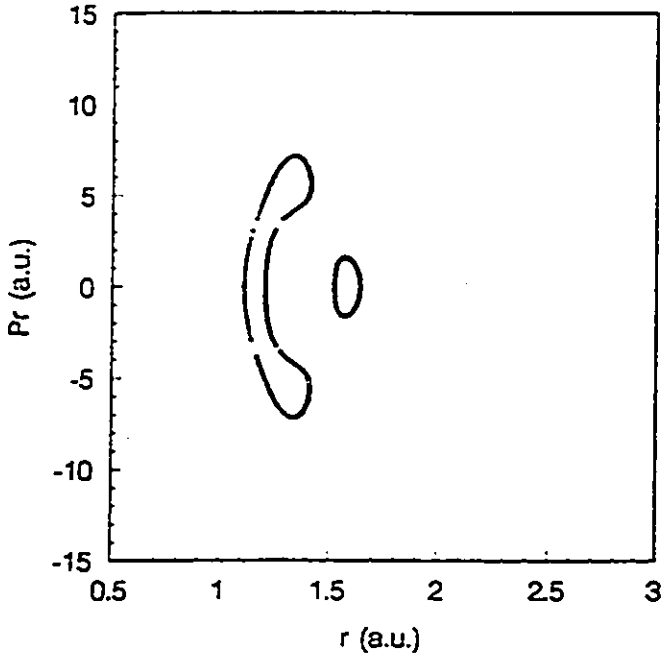

Fig. 3.10a The surface of section for H_2 dynamics generated using Nosé-Hoover equations. Q = 25, T = 4000K, initial conditions r = 1.5 a.u. and p_r = 0.0 a.u.

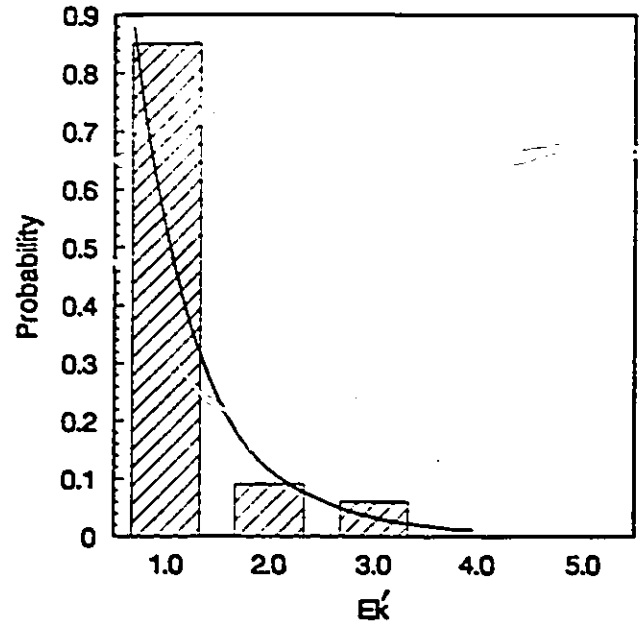

Fig. 3.10b The kinetic energy distribution, normalized to 4000K, corresponding to Fig. 3.10a.

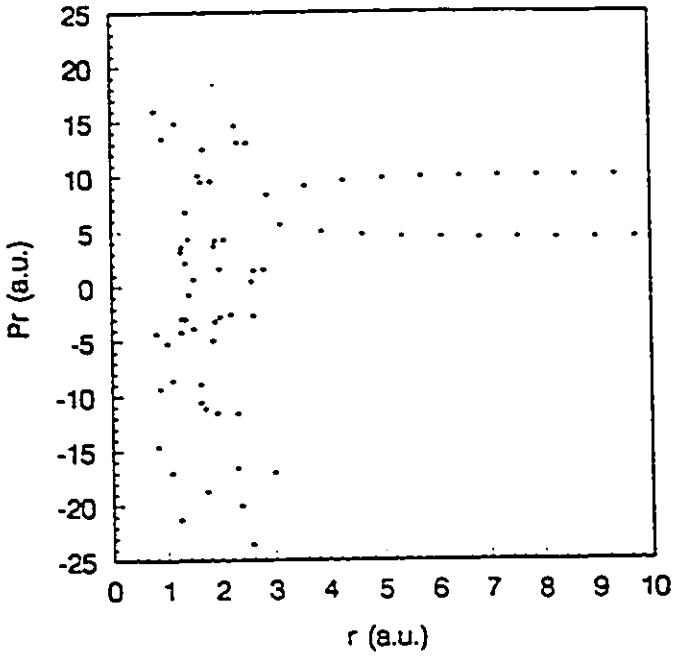

Fig. 3.11a The surface of section for H_2 dynamics generated using Nosé-Hoover equations. Q = 25, T = 17000K, initial conditions r = 3.3 a.u. and p_r = 0.0 a.u.

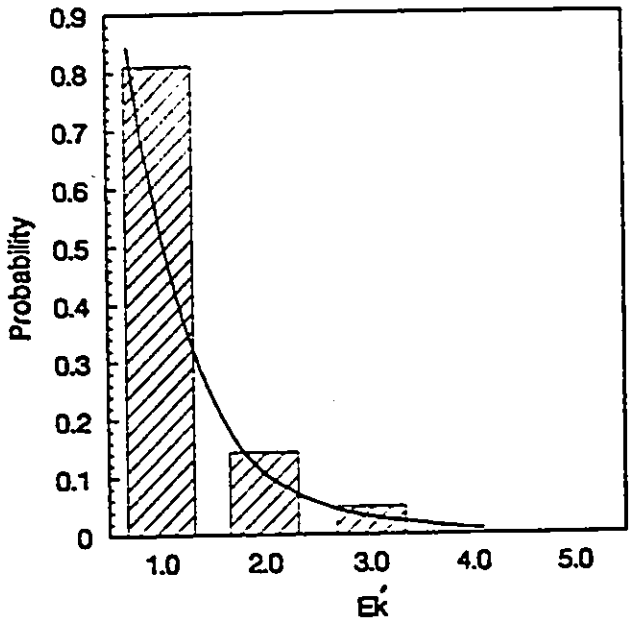

Fig. 3.11b The kinetic energy distribution, normalized to 17000K, corresponding to Fig. 3.11a.

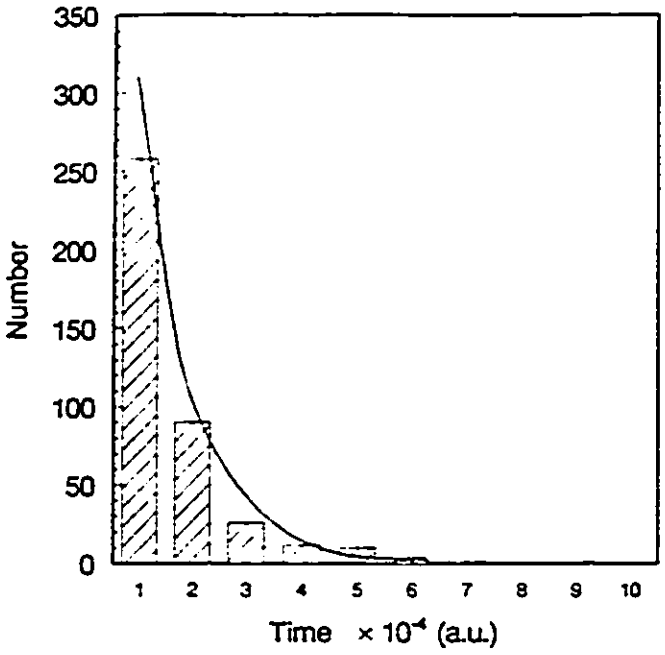

Fig. 3.12 The lifetime distribution for H_2 dissociation at T = 17000K, calculated using Nosé-Hoover equations.

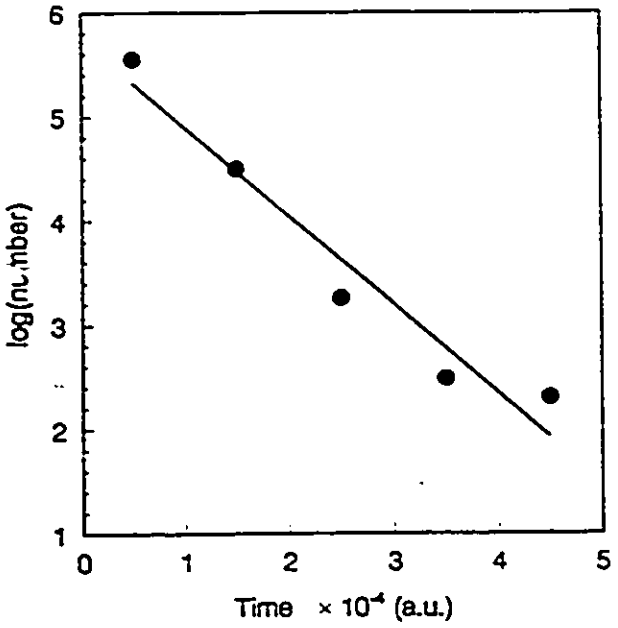

Fig. 3.13 Least-squares fit for the rate constant of H_2 dissociation at T = 17000K, calculated using Nosé-Hoover equations. $k_d = 3.52 \pm 0.48 \times 10^{12}$ sec.$^{-1}$

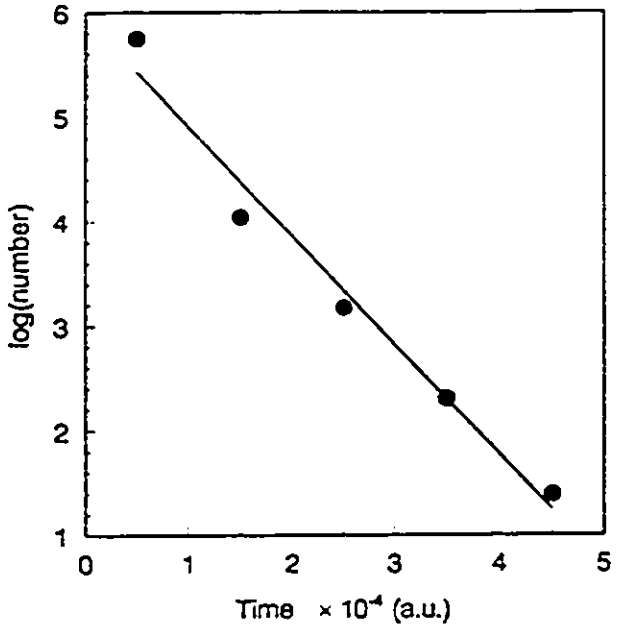

Fig. 3.14 Least-squares fit for the rate constant of H_2 dissociation at T = 19000K, calculated using Nosé-Hoover equations. $k_d = 4.33 \pm 0.39 \times 10^{12}$ sec.$^{-1}$

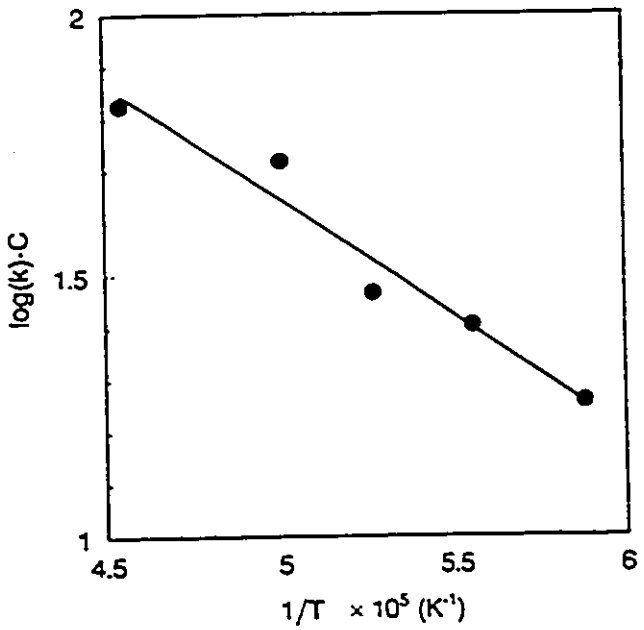

Fig. 3.15 Arrhenius plot of a least-squares fit for the activation energy of H_2 dissociation, calculated using Nosé-Hoover equations. $E_a = 3.55 \pm 0.48$ eV. $C = \log(10^{12}) = 27.63$.

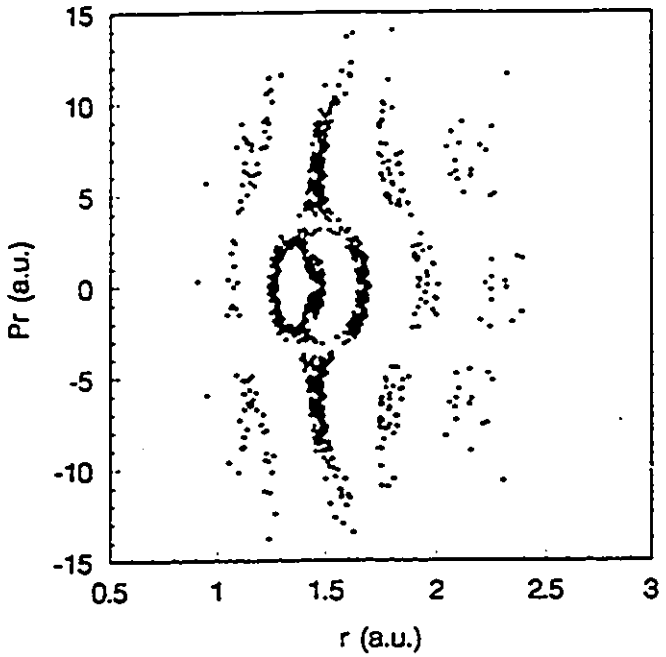

Fig. 3.16a The surface of section for H_2 dynamics generated using Nosé-Hoover equations, including rotation. Q = 17, T = 4000K, initial conditions r = 3.3 a.u. and p_r = 0.0 a.u.

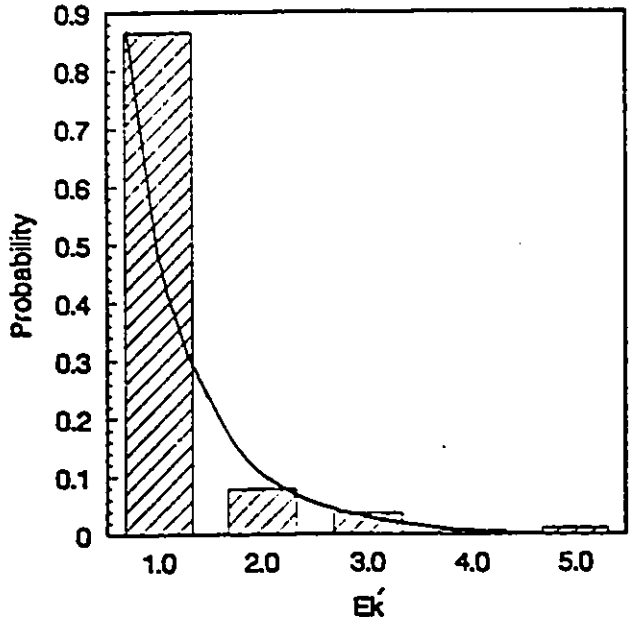

Fig. 3.16b The kinetic energy distribution, normalized to 4000K, corresponding to Fig. 3.16a.

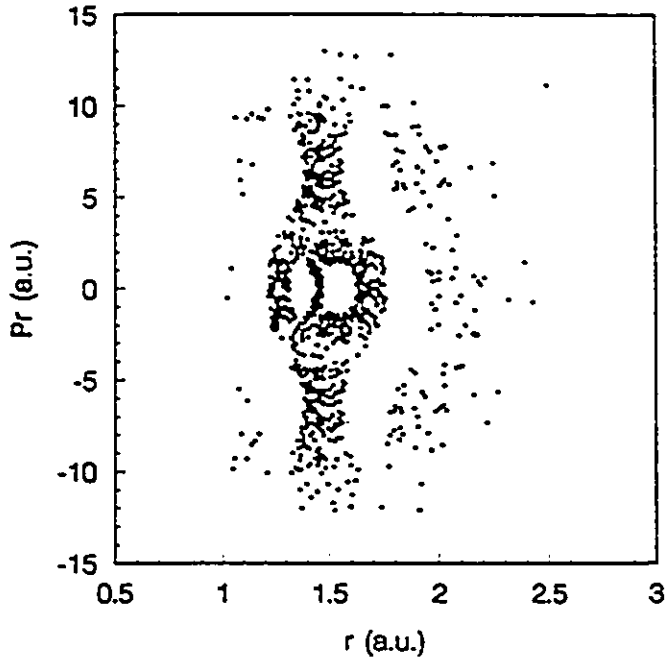

Fig. 3.17a The surface of section for H_2 dynamics generated using Nosé-Hoover equations, including rotation. Q = 20, T = 4000K, initial conditions r = 3.3 a.u. and p_r = 0.0 a.u.

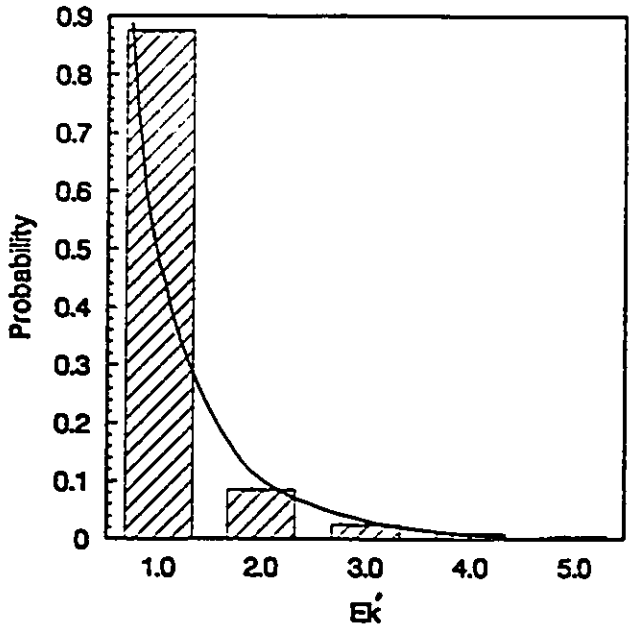

Fig. 3.17b The kinetic energy distribution, normalized to 4000K, corresponding to Fig. 3.17a.

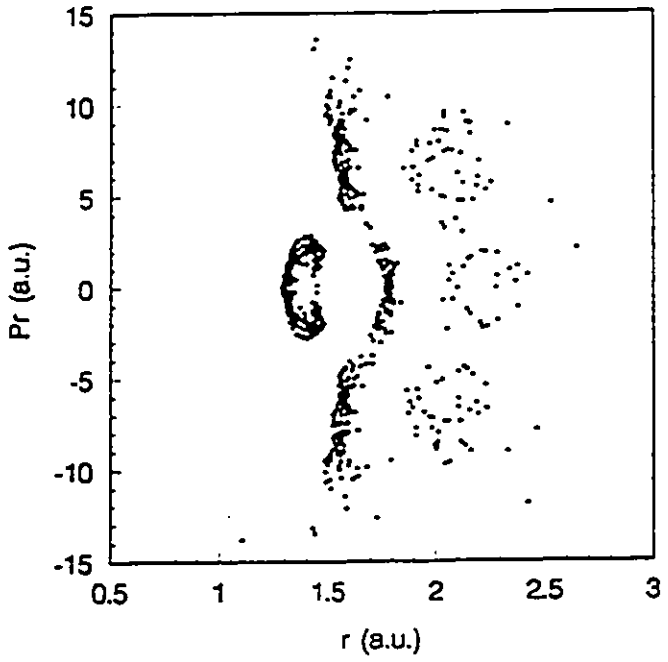

Fig. 3.18a The surface of section for H_2 dynamics generated using Nosé-Hoover equations, including rotation. Q = 25, T = 4000K, initial conditions r = 3.3 a.u. and p_r = 0.0 a.u.

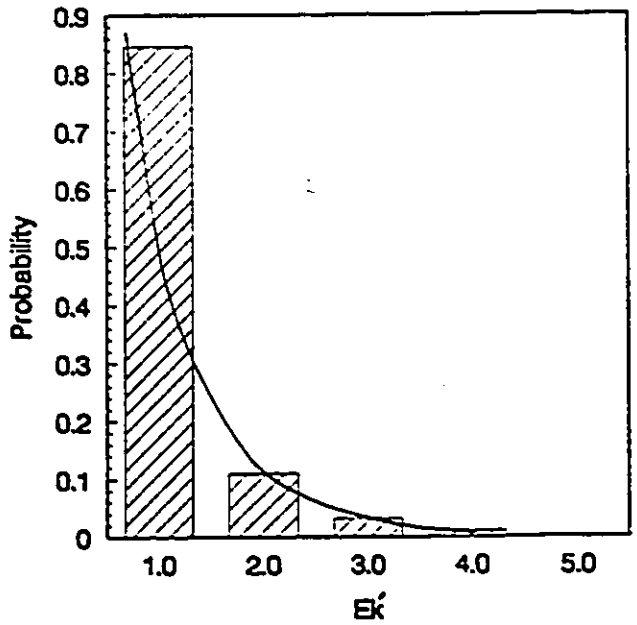

Fig. 3.18b The kinetic energy distribution, normalized to 4000K, corresponding to Fig. 3.18a.

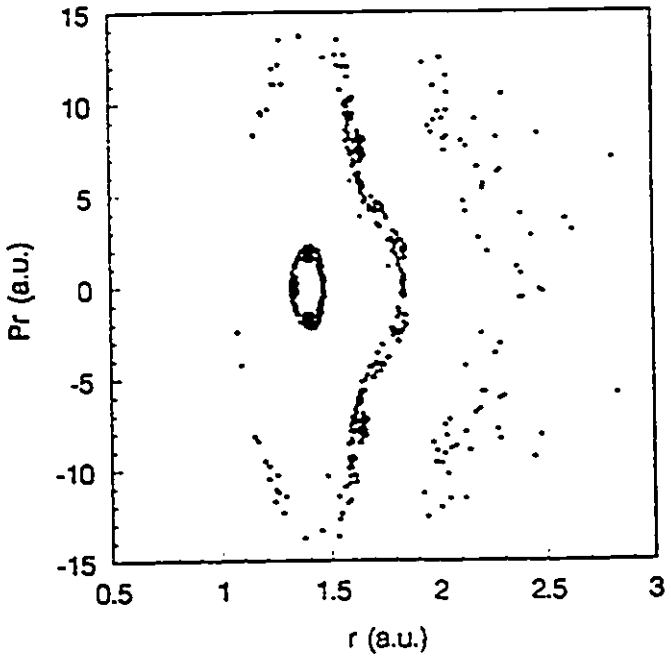

Fig. 3.19a The surface of section for H_2 dynamics generated using Nosé-Hoover equations, including rotation. Q = 30, T = 4000K, initial conditions r = 3.3 a.u. and p_r = 0.0 a.u.

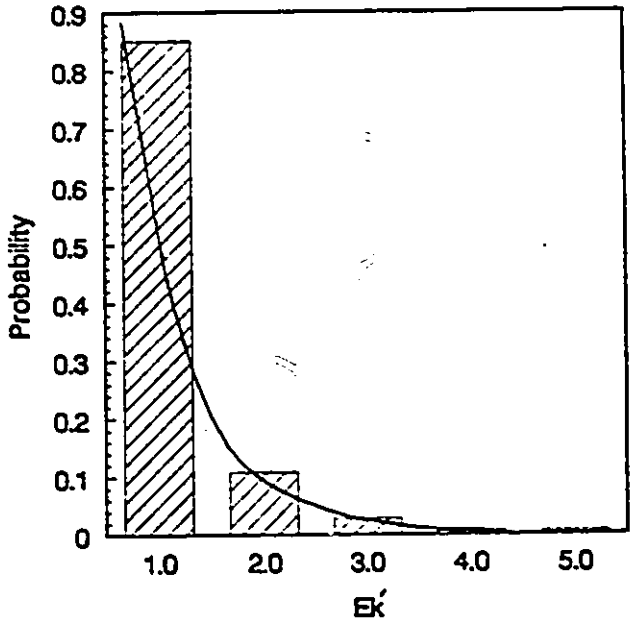

Fig. 3.19b The kinetic energy distribution, normalized to 4000K, corresponding to Fig. 3.19a.

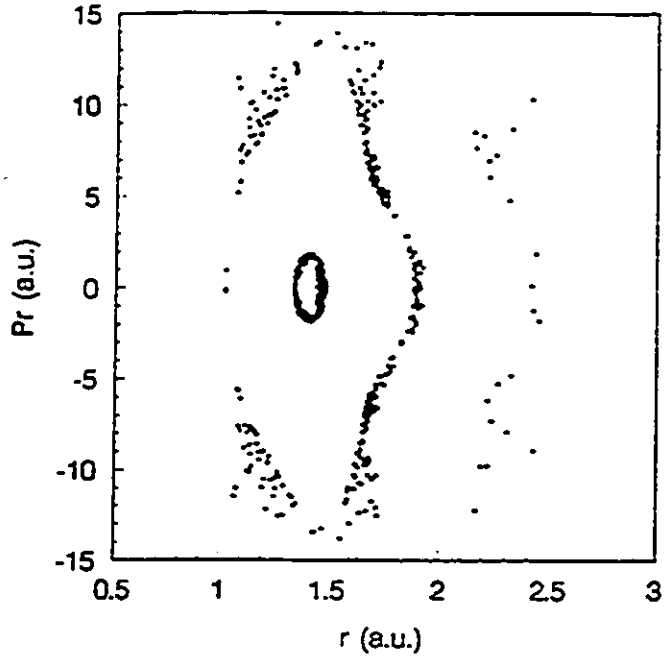

Fig. 3.20a The surface of section for H_2 dynamics generated using Nosé-Hoover equations, including rotation. Q = 35, T = 4000K, initial conditions r = 3.3 a.u. and p_r = 0.0 a.u.

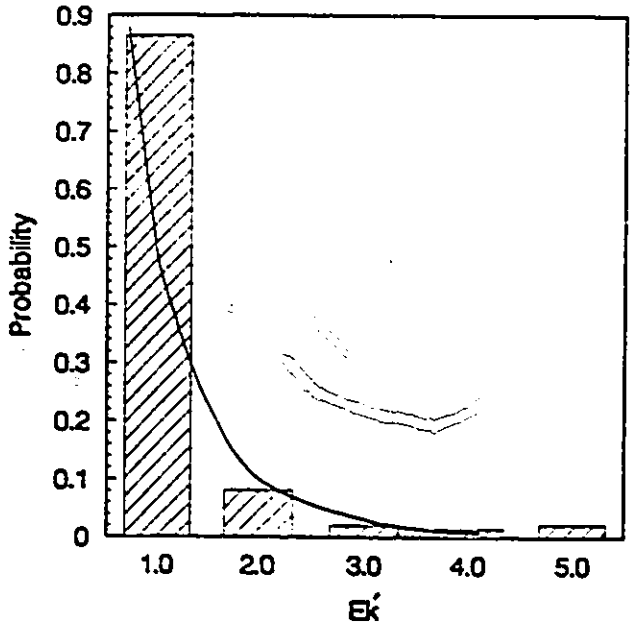

Fig. 3.20b The kinetic energy distribution, normalized to 4000K, corresponding to Fig. 3.20a.

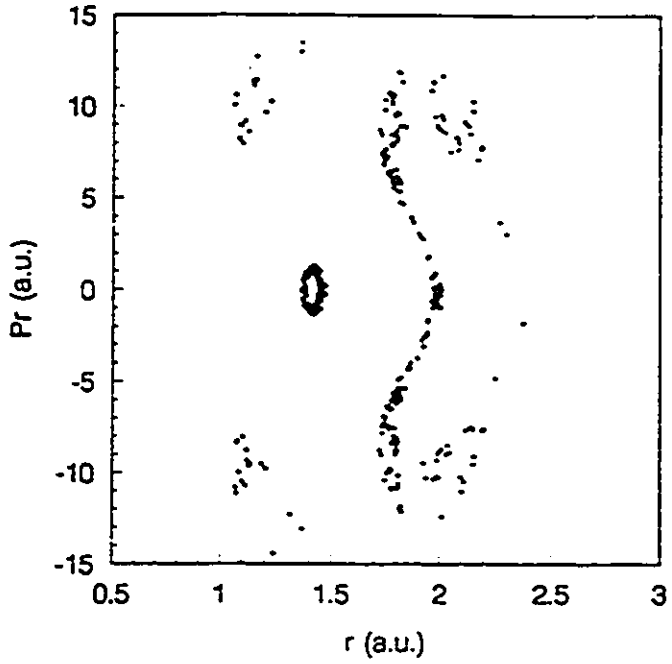

Fig. 3.21a The surface of section for H_2 dynamics generated using Nosé-Hoover equations, including rotation. Q = 40, T = 4000K, initial conditions r = 3.3 a.u. and p_r = 0.0 a.u.

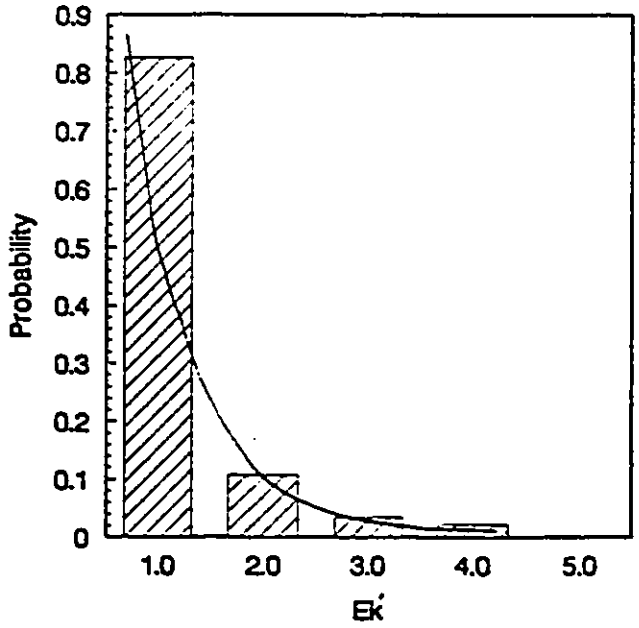

Fig. 3.21b The kinetic energy distribution, normalized to 4000K, corresponding to Fig. 3.21a.

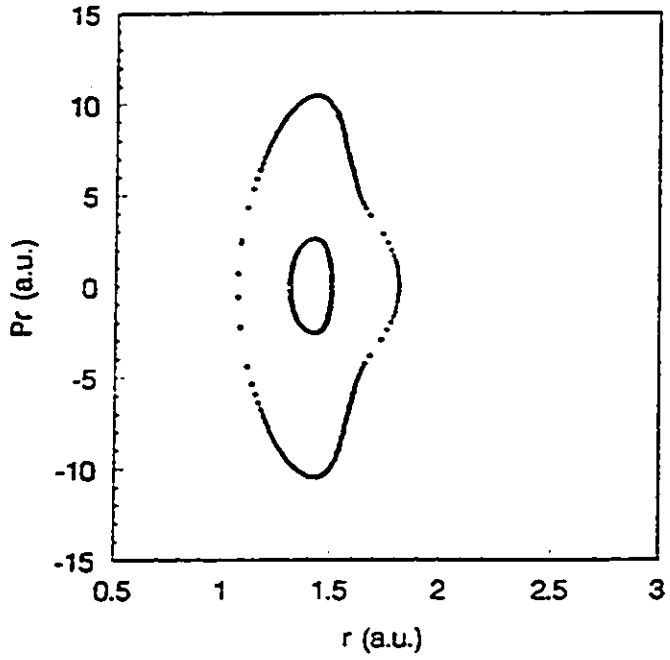

Fig. 3.22a The surface of section for H_2 dynamics generated using Nosé-Hoover equations, including rotation. Q = 30, T = 4000K, initial conditions r = 1.5 a.u. and p_r = 0.0 a.u.

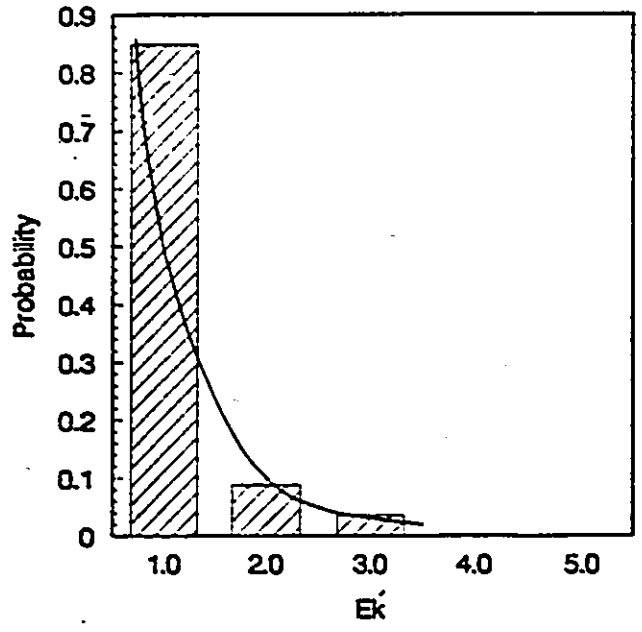

Fig. 3.22b The kinetic energy distribution, normalized to 4000K, corresponding to Fig. 3.22a.

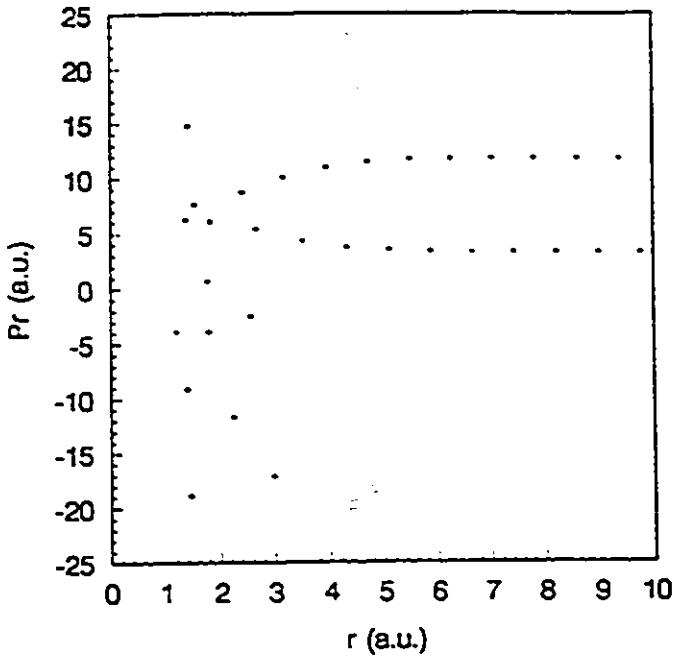

Fig. 3.23a The surface of section for H_2 dynamics generated using Nosé-Hoover equations, including rotation. Q = 30, T = 17000K, initial conditions r = 3.3 a.u. and p_r = 0.0 a.u.

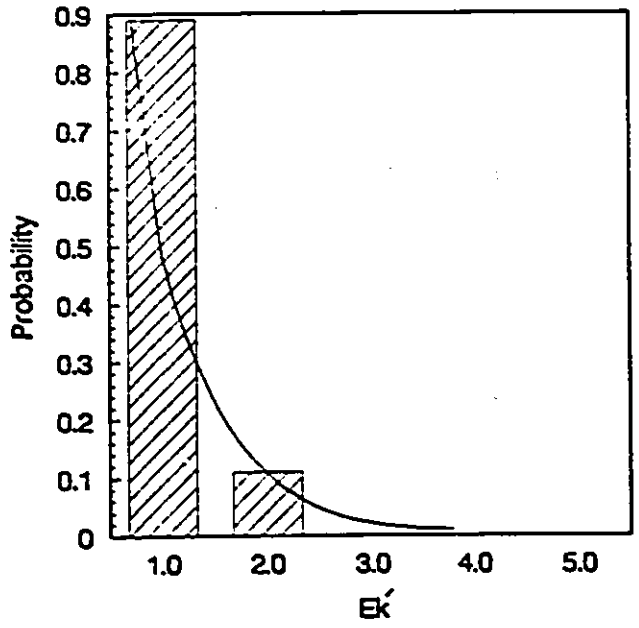

Fig. 3.23b The kinetic energy distribution, normalized to 17000K, corresponding to Fig. 3.23a.

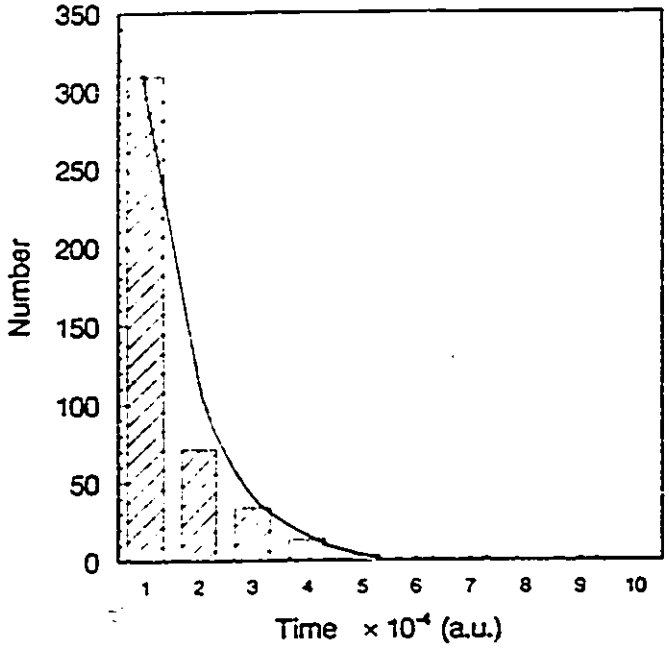

Fig. 3.24 The lifetime distribution for H_2 dissociation at T = 17000K, calculated using Nosé-Hoover equations, including rotation.

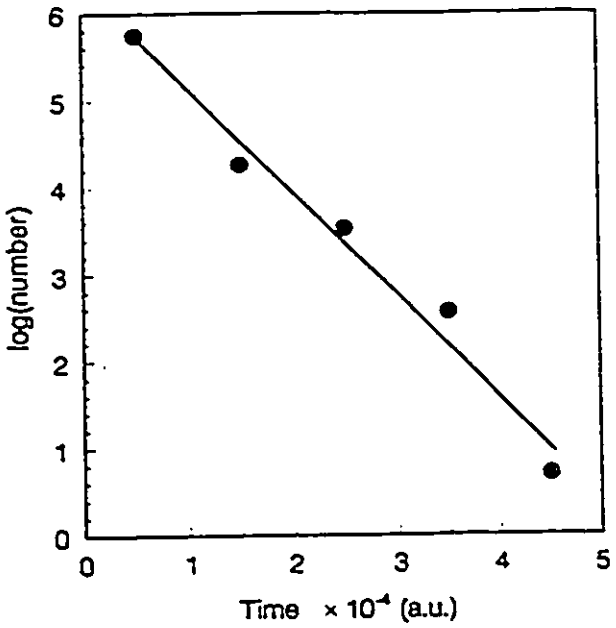

Fig. 3.25 Least-squares fit for the rate constant of H_2 dissociation at T = 17000K, calculated using Nosé-Hoover equations, including rotation.
$k_d = 4.88 \pm 0.44 \times 10^{12}$ sec.$^{-1}$

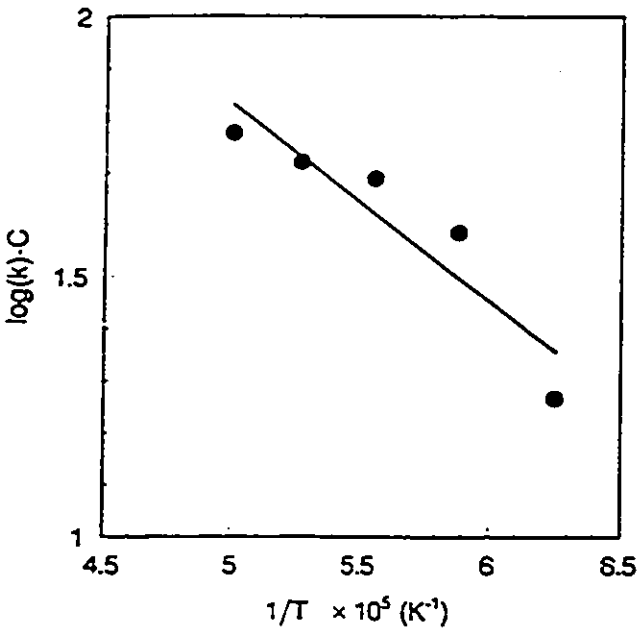

Fig. 3.26 Arrhenius plot of a least-squares fit for the activation energy of H_2 dissociation, calculated using Nosé-Hoover equations, including rotation.
$E_a = 3.00 \pm 0.77$ eV. $C = \log(10^{12}) = 27.63$.

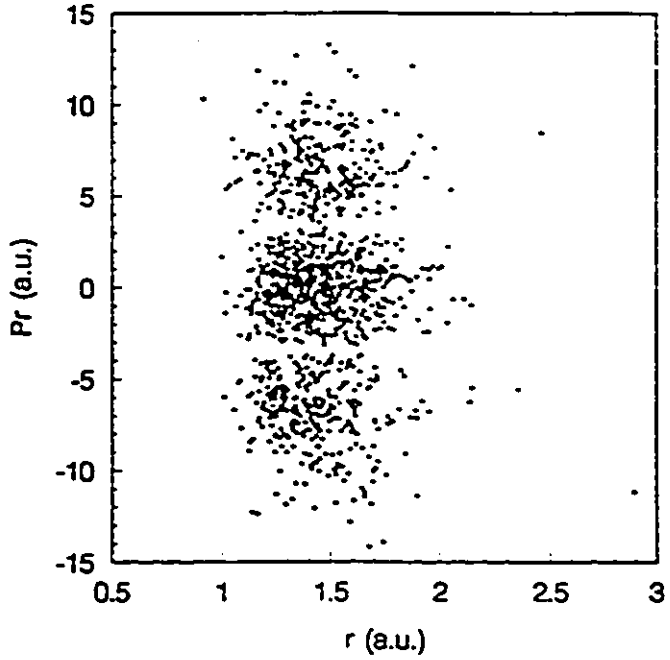

Fig. 4.1a The surface of section for H_2 dynamics generated using modified Nosé-Hoover equations. $Q_1 = Q_2 = 15$, T = 4000K, initial conditions r = 3.3 a.u. and $p_r = 0.0$ a.u.

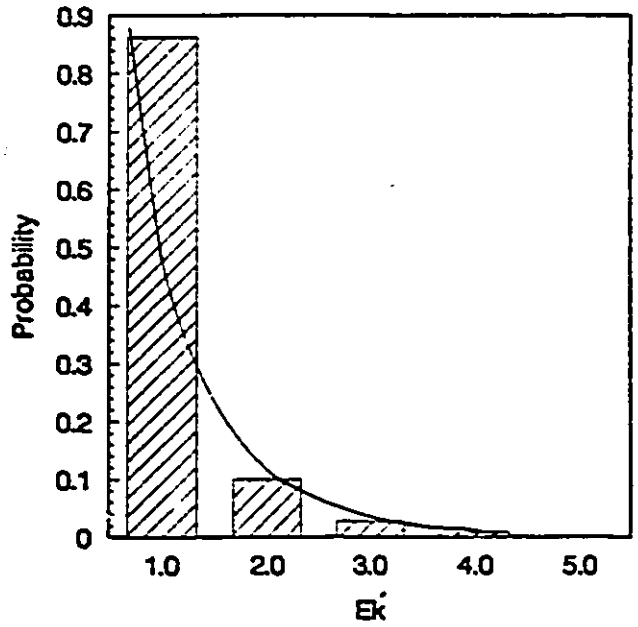

Fig. 4.1b The kinetic energy distribution, normalized to 4000K, corresponding to Fig. 4.1a.

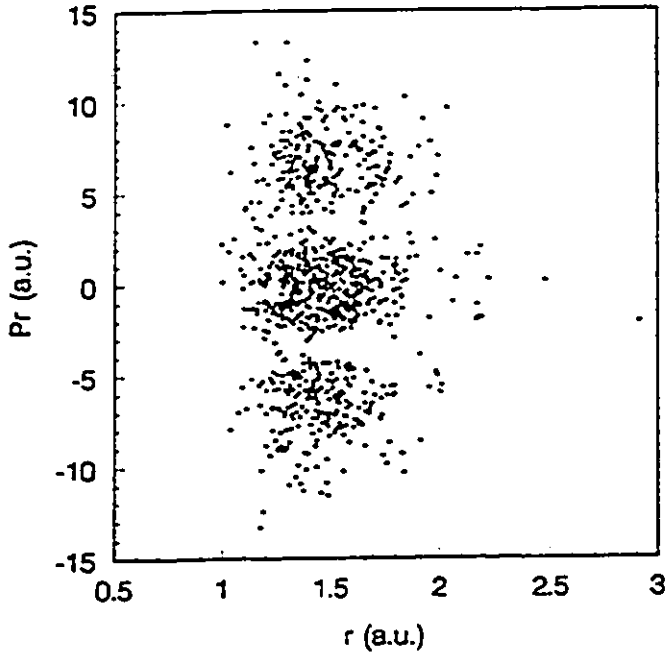

Fig. 4.2a The surface of section for H_2 dynamics generated using modified Nosé-Hoover equations. $Q_1 = Q_2 = 25$, T = 4000K, initial conditions r = 3.3 a.u. and $p_r = 0.0$ a.u.

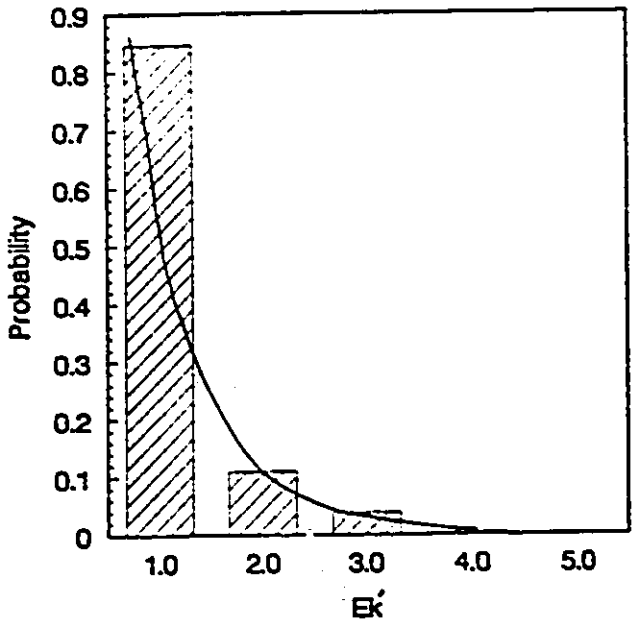

Fig. 4.2b The kinetic energy distribution, normalized to 4000K, corresponding to Fig. 4.2a.

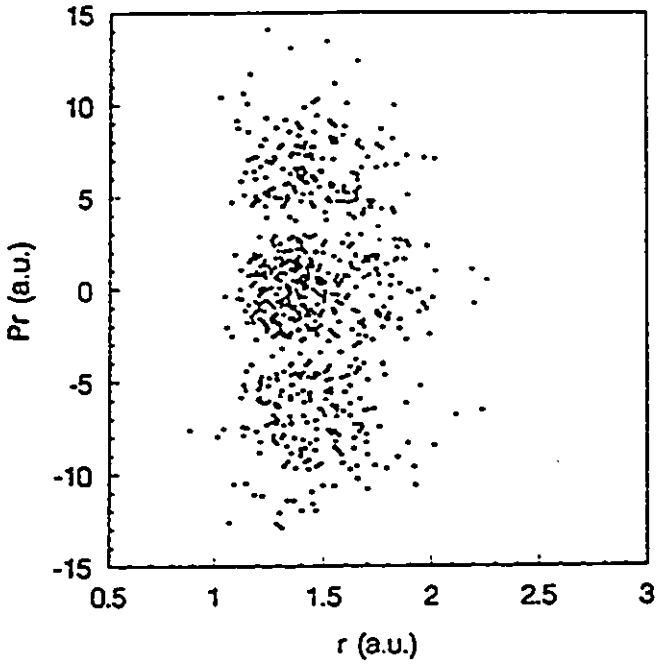

Fig. 4.3a The surface of section for H_2 dynamics generated using modified Nosé-Hoover equations. $Q_1 = Q_2 = 35$, T = 4000K, initial conditions r = 3.3 a.u. and $p_r = 0.0$ a.u.

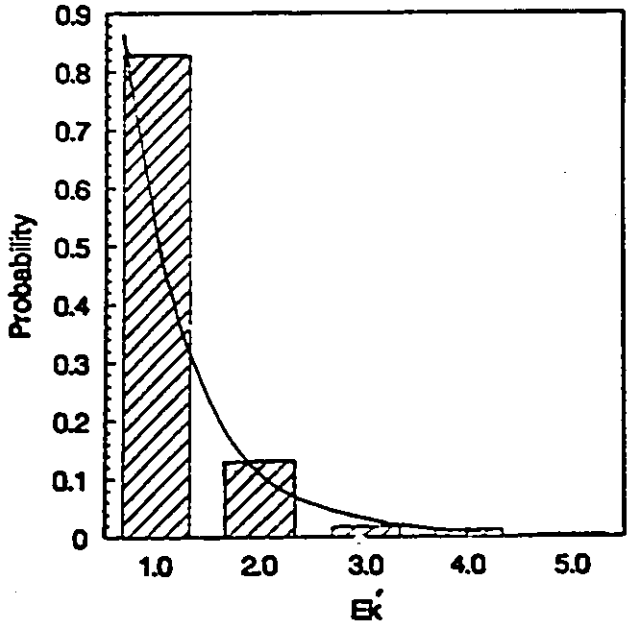

Fig. 4.3b The kinetic energy distribution, normalized to 4000K, corresponding to Fig. 4.3a.

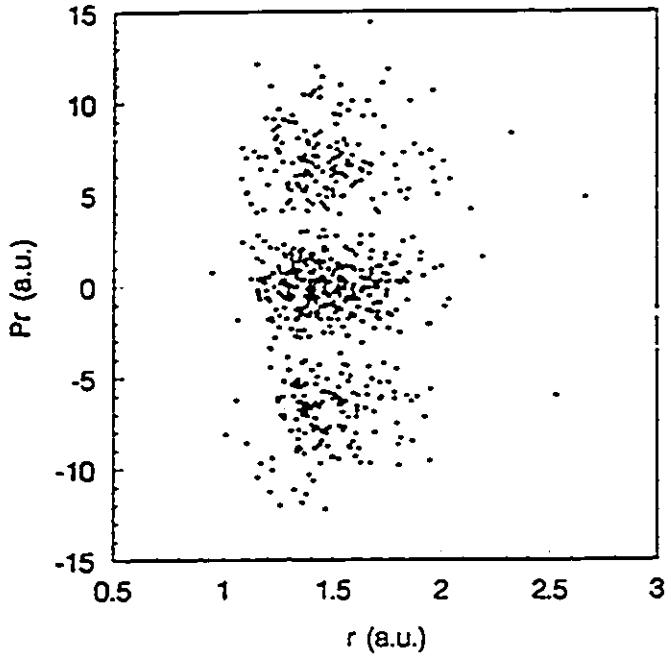

Fig. 4.4a The surface of section for H_2 dynamics generated using modified Nosé-Hoover equations. $Q_1 = Q_2 = 45$, T = 4000K, initial conditions r = 3.3 a.u. and $p_r = 0.0$ a.u.

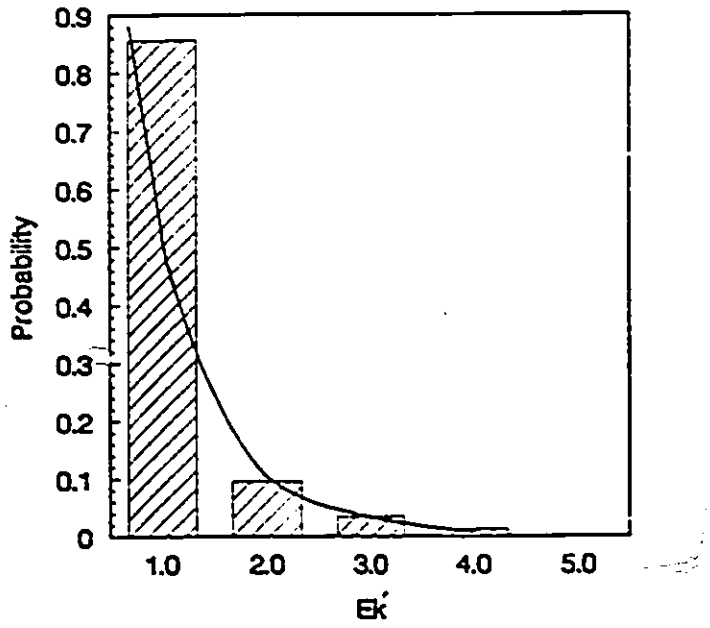

Fig. 4.4b The kinetic energy distribution, normalized to 4000K, corresponding to Fig. 4.4a.

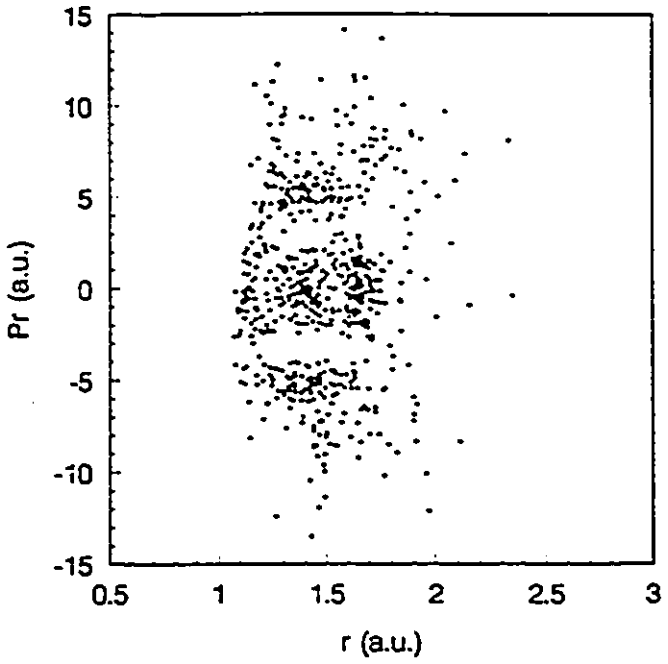

Fig. 4.5a The surface of section for H_2 dynamics generated using modified Nosé-Hoover equations. $Q_1 = Q_2 = 55$, T = 4000K, initial conditions r = 3.3 a.u. and $p_r = 0.0$ a.u.

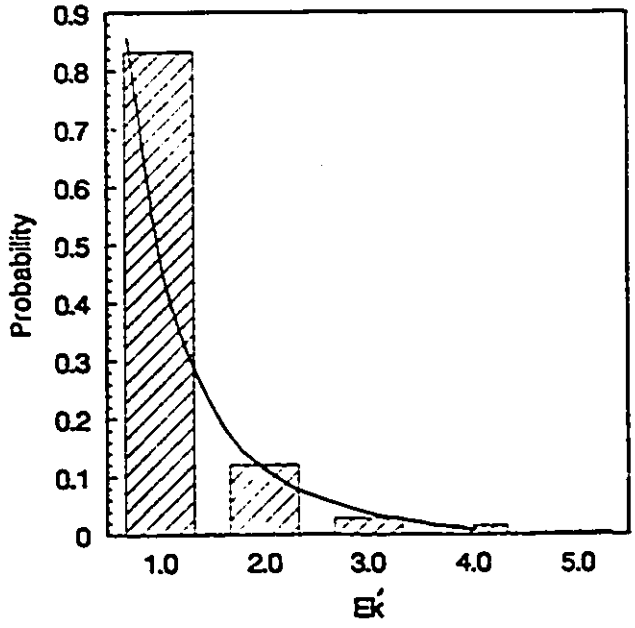

Fig. 4.5b The kinetic energy distribution, normalized to 4000K, corresponding to Fig. 4.5a.

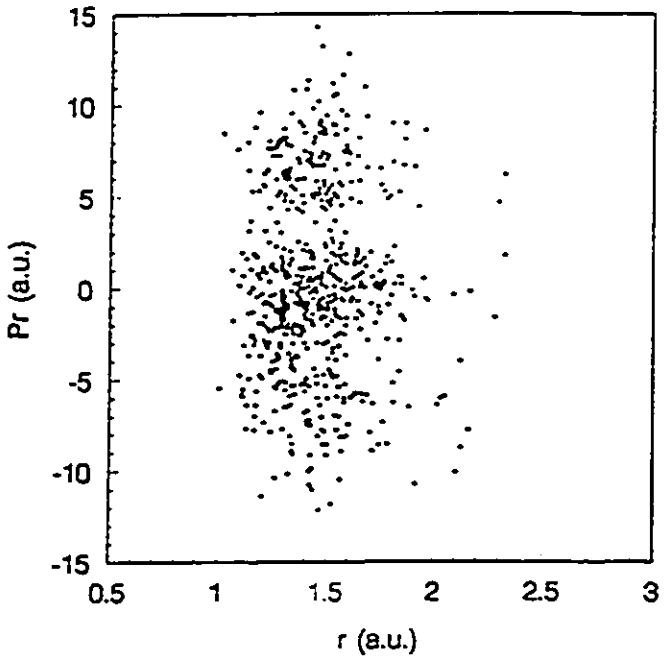

Fig. 4.6a The surface of section for H_2 dynamics generated using modified Nosé-Hoover equations. $Q_1 = 15$, $Q_2 = 55$, T = 4000K, initial conditions r = 3.3 a.u. and $p_r = 0.0$ a.u.

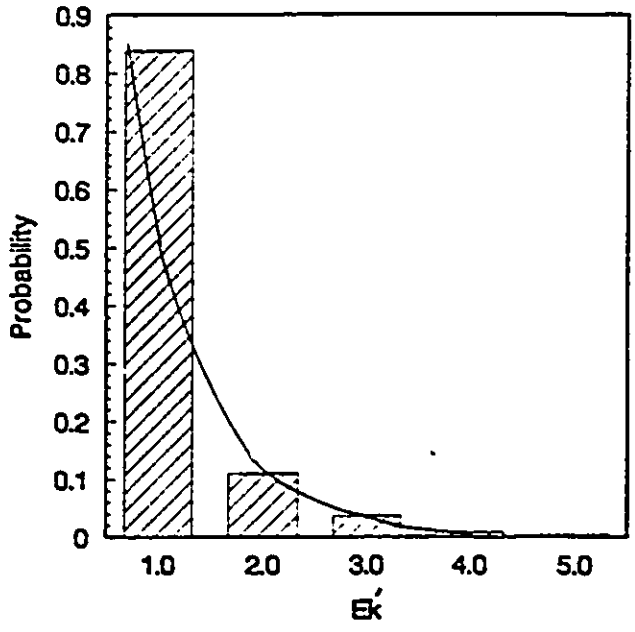

Fig. 4.6b The kinetic energy distribution, normalized to 4000K, corresponding to Fig. 4.6a.

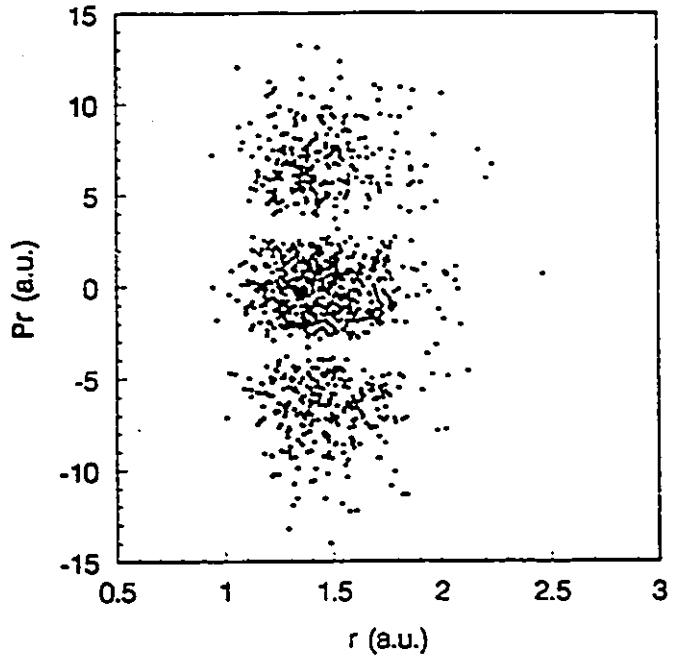

Fig. 4.7a The surface of section for H_2 dynamics generated using modified Nosé-Hoover equations. $Q_1 = 55$, $Q_2 = 15$, T = 4000K, initial conditions r = 3.3 a.u. and $p_r = 0.0$ a.u.

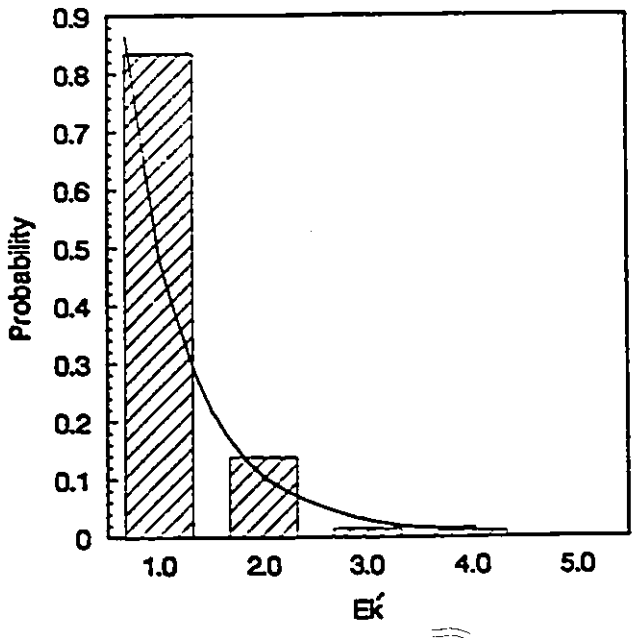

Fig. 4.7b The kinetic energy distribution, normalized to 4000K, corresponding to Fig. 4.7a.

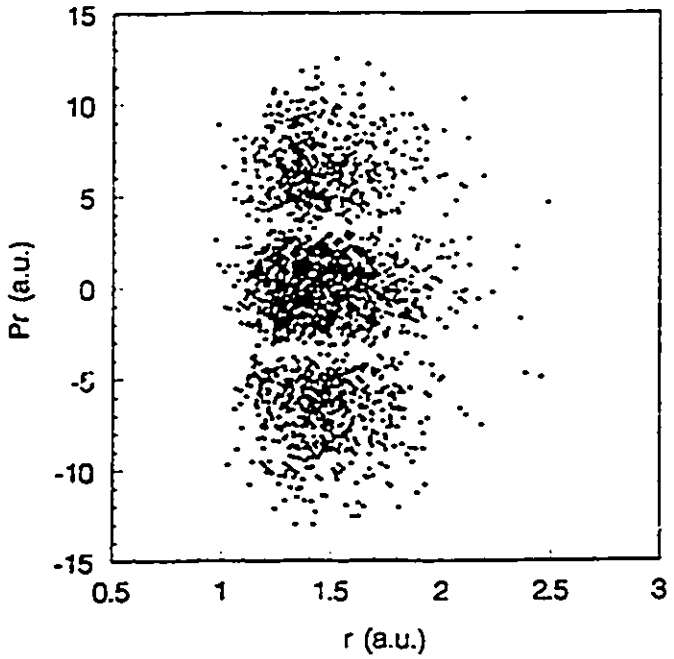

Fig. 4.8a The surface of section for H_2 dynamics generated using modified Nosé-Hoover equations. $Q_1 = Q_2 = 3.5$, T = 4000K, initial conditions r = 3.3 a.u. and $p_r = 0.0$ a.u.

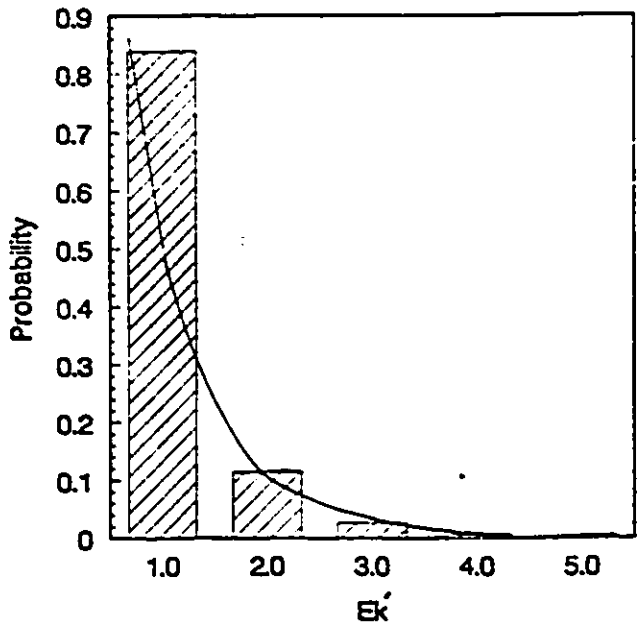

Fig. 4.8b The kinetic energy distribution, normalized to 4000K, corresponding to Fig. 4.8a.

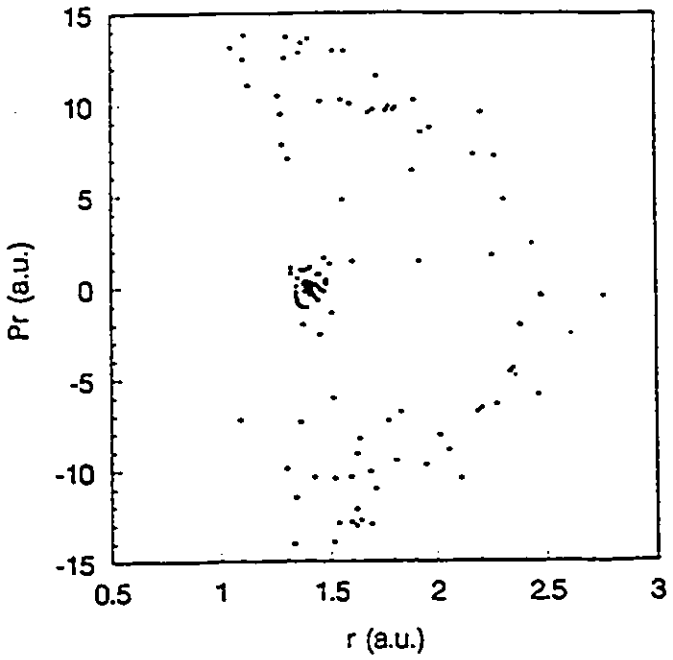

Fig. 4.9a The surface of section for H_2 dynamics generated using modified Nosé-Hoover equations. $Q_1 = Q_2 = 700$, T = 4000K, initial conditions r = 3.3 a.u. and $p_r = 0.0$ a.u.

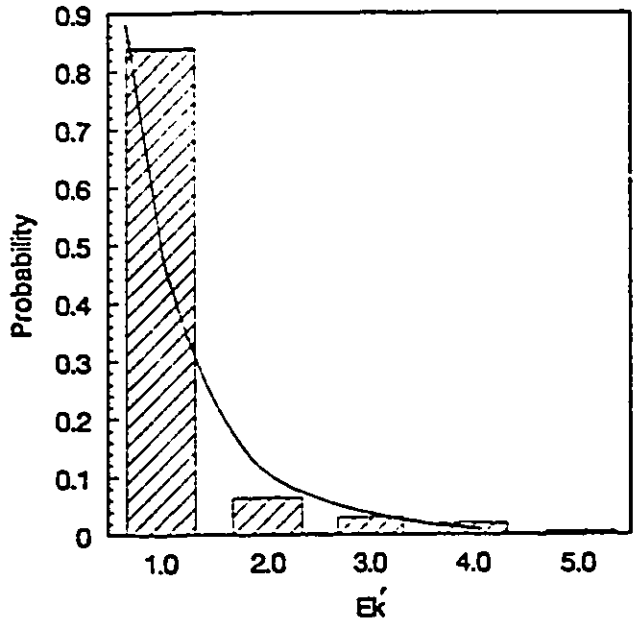

Fig. 4.9b The kinetic energy distribution, normalized to 4000K, corresponding to Fig. 4.9a.

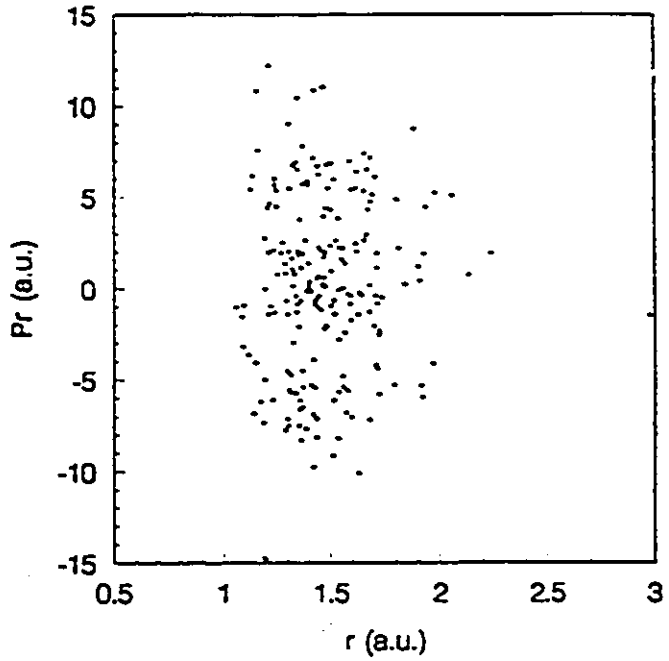

Fig. 4.10a The surface of section for H_2 dynamics generated using modified Nosé-Hoover equations. $Q_1 = 3.5$, $Q_2 = 700$, T = 4000K, initial conditions r = 3.3 a.u. and $p_r = 0.0$ a.u.

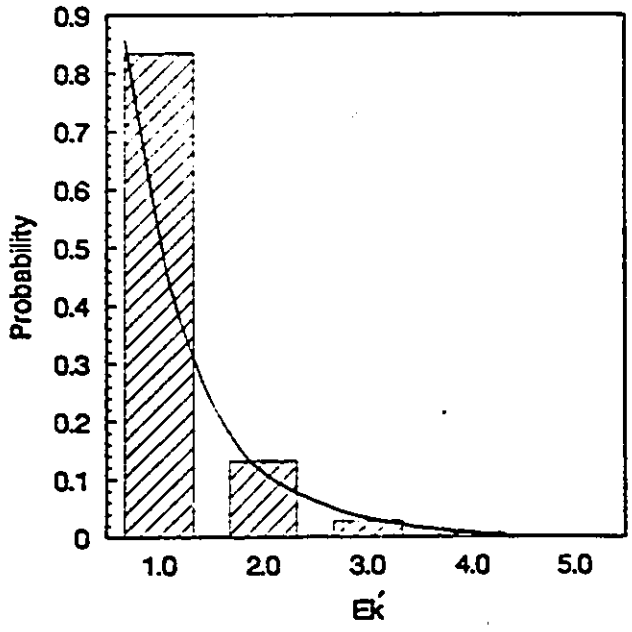

Fig. 4.10b The kinetic energy distribution, normalized to 4000K, corresponding to Fig. 4.10a.

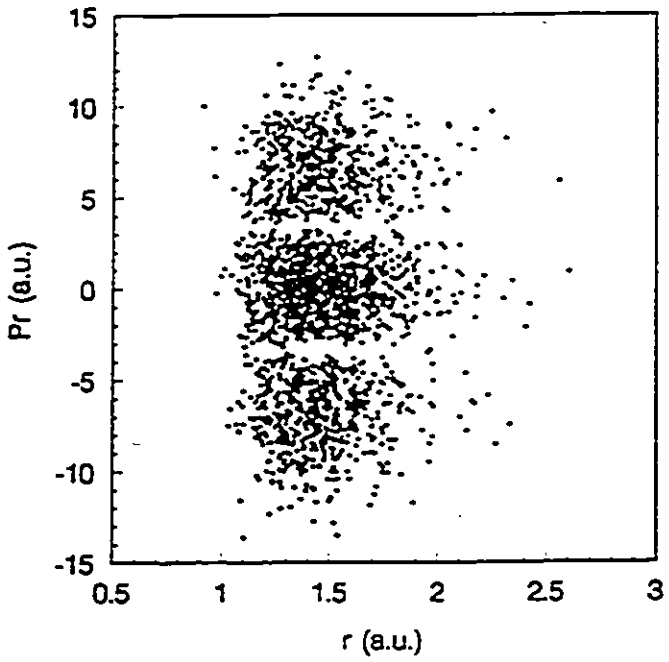

Fig. 4.11a The surface of section for H_2 dynamics generated using modified Nosé-Hoover equations. $Q_1 = 700$, $Q_2 = 3.5$, T = 4000K, initial conditions r = 3.3 a.u. and $p_r = 0.0$ a.u.

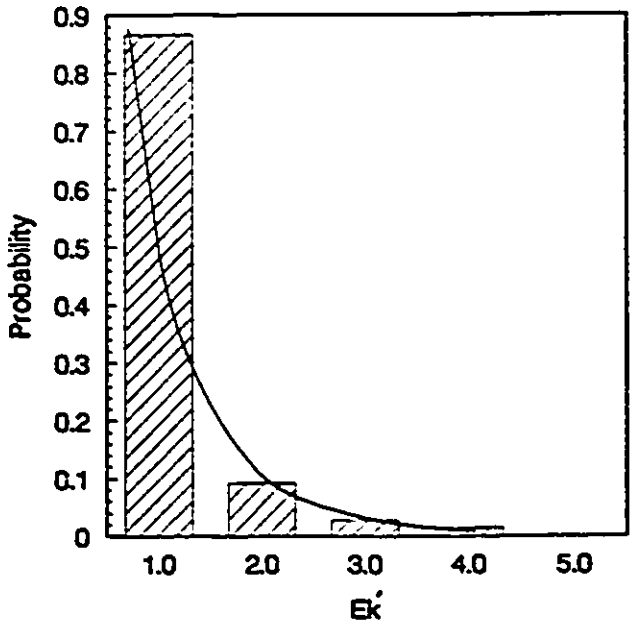

Fig. 4.11b The kinetic energy distribution, normalized to 4000K, corresponding to Fig. 4.11a.

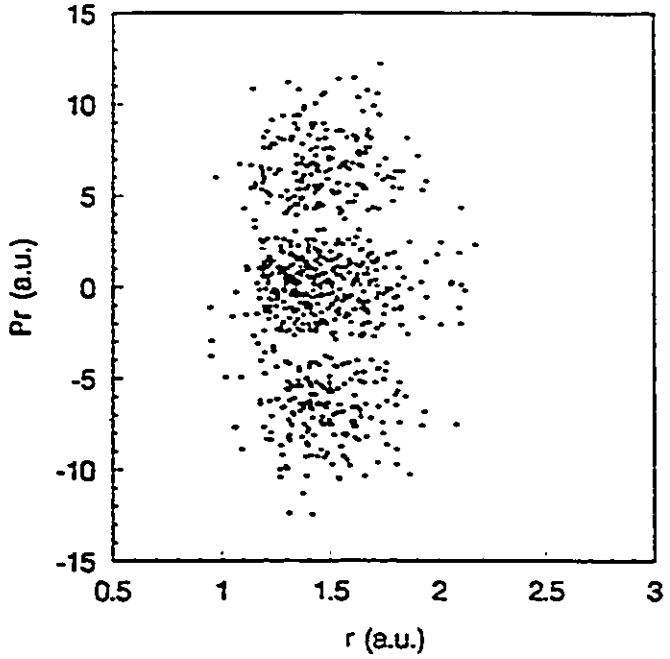

Fig. 4.12a The surface of section for H_2 dynamics generated using modified Nosé-Hoover equations. $Q_1 = Q_2 = 35$, T = 4000K, initial conditions r = 1.5 a.u. and $p_r = 0.0$ a.u.

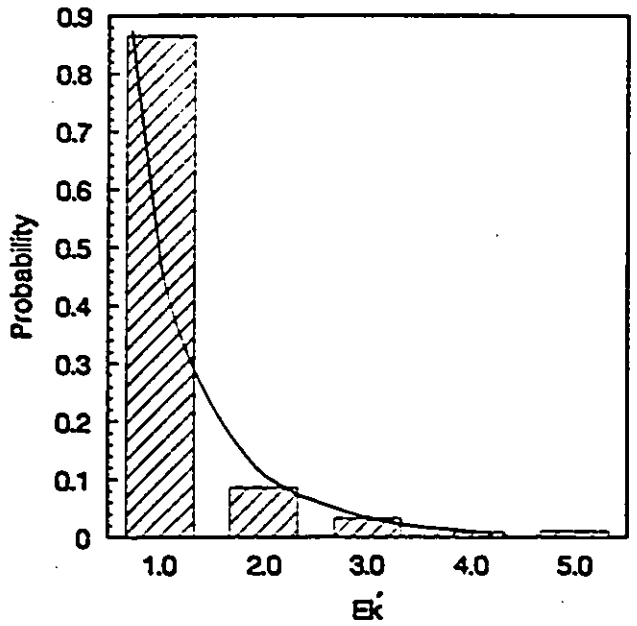

Fig. 4.12b The kinetic energy distribution, normalized to 4000K, corresponding to Fig. 4.12a.

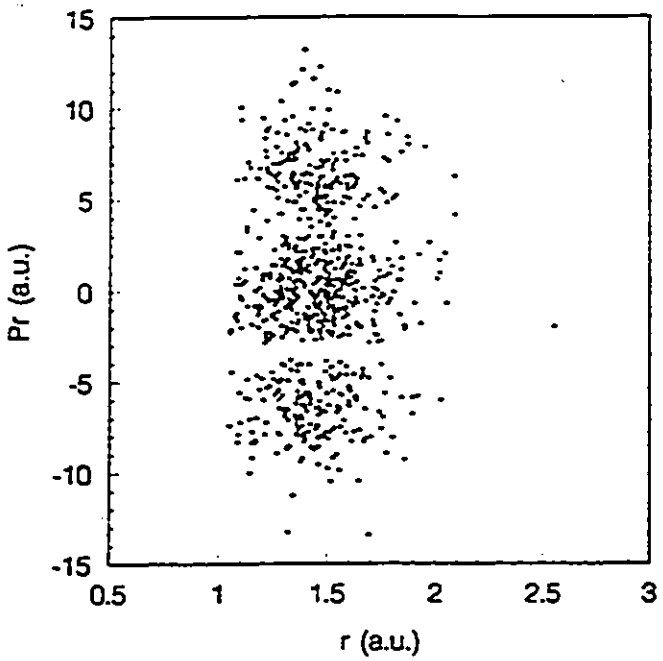

Fig. 4.13a The surface of section for H_2 dynamics generated using modified Nosé-Hoover equations. $Q_1 = Q_2 = 35$, T = 4000K, initial conditions r = 1.3 a.u. and $p_r = 0.0$ a.u.

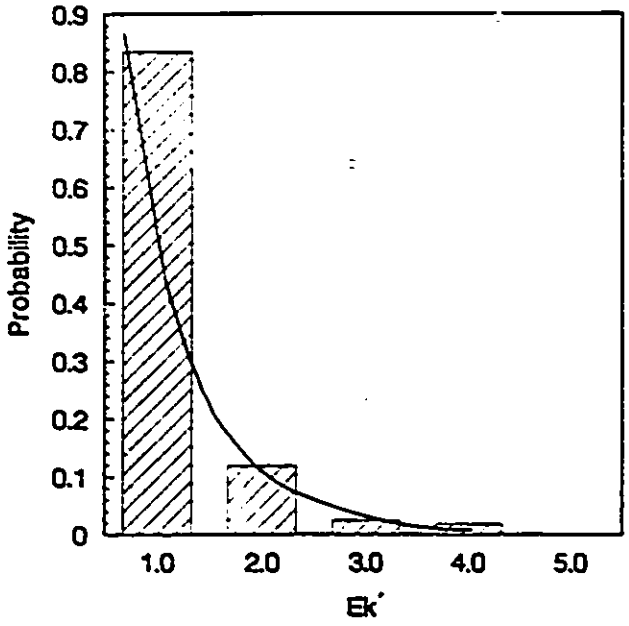

Fig. 4.13b The kinetic energy distribution, normalized to 4000K, corresponding to Fig. 4.13a.

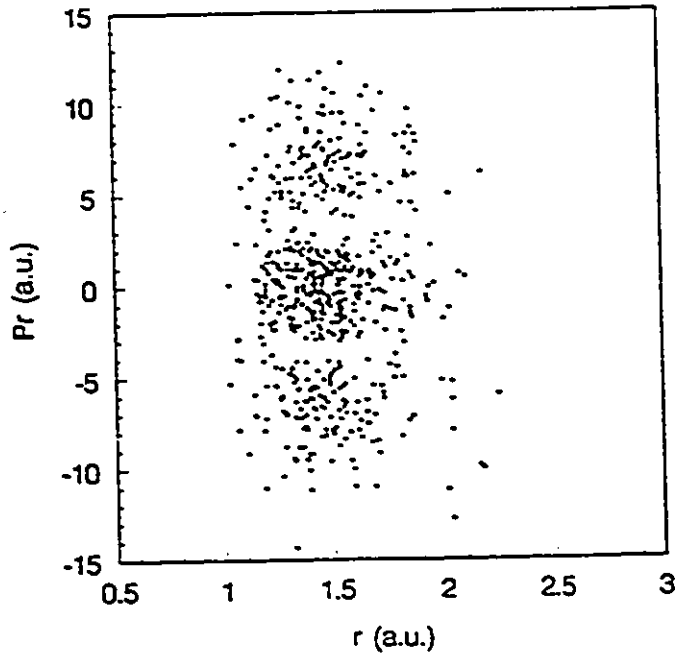

Fig. 4.14a The surface of section for H_2 dynamics generated using modified Nosé-Hoover equations. $Q_1 = 15$, $Q_2 = 55$, T = 4000K, initial conditions r = 1.5 a.u. and $p_r = 0.0$ a.u.

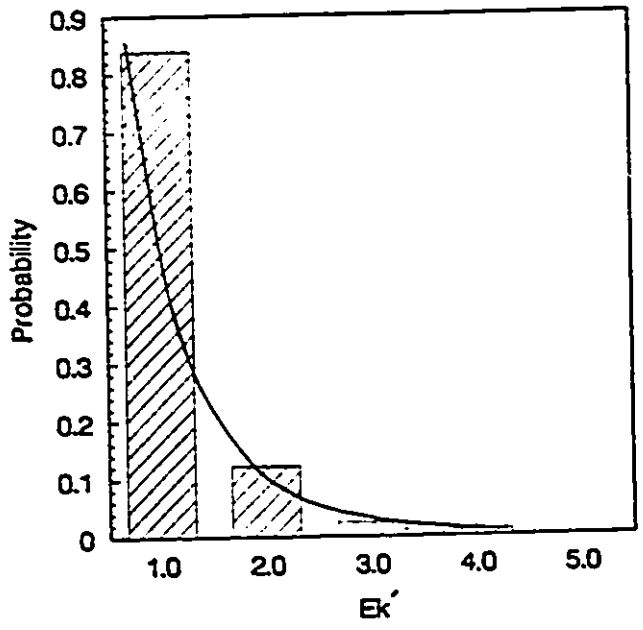

Fig. 4.14b The kinetic energy distribution, normalized to 4000K, corresponding to Fig. 4.14a.

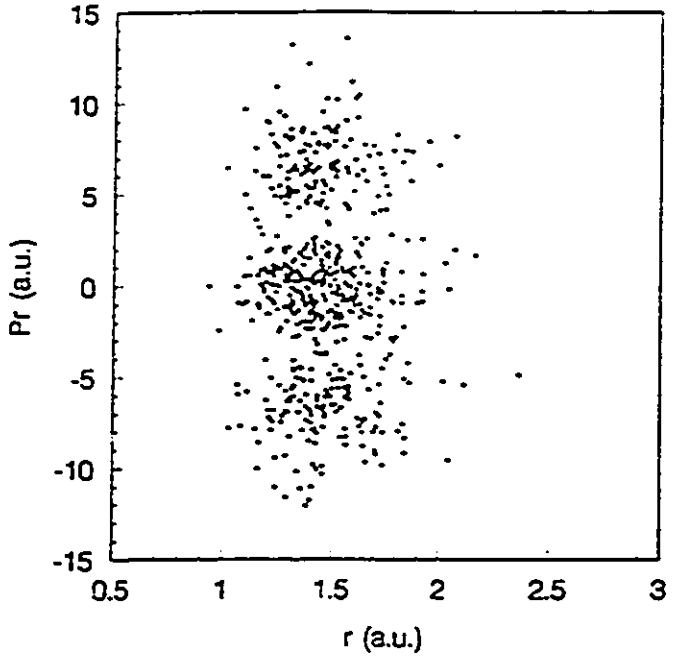

Fig. 4.15a The surface of section for H_2 dynamics generated using modified Nosé-Hoover equations. $Q_1 = 15$, $Q_2 = 55$, T = 4000K, initial conditions r = 1.3 a.u. and $p_r = 0.0$ a.u.

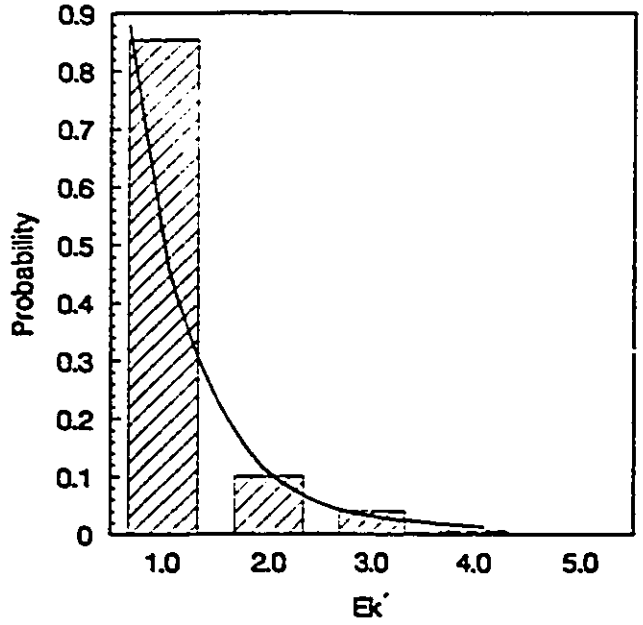

Fig. 4.15b The kinetic energy distribution, normalized to 4000K, corresponding to Fig. 4.15a.

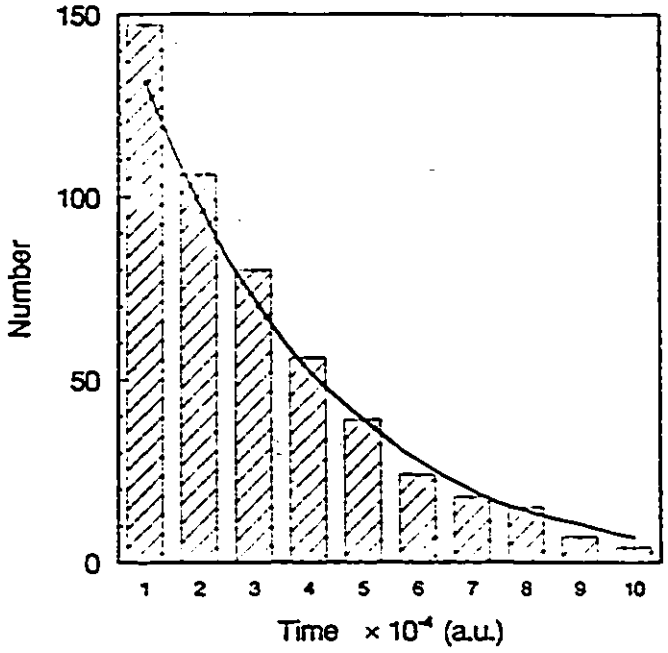

Fig. 4.16 The lifetime distribution for H_2 dissociation at T = 7250K, calculated using modified Nosé-Hoover equations.

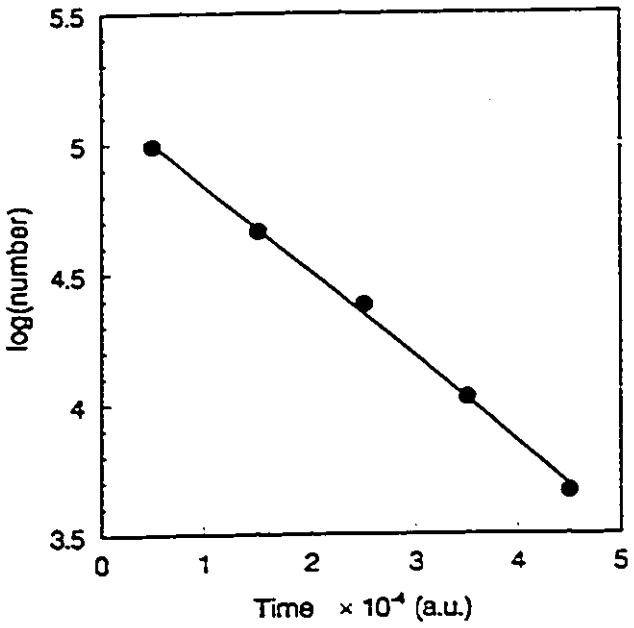

Fig. 4.17 Least-squares fit for the rate constant of H_2 dissociation at T = 7250K, calculated using modified Nosé-Hoover equations. $k_d = 1.36 \pm 0.04 \times 10^{12}$ sec.$^{-1}$

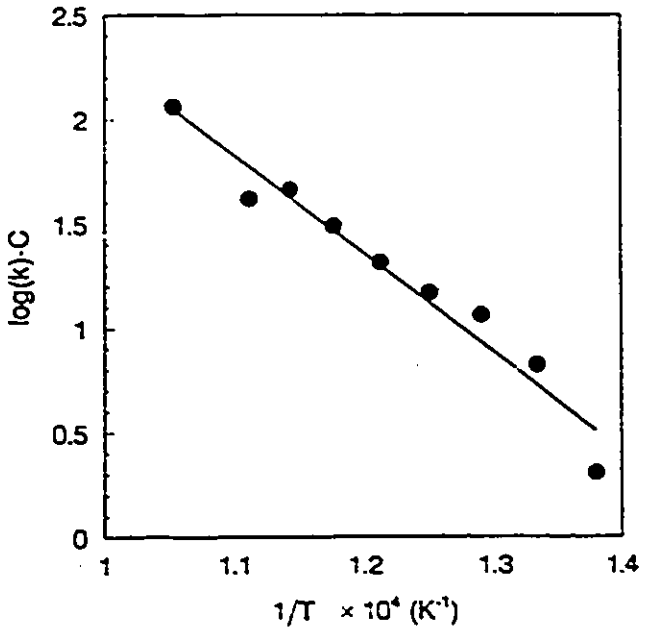

Fig. 4.18 Arrhenius plot of a least-squares fit for the activation energy of H_2 dissociation, calculated using modified Nosé-Hoover equations.
$E_a = 3.78 \pm 0.33$ eV. $C = \log(10^{12}) = 27.63$.

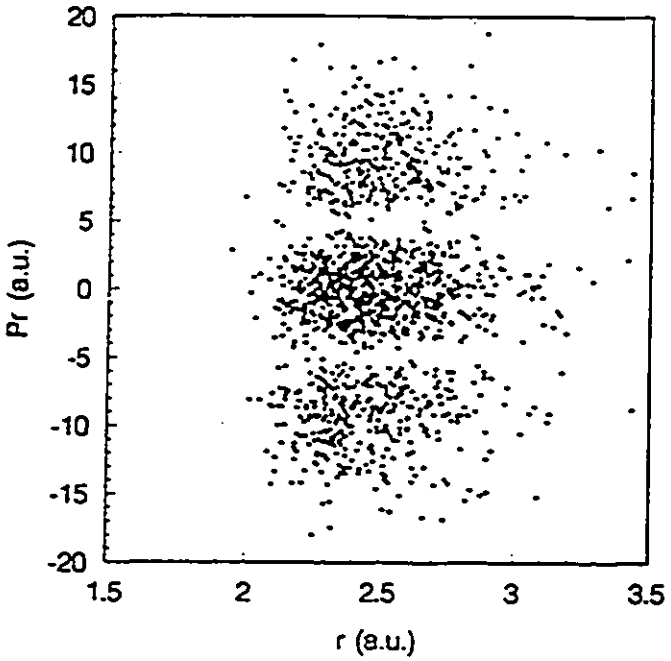

Fig. 4.19a The surface of section for HCl dynamics generated using modified Nosé-Hoover equations. $Q_1 = Q_2 = 10$, T = 4000K, initial conditions r = 2.6 a.u. and $p_r = 0.0$ a.u.

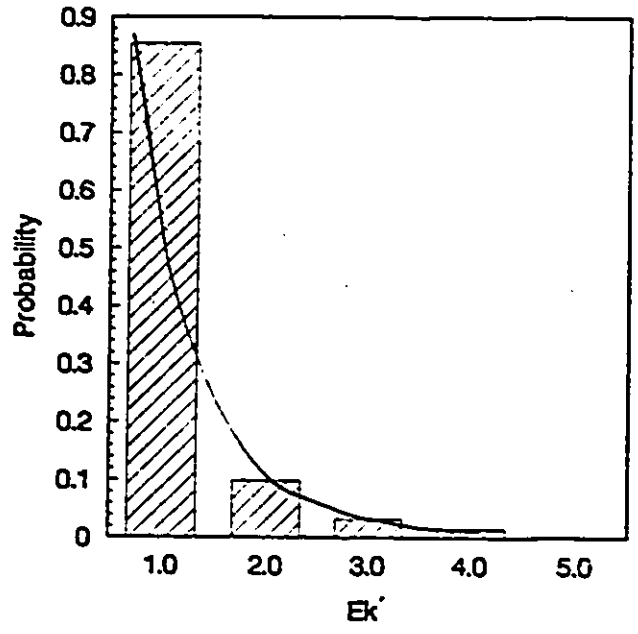

Fig. 4.19b The kinetic energy distribution, normalized to 4000K, corresponding to Fig. 4.19a.

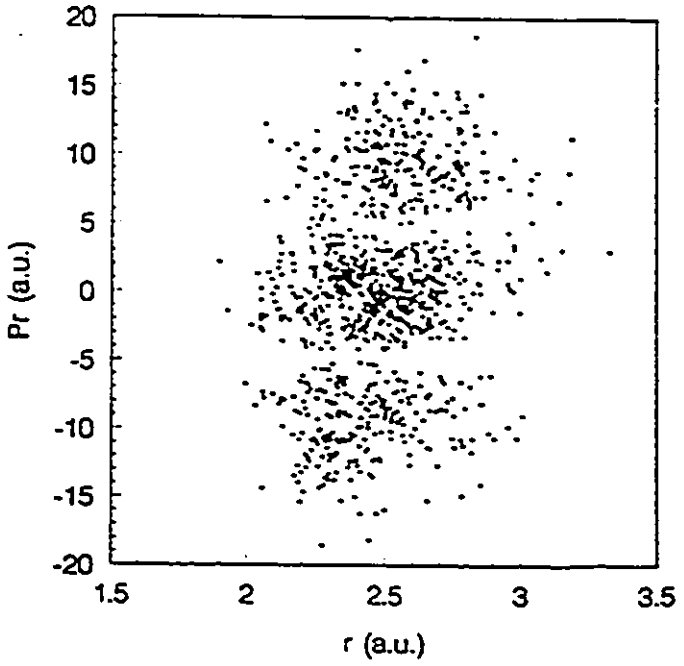

Fig. 4.20a The surface of section for HCl dynamics generated using modified Nosé-Hoover equations. $Q_1 = Q_2 = 20$, T = 4000K, initial conditions r = 2.6 a.u. and $p_r = 0.0$ a.u.

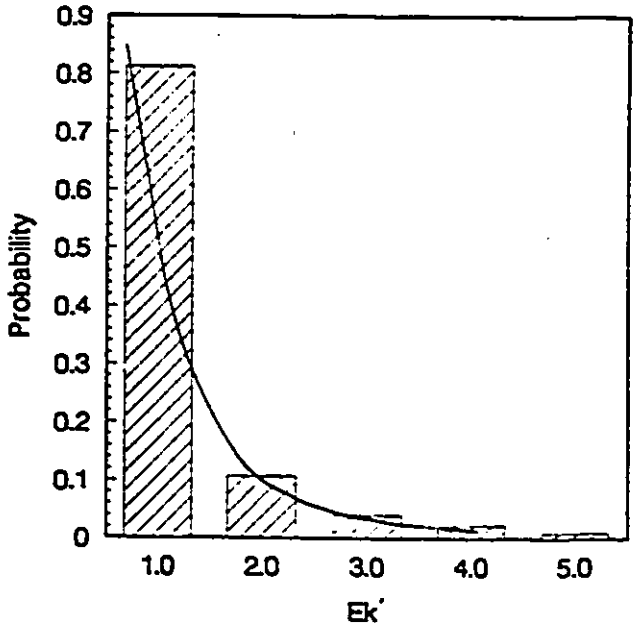

Fig. 4.20b The kinetic energy distribution, normalized to 4000K, corresponding to Fig. 4.20a.

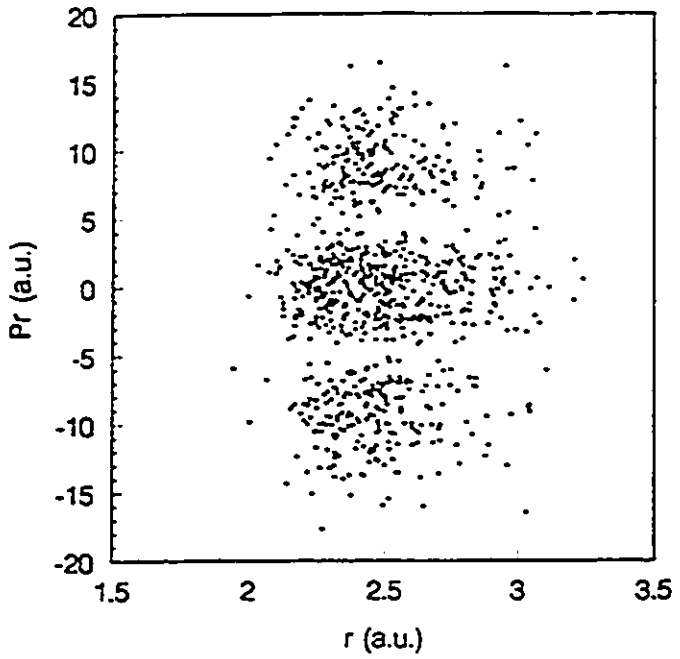

Fig. 4.21a The surface of section for HCl dynamics generated using modified Nosé-Hoover equations. $Q_1 = Q_2 = 30$, T = 4000K, initial conditions r = 2.6 a.u. and $p_r = 0.0$ a.u.

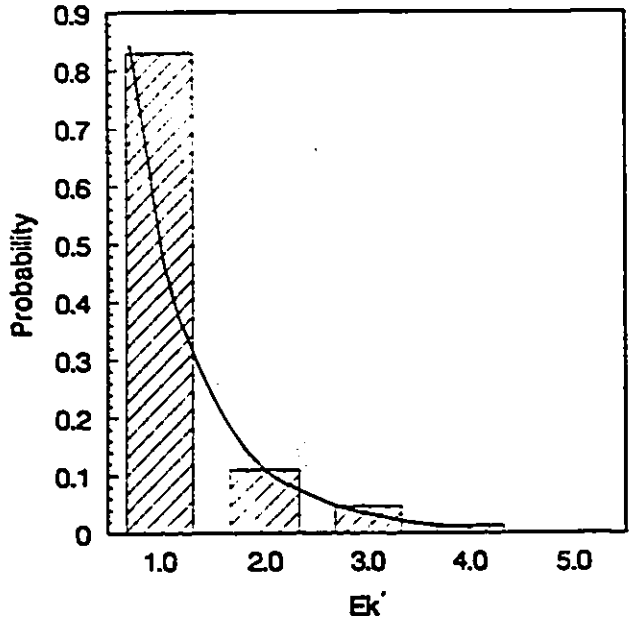

Fig. 4.21b The kinetic energy distribution, normalized to 4000K, corresponding to Fig. 4.21a.

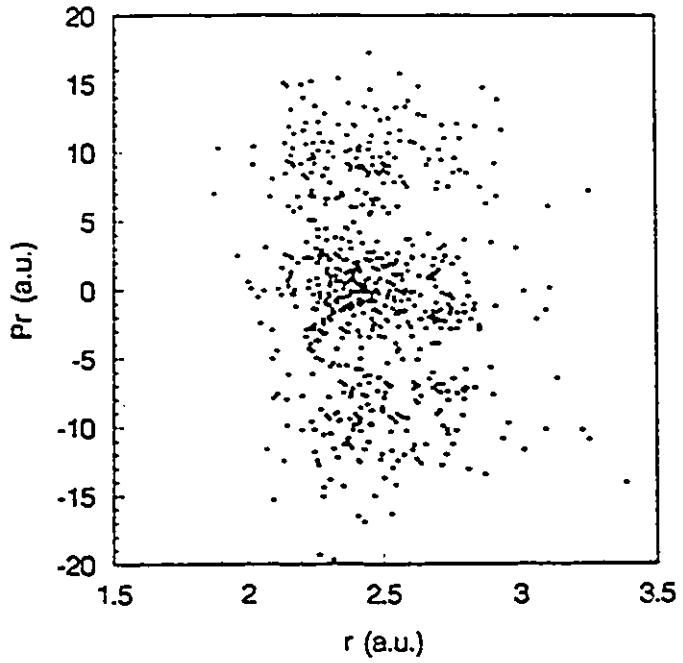

Fig. 4.22a The surface of section for HCl dynamics generated using modified Nosé-Hoover equations. $Q_1 = Q_2 = 40$, T = 4000K, initial conditions r = 2.6 a.u. and $p_r = 0.0$ a.u.

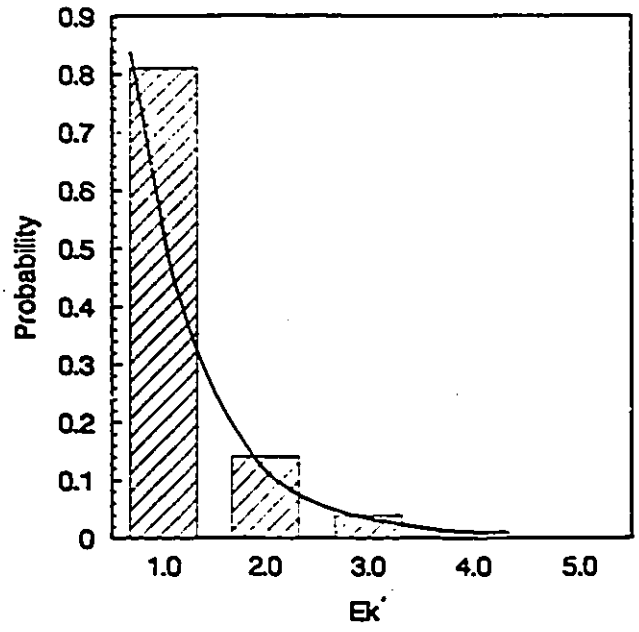

Fig. 4.22b The kinetic energy distribution, normalized to 4000K, corresponding to Fig. 4.22a.

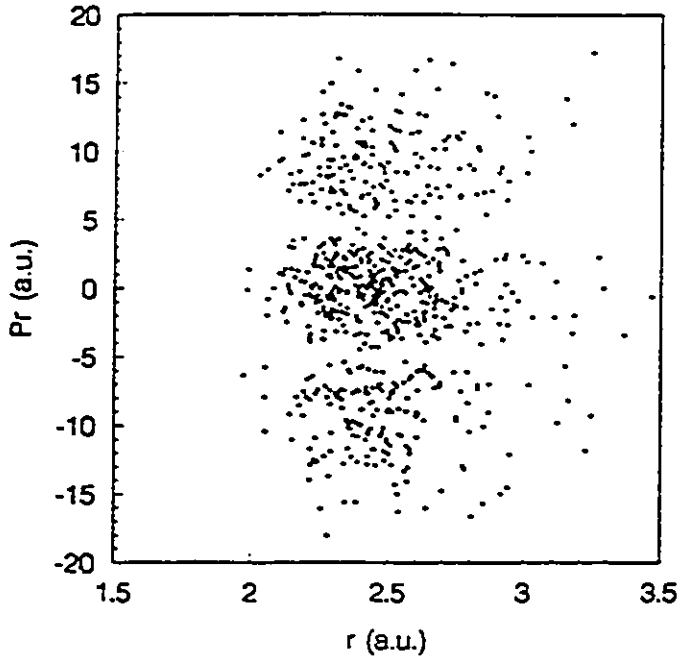

Fig. 4.23a The surface of section for HCl dynamics generated using modified Nosé-Hoover equations. $Q_1 = 10$, $Q_2 = 40$, T = 4000K, initial conditions r = 2.6 a.u. and $p_r = 0.0$ a.u.

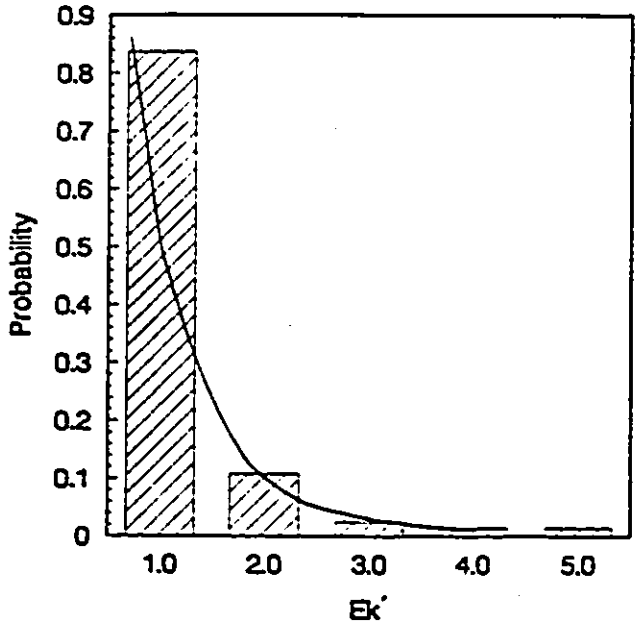

Fig. 4.23b The kinetic energy distribution, normalized to 4000K, corresponding to Fig. 4.23a.

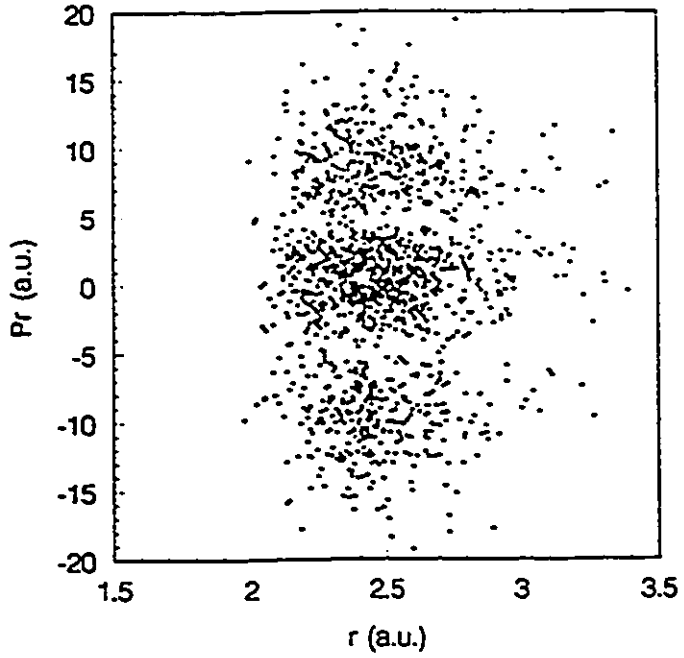

Fig. 4.24a The surface of section for HCl dynamics generated using modified Nosé-Hoover equations. $Q_1 = 40$, $Q_2 = 10$, T = 4000K, initial conditions r = 2.6 a.u. and $p_r = 0.0$ a.u.

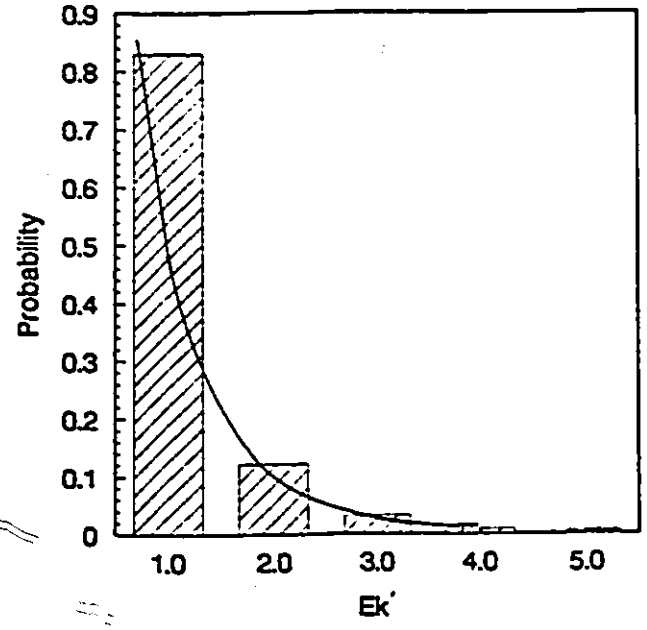

Fig. 4.24b The kinetic energy distribution, normalized to 4000K, corresponding to Fig. 4.24a.

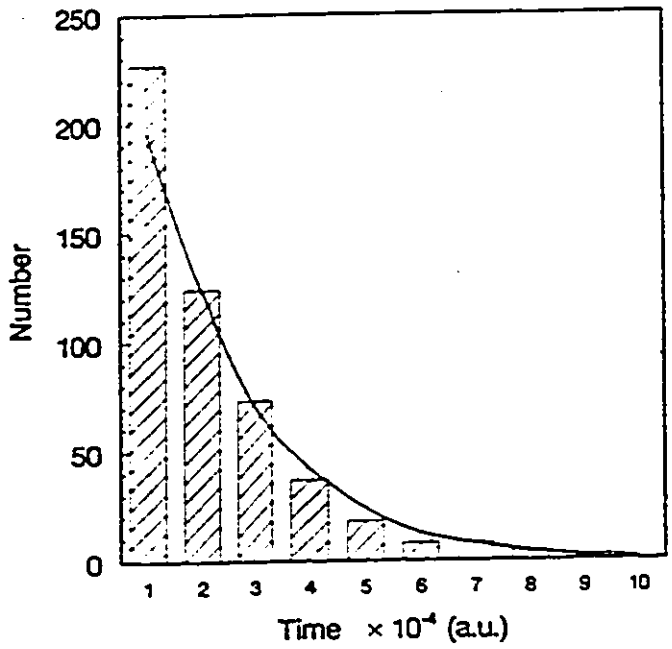

Fig. 4.25 The lifetime distribution for HCl dissociation at T = 7250K, calculated using modified Nosé-Hoover equations.

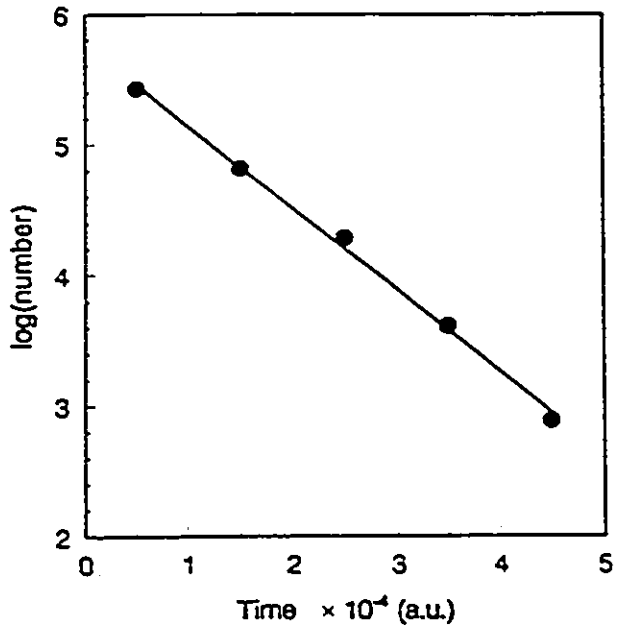

Fig. 4.26 Least-squares fit for the rate constant of HCl dissociation at T = 7250K, calculated using modified Nosé-Hoover equations. $k_d = 2.59 \pm 0.09 \times 10^{12}$ sec.$^{-1}$

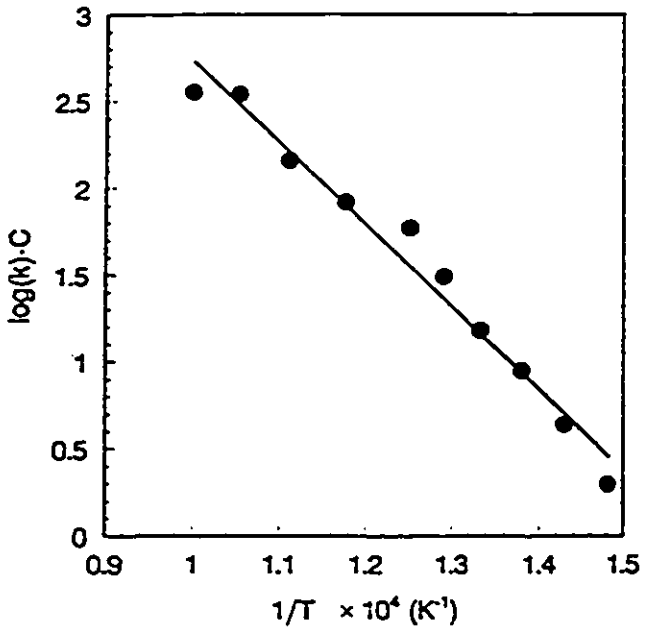

Fig. 4.27 Arrhenius plot of a least-squares fit for the activation energy of HCl dissociation, calculated using modified Nosé-Hoover equations.
$E_a = 3.89 \pm 0.23$ eV. $C = \log(10^{12}) = 27.63$.

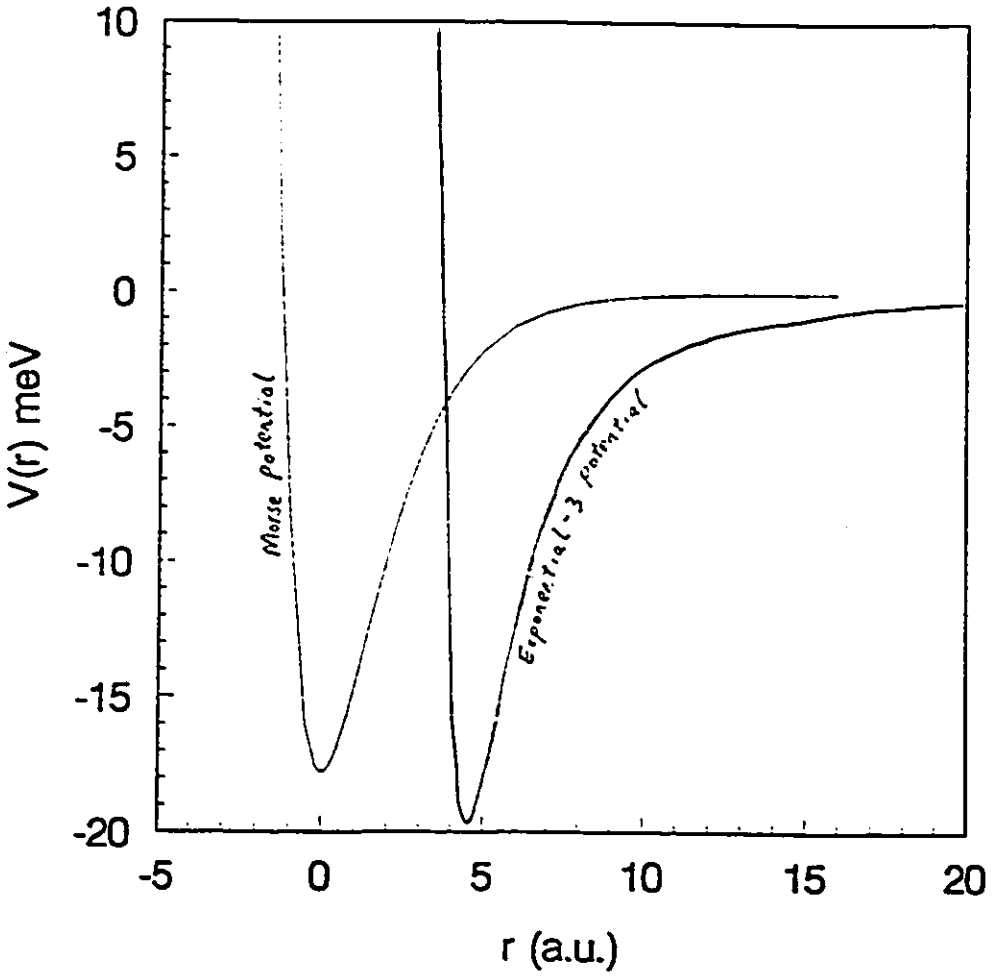

Fig. 5.A The Morse potential and the exponential-3 potential curves for the H/LiF (001) system.

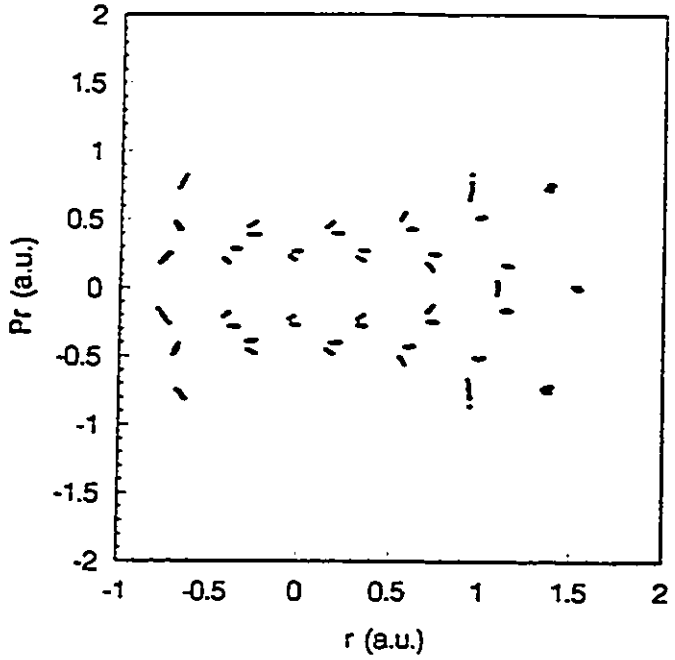

Fig. 5.1a The surface of section for H/LiF dynamics generated using Nosé-Hoover equations with the Morse potential function. Q = 15, T = 20K, initial conditions r = 1.5 a.u. and p_r = 0.0 a.u.

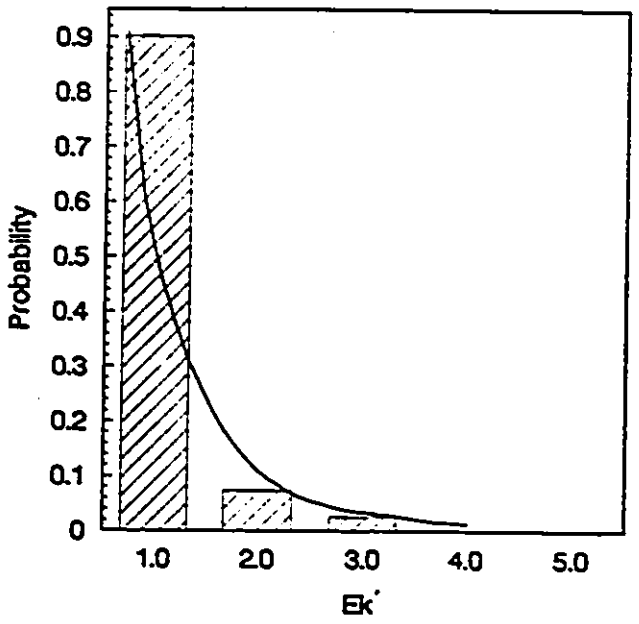

Fig. 5.1b The kinetic energy distribution, normalized to 20K, corresponding to Fig. 5.1a.

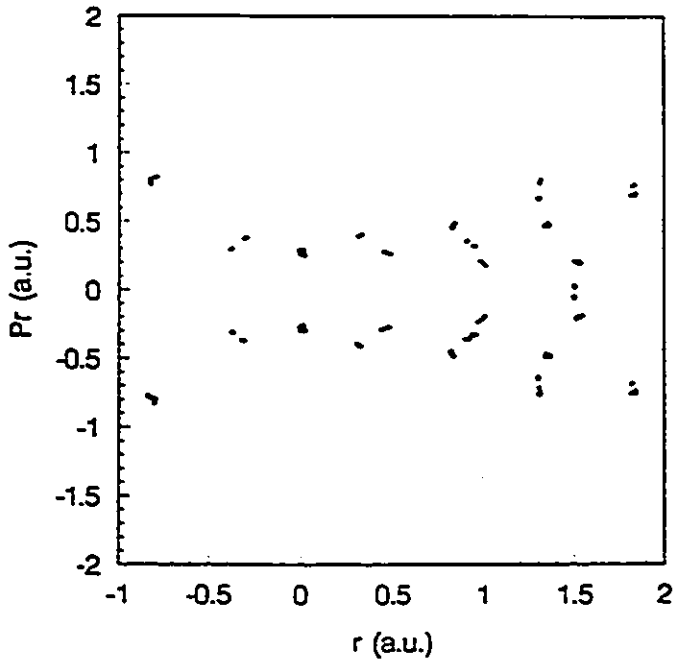

Fig. 5.2a The surface of section for H/LiF dynamics generated using Nosé-Hoover equations with the Morse potential function. Q = 25, T = 20K, initial conditions r = 1.5 a.u. and p_r = 0.0 a.u.

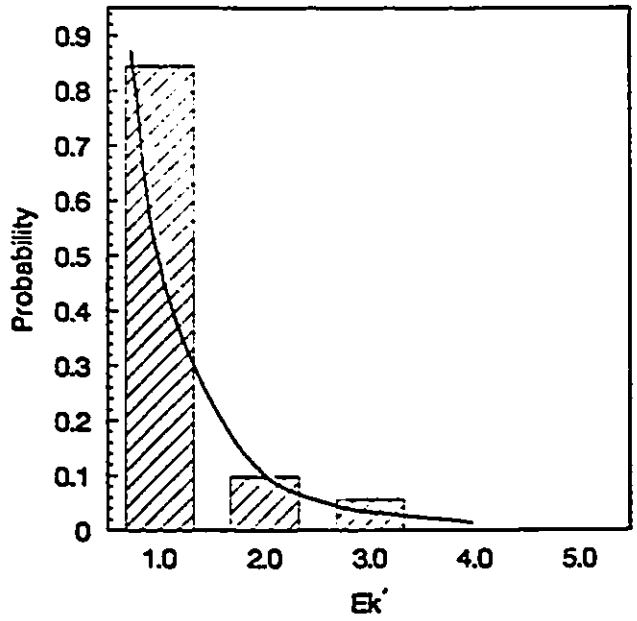

Fig. 5.2b The kinetic energy distribution, normalized to 20K, corresponding to Fig. 5.2a.

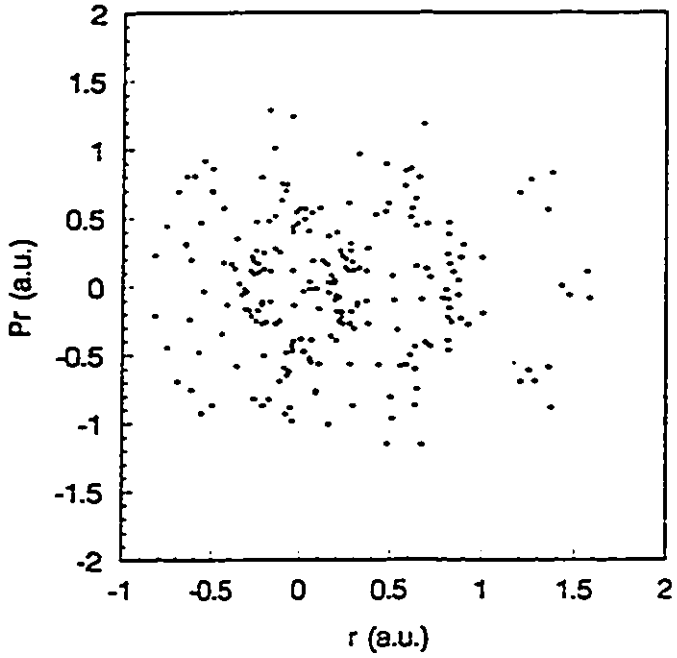

Fig. 5.3a The surface of section for H/LiF dynamics generated using Nosé-Hoover equations with the Morse potential function. Q = 35, T = 20K, initial conditions r = 1.5 a.u. and p_r = 0.0 a.u.

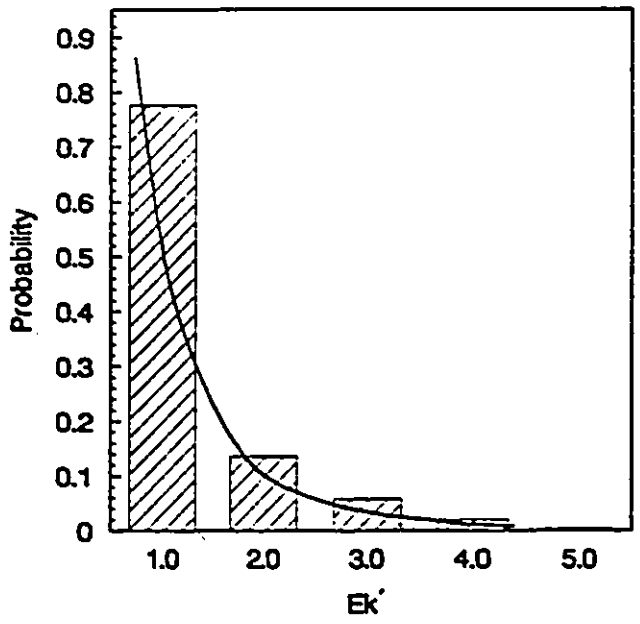

Fig. 5.3b The kinetic energy distribution, normalized to 20K, corresponding to Fig. 5.3a.

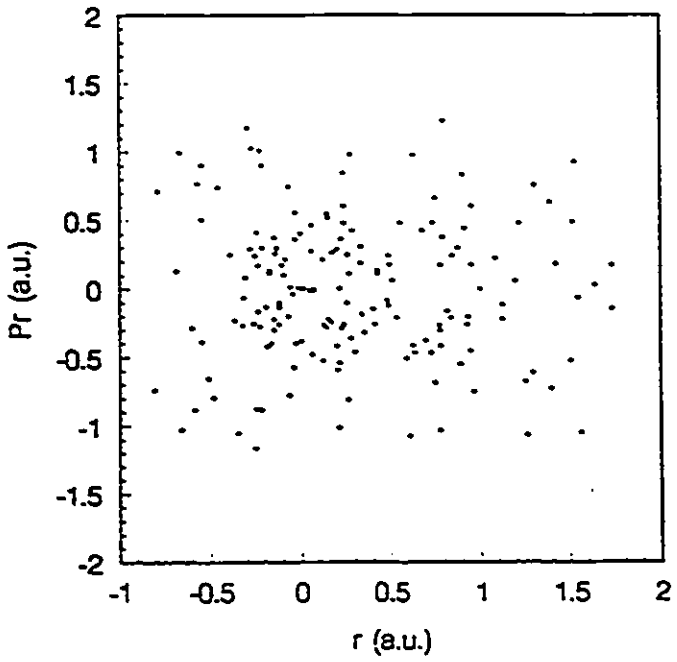

Fig. 5.4a The surface of section for H/LiF dynamics generated using Nosé-Hoover equations with the Morse potential function. Q = 45, T = 20K, initial conditions r = 1.5 a.u. and p_r = 0.0 a.u.

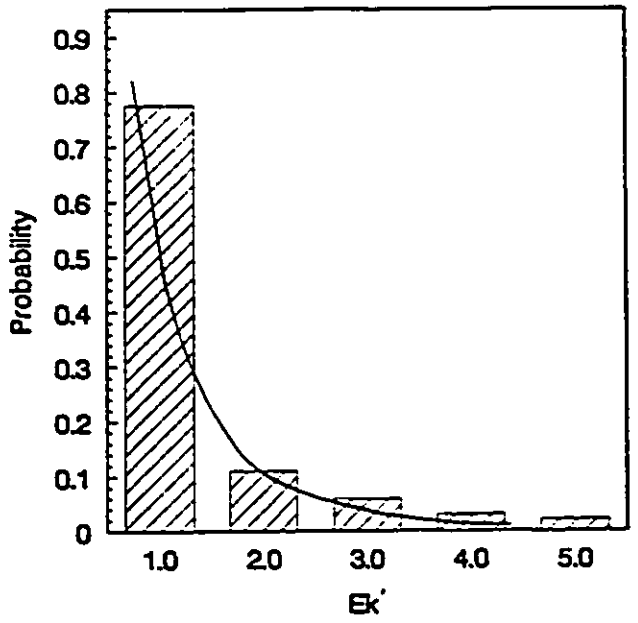

Fig. 5.4b The kinetic energy distribution, normalized to 20K, corresponding to Fig. 5.4a.

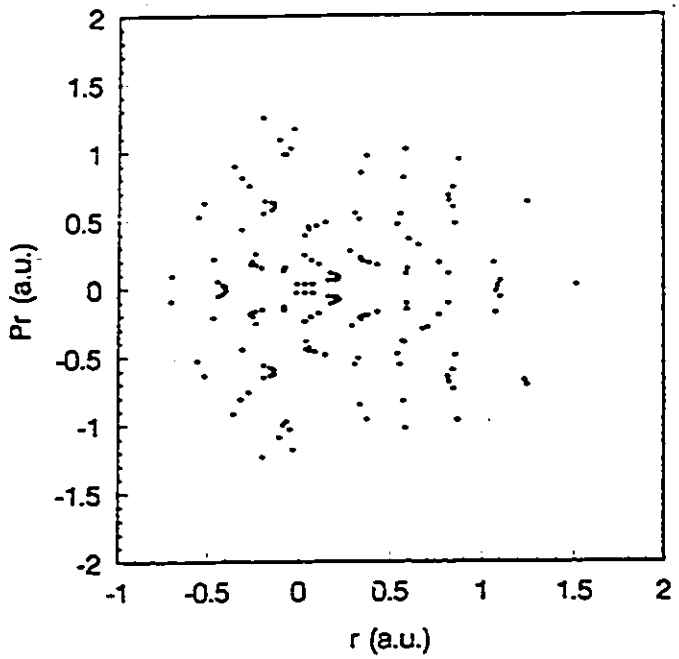

Fig. 5.5a The surface of section for H/LiF dynamics generated using Nosé-Hoover equations with the Morse potential function. Q = 55, T = 20K, initial conditions r = 1.5 a.u. and p_r = 0.0 a.u.

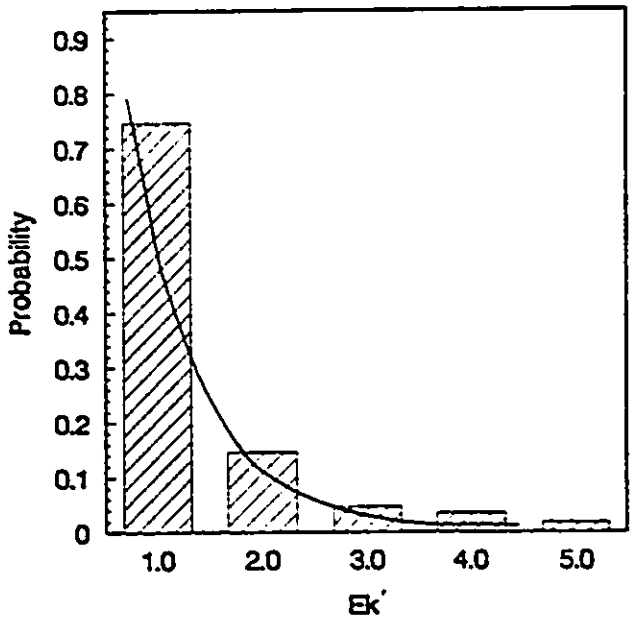

Fig. 5.5b The kinetic energy distribution, normalized to 20K, corresponding to Fig. 5.5a.

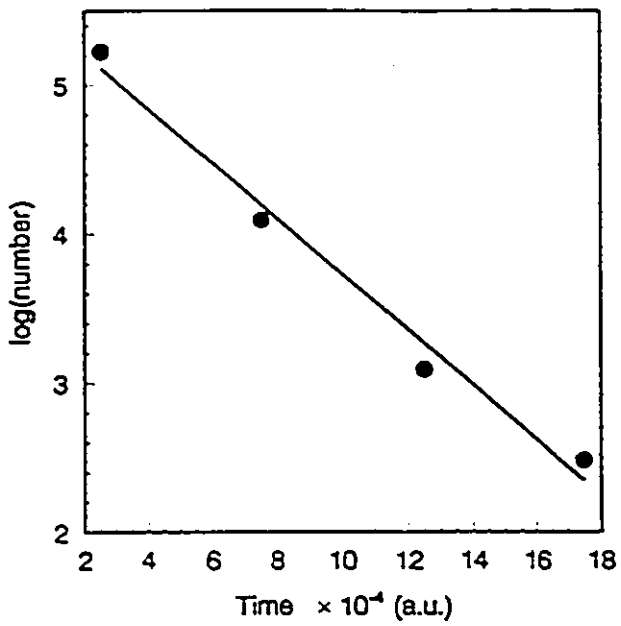

Fig. 5.6 Least-squares fit for the rate constant of desorption at T = 120K, calculated using Nosé-Hoover equations with the Morse potential function.
$k_d = 0.76 \pm 0.07 \times 10^{12}$ sec.$^{-1}$

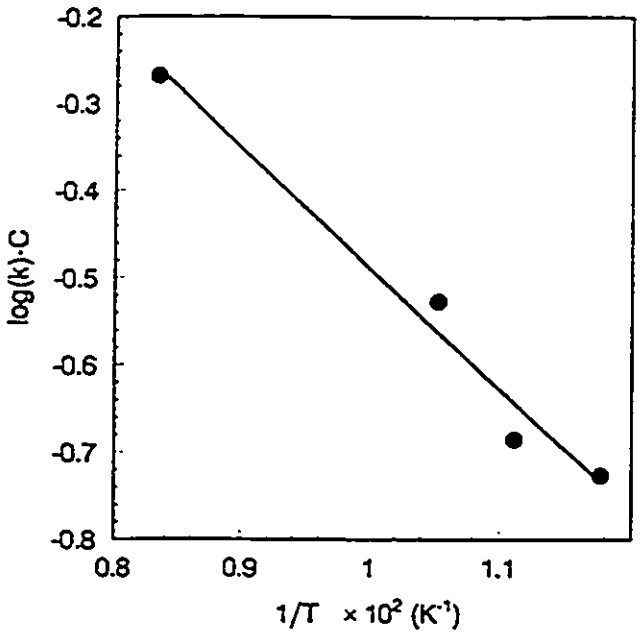

Fig. 5.7 Arrhenius plot for the activation energy of H atom desorption, calculated using Nosé-Hoover equations with the Morse potential function.
E_a = 6.06 ± 1.33 meV. C = log(10^{12}) = 27.63.

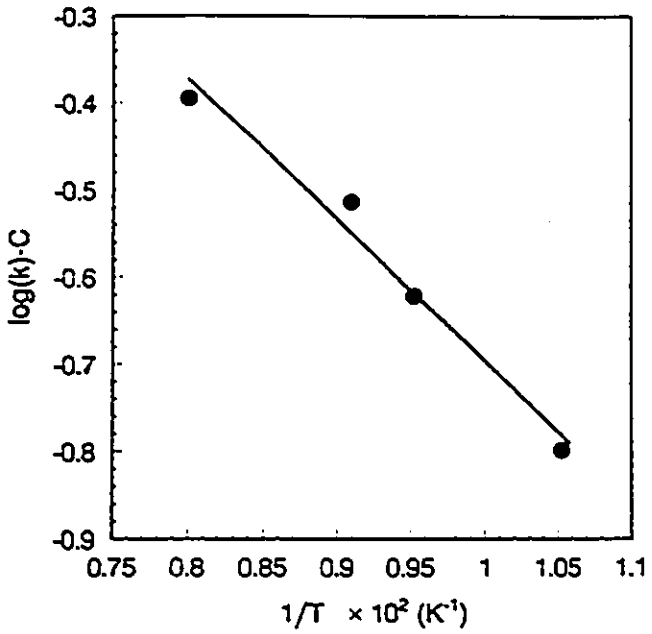

Fig. 5.8 Arrhenius plot for the activation energy of H atom desorption, calculated using Nosé-Hoover equations with the exponential-3 potential function.
E_a = 6.32 ± 1.53 meV. C = log(10^{12}) = 27.63.

Claims to Original Research

I applied the Nosé-Hoover equations of motion to the thermal dissociation of a diatomic molecule, H_2, in an inert gas. I calculated the pseudo-unimolecular rate constant and activation energy of thermal dissociation.

I added a rotation term to the Nosé-Hoover equations of motion for a diatomic molecule. I calculated the pseudo-unimolecular rate constant and activation energy of thermal dissociation with the Nosé-Hoover equations of motion including rotation.

I applied the modified Nosé-Hoover equations of motion to the thermal dissociation of the homonuclear diatomic molecule, H_2, and the heteronuclear diatomic molecule, HCl. I calculated the pseudo-unimolecular rate constant and activation energy for both H_2 and HCl thermal dissociation.

I demonstrated an example that the Nosé-Hoover equations of motion can be applied to the thermal desorption of H atoms from the LiF (001) surface, where other approaches may not be feasible.

Appendix A

Definition of Symbols Used

Symbol	Interpretation
a_i	amplitude of pendulum motion
A(q,p)	any ensemble property in the extended system
$<A>$	ensemble average of any property A in the N-particle system
$<A_{ES}>$	ensemble average of any property A in the extended system
AB	any diatomic molecule
α	Morse potential or exponential-3 potential parameter which relates to bond strength
D_e	classical dissociation energy or classical desorption energy, *i.e.*, depth of the potential well
D_0	spectroscopic dissociation energy
D_e^{ef}	classical effective dissociation energy
D_0^{ef}	effective dissociation energy
$D_0(J_i)$	dissociation energy at the vibrational level $v' = 0$ and the rotational state J_i
$D_0^{ef}(J_i)$	effective dissociation energy at the vibrational level $v' = 0$ and the rotational state J_i
ε_i	i-th energy level of the molecule
E	energy of each imaginary replication

E_a	activation energy
E_i	energy of imaginary replication in state i
E_k	kinetic energy
E_k'	kinetic energy normalized to temperature indicated
E_r	total rotational kinetic energy for a linear rigid rotor
E_{1r}	rotational kinetic energy for one-dimensional rotational motion
E_t	total energy of all imaginary replications in an actual system
E_{ES}	total energy of the extended system
f	number of degrees of freedom of an N-particle system
f(x)	arbitrary function
g_i	degeneracy of state i
$\phi(x)$	arbitrary function
ζ	set equal to p_ζ/Q in Subsection §2.3.1: a variable in the Nosé-Hoover equations of motion
F_i	force acting on particle i
F	force acting on the centre of mass of molecule AB
g(x)	arbitrary function
h	Planck's constant, $h = 6.62608 \times 10^{-34}$ J s
H	enthalpy
$H(r,p_r)$	Hamiltonian of an N-particle system (or the physical system, according to Nosé)
H_{ES}	total Hamiltonian of the extended system

$H_0(q,p)$	Hamiltonian of N particles in the extended system
$[H_2]$	concentration of hydrogen
I	moment of inertia
J_i	i-th rotational state
k	Boltzmann constant. $k = 1.38066 \times 10^{-23}$ (J/K)
k_d	pseudo-unimolecular rate constant of dissociation or desorption
k_i	rate constant of dissociation at the i-th step
L_i	angular momentum for one-dimensional rotation of a linear rigid rotor
m_i	mass of particle i
m_A	mass of atom A
m_B	mass of atom B
m_H	mass of hydrogen atom
M	inert gas molecule or inert collision partner
[M]	concentration of inert gas
n_i	number of molecules in i-th energy level
n_{xi}	number of imaginary replications in i state
N	number of particles in each imaginary replication
N_x	total number of imaginary replications in an actual system
N_{diss}	exponential decay number of dissociated molecules
N_{tot}	total number of molecules in dissociation reaction
ρ	equilibrium distribution function
ρ_{ES}	distribution function of the extended system

p_i	momentum of particle i in the extended system
p_r	momentum of one-dimensional motion; momentum of the centre of mass of a diatomic molecule; or momentum of an atom
p_n	momentum of particle i in the N-particle system
p_s	generalized momentum conjugate to the variable s; for consistency, replacement of the symbol ζ in the Nosé-Hoover equations of motion
P	pressure
$P(E_k')$	probability of the exact Boltzmann distribution
Q or Q_1, Q_2	Nosé parameter
q_i	coordinate of particle i in the extended system
(q,p)	coordinate and momentum of N particles in the extended system
r	coordinate of one-dimensional motion in Subsection §2.1.4; interatomic distance of a diatomic molecule in Chapters 3 and 4; or perpendicular distance between an atom and a surface in Chapter 5
r_i	coordinate of particle i in the N-particle system
R_e	equilibrium bond distance of a diatomic molecule or minimum perpendicular distance between an atom and a surface
(r,p_r)	coordinate and momentum of N particles in the N-particle system
τ	virtual time in the extended system
θ	angular displacement
s	an additional degree of freedom which was introduced by Nosé and which simulates a heat bath in the extended system

δ	Dirac delta function
t	time
t_{mid}	middle value of time for each bar in the histogram of lifetime distribution
t'	$t_{mid} \times 10^{-4}$
t_{new}	new time variable defined by Hoover in Subsection §2.3.1
t_{old}	old time variable defined by Hoover in Subsection §2.3.1
T	temperature
T_v	virial term
μ	reduced mass of a diatomic molecule
$U_{max}(J_i)$	effective rotational barrier at rotational J_i state
v_i'	i-th vibrational level
v	linear velocity of a particle
V	volume
$V_N(q)$	total potential energy of N particles in the extended system
V(r)	potential energy of one-dimensional oscillator; potential energy of a diatomic molecule; or potential energy between an atom and a surface
$V_N(r)$	total potential energy of N particles in the N-particle system
ω	angular velocity
z	molecular partition function
Z	canonical partition function
Z_{ES}	partition function of the extended ensemble

Appendix B

Some Unit Conversions

(1) Atomic Units Converted to cgs Units

Quantity	Atomic Unit	Physical Significance	Other Units
Mass	1	electron mass	9.1091×10^{-28} gram
Length	1	Bohr radius	0.529167×10^{-8} cm
Time	1	time required for electron in first Bohr orbit to travel one Bohr radius	2.41888×10^{-17} second
Energy	1	Twice the ground-state energy of a hydrogen atom if nuclear motion is neglected	4.35942×10^{-11} erg

Example: convert mass of a hydrogen atom from cgs unit to atomic unit.

The mass of a hydrogen atom is 1.6735×10^{-24} gram. Divided this value by electron mass, *i.e.*, 9.1091×10^{-28} gram, the mass

of a hydrogen atom is converted to 1837.1645 a.u.

(2) Energy Conversion Factors

	eV	kcal/mole	cm^{-1}	K	a.u.
eV	1	23.0609	8.06573×10^{1}	1.16049×10^{4}	3.67502×10^{-2}
kcal/mole	4.33634×10^{-2}	1	3.49757×10^{2}	5.03228×10^{2}	1.59362×10^{-3}
cm^{-1}	1.23981×10^{-4}	2.85911×10^{-3}	1	1.43879	4.55633×10^{-6}
K	8.61705×10^{-5}	1.98717×10^{3}	6.95028×10^{-1}	1	3.16678×10^{-6}
a.u.	27.2107	6.27503×10^{2}	2.19474×10^{5}	3.15777×10^{5}	1

Example: convert 4000K to eV unit.

The fifth row in above table shows that 1K equals 8.61705×10^{-5} eV. Therefore, $8.61705\times10^{-5}\times4000 = 0.34$ eV.

Appendix C

Formula Derivation

A purely exponential decay probability is

$$\frac{N_{diss}}{N_{tot}} = \frac{e^{-a\,t'}}{\int_0^{\infty} e^{-a\,t'}\,dt'} , \qquad (C.\ 1)$$

where a is a parameter which controls the rate of exponential decay.

Since

$$\int_0^{\infty} e^{-a\,t'}\,dt' = \frac{1}{a} , \qquad (C.\ 2)$$

the exponential decay number of dissociated molecules. N_{diss}, can be expressed as

$$N_{diss} = N_{tot}\ a\ e^{-a\,t'} . \qquad (C.\ 3)$$

Appendix D

Program Flow Chart